A DIAGNOSTIC STUDY OF ANTARCTIC FOG

by

Matthew A. Lazzara

A dissertation submitted in partial fulfillment of

the requirements for the degree of

Doctor of Philosophy

(Atmospheric and Oceanic Sciences)

at the

UNIVERSITY OF WISCONSIN-MADISON

2008

A DIAGNOSTIC STUDY OF ANTARCTIC FOG

Matthew A. Lazzara

Under the supervision of Professor Steven A. Ackerman

At the University of Wisconsin-Madison

The United States Antarctic Program (USAP) is the largest scientific research program in the Antarctic and requires a considerable aviation operation. Of the more than 700 flights planned each year, nearly 175 are aborted due to bad weather conditions. Although fog is one of the top three forecast problems related to flights aborted due to weather, it is largely unstudied. This investigation examines fog that affects the important Antarctic research station, McMurdo Station, Antarctica and its nearby airfields. The objective of this research is to acquire an understanding of fog occurrence in the region. This understanding is gained through analyses of surface based weather observations, satellite measurements and numerical weather prediction models.

Multi-channel satellite observations indicate that most austral summer fog events are "advective" in nature. This is supported by weather observations from McMurdo Station and nearby airfields where fog occurs at moderate wind speeds, and primarily from the eastward direction. Analyses using both a back trajectory model and mesoscale numerical model are consistent with this finding. The primary source region for fog is found to be from the southeast over the Ross Ice Shelf (72% of the cases studied), while only a minority of cases (23%) reveals

a secondary source of fog from the north along the Scott Coast with airflow influences from the East Antarctic Plateau.

McMurdo experiences two fog seasons with a primary peak in January and a secondary peak in September. Fog events are often short lived – typically 1 to 3 hours, though some can last up to 30 hours. Over the last 30 years there has been a decreasing trend in fog occurrence at McMurdo. Time series analysis between the observed fog variability and large-scale circulations (e.g., El Nino, Antarctic Oscillation) yielded no correlations, while there is only a limited relationship of fog occurrence to ice concentration in nearby Lewis Bay and McMurdo Sound. Fog is more likely to take place at the nearby airfields rather than at McMurdo Station, which is consistent with the advective nature of the fog.

Recent developments in the last 10 years have added new tools to examine fog occurrence in Antarctica. With the launch of the Earth Observing Satellite Terra in 1999, the depiction of fog and low clouds is possible in the Antarctic using the Moderate-Resolution Imaging Spectroradiometer (MODIS) onboard these satellites. A multi-channel fog and low cloud depiction method has been developed using the MODIS satellite observations via principal component analysis. A basic validation was conducted using observations from the University of Wisconsin Automatic Weather Station (AWS) network. In early 2001, the Antarctic Mesoscale Prediction System (AMPS) was first run over the Antarctic. AMPS, used in an analysis mode, and a back trajectory model are combined with traditional meteorological observing systems such as radiosondes and surface observations. This combination provides a more complete means for the analysis of fog in the Antarctic. Having identified the source regions of fog and developed a satellite depiction method for fog, forecasters have additional tools for improving

the monitoring and forecasting of fog events.

Acknowledgements

Dedication

In memory of my mother: Janet Lazzara
November 24, 1946 - January 9, 2002

Table of Contents

List of Tables

List of Figures

Chapter 1: Introduction: History and Objectives

Fog is defined in the American Meteorological Society's (AMS) *Glossary of Meteorology* as (AMS 2000):

> "… water droplets suspended in the atmosphere in the vicinity of the earth's surface that affect visibility. According to international definition, fog reduces visibility below 1 kilometer (0.62 miles). Fog differs from cloud only in that the base of the fog is at the earth's surface while clouds are above the surface…"

It is a phenomenon that occurs all over the world, including in Antarctica. This chapter introduces the impacts fog has in the Antarctic and outlines the objectives of this dissertation.

1. Background

Serious exploration of the Antarctic began in the late nineteenth century. Fog was a weather phenomenon that affected the lives of those early Antarctic explorers. Dr. E.A. Wilson, Sir Robert Falcon Scott's chief scientist during an early British Antarctic expedition, took time to sketch a fog event that clearly showed reduced visibility and an obscured horizon (Figure 1). From his book *The Voyage of 'Discovery*,' Scott describes the following fog event from 29 November 1902 on the Ross Ice Shelf (Scott 1905):

> "November, 29... Shortly after four o'clock today we observed the most striking atmospheric phenomenon we have yet seen in these regions. We were enveloped in a light, thin stratus cloud of small ice-crystal; it could not have extended to any height, the sun was only lightly veiled. From these drifting crystals above, the sun's rays were reflected in such an extraordinary manner that the whole arch of the heavens was traced with circles and lines of brilliant prismatic or white light.

> The coloured circles of a bright double halo were touched or intersected by one which ran about us parallel to the horizon; above this, again, a gorgeous prismatic ring encircled the zenith; away from the sun was a white fogbow, with two bright mock suns where it intersected the horizon circle. The whole effect was almost bewildering, and its beauty is far beyond the descriptive powers of my sledging pencil. We have often seen double halos, fogbows, mock suns, and even indication of other circles, but we have never been privileged to witness a display that approaches in splendour that of to-day. We stopped whilst Wilson took notes of the various light effects. If it is robbed of some of the beauties of a milder climate, our region has certainly pictures of its own to display."

Clearly, this fog event with accompanying atmospheric optical effects made a significant impression on Scott and his party.

Another of Scott's men, Lt. E. Evans, made similar notes in his diary regarding the fog events that the party witnessed on their second expedition to Antarctica, camped near the Beardmore Glacier (Evans 1921):

> "We commended the day unluckily, for a low stratus cloud had spread like a tablecloth over the Beardmore and filled up the glacier with mist...The air was thick with countless myriads of tiny floating ice crystals, and the great hummocs of ice stood weirdly shapen as they loomed through the frozen mist." (16 January 1911)

Fog-bow - on the Great Ice Barrier.

Figure 1.   Fogbow as drawn by E.A. Wilson, from his "Diary of the Terra Nova Expedition" (*Courtesy of the Scott Polar Research Institute, University of Cambridge*).

American explorer Adm. Richard E. Byrd made similar comments about fog during his journeys to the Antarctic. This example is described from off -shore (Byrd 1935):

"The fog was somewhat disquieting. We were still in it on the 16th, 1200 miles southeast of Wellington [New Zealand]. Sometimes it would lift a bit for a few hours, then shut in again, thick as wool." (15 December 1934)

Figure 2 shows an example of the fog Byrd's early expeditions encountered in the Bay of Whales. These initial observations are the starting point of observing and coping with this problem faced by all those who explore, study or travel to Antarctica.

Figure 2. The caption from Byrd's 1935 book *Little America* states: "A Welcome Sight: The *City of New York*, only her upper works showing above the sea smoke, returns to the Bay of Whales. The first thing the men at Little America had seen from civilization in a year." (Byrd 1935) (*Courtesy of Richard E. Bryd, III*)

The International Geophysical Year (IGY) in 1957 and the advent of the weather satellite in 1960 catalyzed change in the investigations of the polar region by meteorologists. These events signaled the beginning of routine weather observing at Antarctic manned stations, and the possibility of spatial and temporal monitoring from satellite platforms. However, meteorologists had to wait until the late 1970s before the polar-orbiting satellite platform offered sufficiently high quality data and imagery suitable for forecasting and research purposes (Lazzara et al. 2003). On the heels of improved satellite communications in the late 1970s, automatic weather stations (AWS) began offering observations away from manned stations (e.g., Stearns and Weidner 1990).

In reviewing literature on fog, as related to the Antarctic, it is clear that this specialized field involves the intersection of three distinct areas of meteorology. This thesis falls into the small intersection of fog research, polar meteorology and satellite meteorology. There have been no formal studies of fog conducted in Antarctica, in spite of the fact that fog remains one of the top three forecast problems for the United States Antarctic Program (USAP) (Cayette personal communications, 2000).   The topic for this thesis is motivated by both its practicality and by its timeliness, as new data have recently become available from satellite, ground-based observations, and numerical models. The use of principal component analysis on the satellite imagery offers a new depiction of Antarctic fog/low clouds. This technique is important as it allows for the satellite observations to be effective for operational monitoring of fog and gives a focus of this study: used reliably in gaining understanding of fog in this region of the Antarctic. The use of satellite observations in comparison with a meteorological analysis from a modern mesoscale prediction system and back trajectory analysis provides the opportunity to improve understanding of fog behavior in this part of the world.

2. Statement of the Problem

In operation for over fifty years, McMurdo Station, Ross Island, Antarctica is affected by the occurrence of fog (Mullen 1987, NSFA 1990, Cayette 1998 and 1999, Stearns and Weidner 1999, Turner and Pendlebury 2000). In recent years, fog has been characterized as one of the main problems faced by operational forecasters. Blowing snow and precipitation are listed as

well (Cayette, personal communications 2000). Fog events that occur near and over the Ross Island region of Antarctica pose a significant problem because their onset can be extremely unpredictable and has significant impact on USAP aviation operations (Mullen 1987, Cayette personal communications, 2000). One unverified theory has been put forth regarding formation of fog in this region. This theory stated that the precursor is flow of cold air off of Ross Island and a situation with light winds and cooling temperatures take place just before the onset of fog (Stearns and Weidner 1999). No other formal studies of Antarctic fog exist.

The focus of this investigation aims to find deeper understanding of these fog events. To improve our understanding, climatology of fog needs to be defined for the area. This study examines fog and its environment by reviewing more than 30 years of weather observations from McMurdo Station, along with other nearby observations, to characterize the fogs experienced in the Ross Island region and McMurdo Sound areas. Fog events are then depicted from a space-based instrument, combined with other observations (surface reports for example) along with the analysis from a numerical weather prediction system and back trajectory analysis to develop an understanding of the fog. This dissertation concentrates on fog during the Antarctic summer period from late October to early March, coinciding with the operational field season during which this part of the Antarctic has the most aviation activity.

With the goal of learning about the unstudied meteorological frontier of fog in the Antarctic, this research project has the following objectives:

1. What are the physical, climatological and meteorological characteristics of fog in the Ross Island Region of Antarctica? This dissertation examines the relationship of fog to standard

meteorological variables by comparing observations made during fog and non-fog periods, collecting and measuring fog particles, and seeing if associations with sea ice and large-scale climate phenomena exist.

2. What methods are able to detect and track fog from an advanced satellite platform over the Antarctic, specifically the Ross Island region, during the operational Antarctic field season for the USAP (October to February)? A new method for depicting and enhancing fog/low clouds from satellite observations is introduced.

3. What is (are) the meteorological conceptual model(s) for fog in this part of the world? Based on the available observations along with an analysis from a back trajectory model as well as a mesoscale numerical model, the fog behavior in this region of Antarctica is discussed.

This dissertation offers the first formal study of fog in the Antarctic. Chapter 2 introduces the region and the observations available, and discusses a simple field collection of fog particles at McMurdo Station. The results of this experiment are discussed. Additional context for these observations is also offered, along with suggestions for future fog collection efforts in the Antarctic. Chapter 2 also provides background on the currently known fog types and a description of the vertical structure of fog. A description of the study region and the observations available from the region are also reviewed. Chapter 3 charts a fog-climatology using a dataset of more than 30-years of observations from McMurdo Station via the comparison of basic meteorological variables between fog and non-fog periods. Inspired by multi-year variability, this chapter also includes an analysis of fog and its relation to the nearby sea ice environment and to large-scale climate forcing. Chapter 4 reviews methods to depict fog/low

clouds from satellite and discusses the uses in the Antarctic. A new method is introduced using principal component analysis to depict fog and low clouds during the austral summer period, which is the focus period of this study. The University of Wisconsin AWS network provided a means for a basic validation of this technique. Chapter 5 suggests source regions for fog based on satellite observations in conjunction with an analysis from both a back trajectory model and a mesoscale numerical model. Example cases of fog that illustrate the source regions are also discussed. The thesis closes in Chapter 6 with a summary of this effort's conclusions as well as an outline of future work.

Chapter 2: Fog and Its Environment

1. The Study Area: McMurdo Station, Antarctica and Airfields

McMurdo Station, Antarctica is located at 77° 51' South and 166° 40' East on the Hut Point Peninsula of Ross Island Antarctica (Figure 3). The station is at an elevation of approximately 34 meters at the McMurdo Weather and Operations building, and is assigned the World Meteorological Organization (WMO) block identifier number 89664. Established in March 1956, the station has been open continuously for the last 52 years. It is the main station in the Antarctic for the USAP, which is overseen and managed by the National Science Foundation (NSF). McMurdo Station is located on Winter Quarter's Bay next to the first hut used by Captain Robert Falcon Scott's during the first of his several expeditions to Antarctica. Nearby is the New Zealand's Scott Base located at Pram Point on the other side of Hut Point Peninsula (Figures 4 and 5). McMurdo Station and Scott Base are connected via a road through a saddle point between Crater Hill and Observation Hill. Observation Hill, an extinct volcanic cone, lies at the very tip of Hut Point, Cape Armitage. The complete study area, centered about McMurdo Station, is displayed in Figure 6 and important geographic features and locations are labeled.

Figure 3. A view of McMurdo Station Antarctica as seen from Observation Hill, with Winters Quarter's Bay on the left side and Arrival Heights just outside the field of view of this photo to the right.

Figure 4. An aerial photo of McMurdo Station on Hut Point Peninsula showing the ice runway as well as nearby New Zealand Scott Base at Pram Point, on the other side of Observation Hill and Cape Armitage (*Photographer Unknown*).

Figure 5. An aerial photograph of McMurdo Station from Operation Deep Freeze 1960 which shows the full Hut Point Peninsula with Mt. Erebus in the background, the active volcano at the heart of Ross Island, Antarctica. (*Photo courtesy of Operation Deep Freeze '60, Task Force 43*)
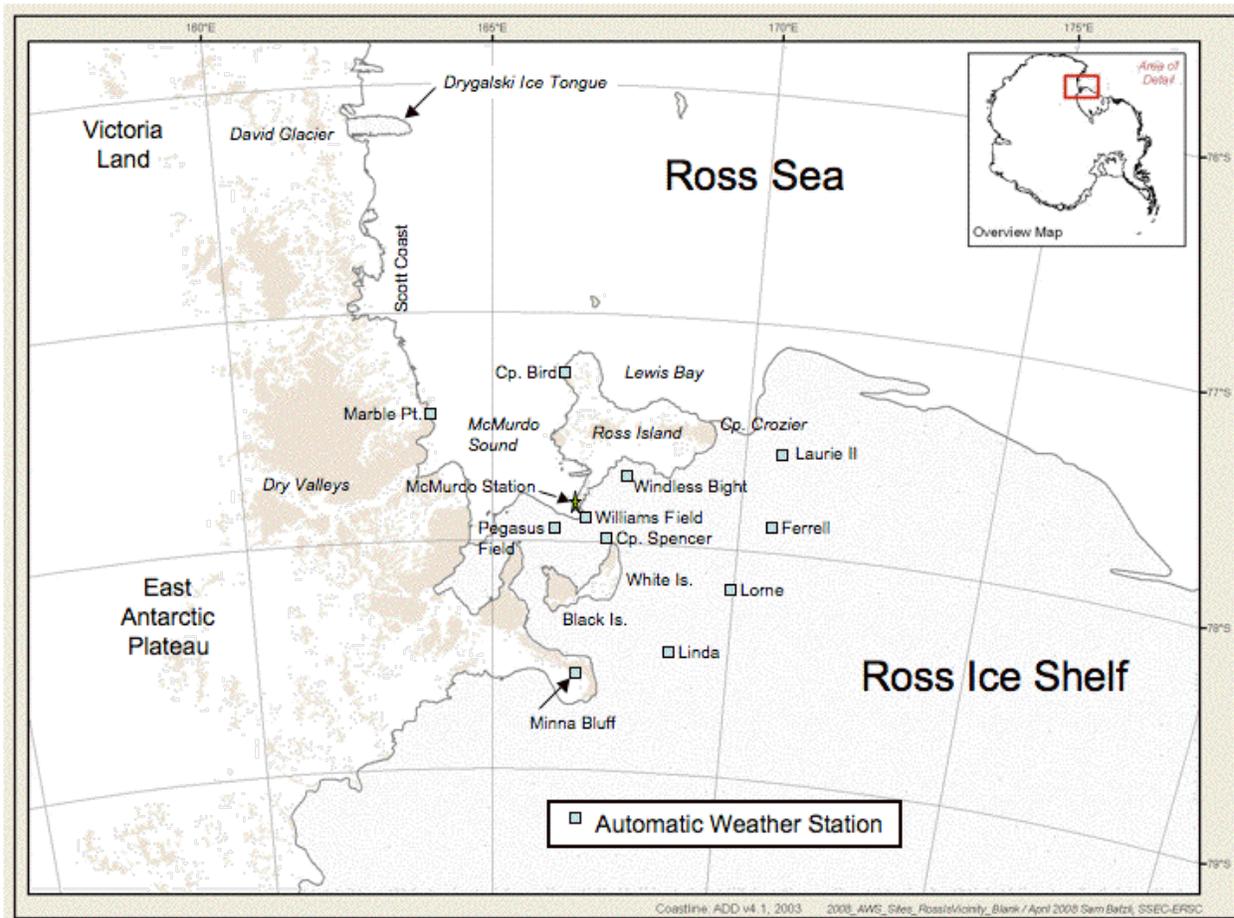
Figure 6. The fog study area centered on Ross Island and McMurdo Sound. AWS locations and important geographic features are labeled in the map.

Three airfields (also commonly known as skiways) are operated by the USAP nearby the station: the Ice Runway, Williams Field and Pegasus Field. Recently, these airfields have been assigned International Civil Aviation Organization (ICAO) identifiers NZIR, NZWD and NZPG, respectively. For many years prior to the 1990s, McMurdo Station was a Naval Air Facility with the ICAO identifier NZCM. Hence, some observations over those years from NZCM are from the longest running airfield, Williams Field. Otherwise, today NZCM is reserved for reference

to McMurdo Station proper. The last decade of the analysis presented here includes some supplemental information supplied by the observers at the nearby airfields.

At the station, synoptic and radiosonde observations are taken year round. For the last several years, surface hourly observations (METAR) are taken at the airfields when they are open during the operating field season (variable dates between late August and early March). It is standard practice that only one radiosonde observation is taken daily during the winter months. Two observations are taken per day during the operational field season (austral summer). The station reports only 6-hourly synoptic observations during the winter, and 3-hourly synoptic observations during the operational field season. McMurdo Station's operating field season does come in line with the cycle of the sun, (Figure 7) and the duration of sunlight. It also points to how McMurdo Station has some limited diurnal variation through the transition seasons. Even during periods of 24 hours of sunlight, there is some elevation change of the sun over the horizon.
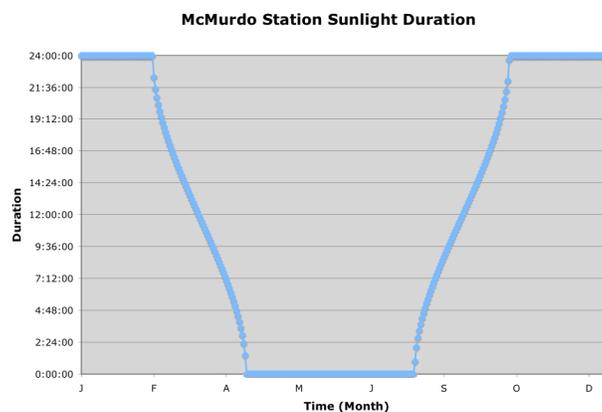
Figure 7. McMurdo Station's sunlight duration as depicted here reveals how the station does have long periods of 24-hour sunlight and 24-hour darkness, with two transition seasons.

Weather observations taken at McMurdo Station occur at Building 165, jointly housing the McMurdo Weather Office (Mac Weather) and McMurdo Operations (Mac Ops). This central building includes air traffic control (Mac Center), and headquarters for the Commander of Operation Deep Freeze (Figure 8).

Figure 8. The weather instrumentation shown here atop Building 165, McMurdo Operations and McMurdo Weather Office is the source of McMurdo Station's synoptic observations.

2. Observational Data

This study primarily uses McMurdo Station synoptic observations to characterize fog and create the first fog climatology from a station in Antarctica. McMurdo Station observations from 1956 though mid-1998 were acquired from the British Antarctic Survey (BAS). This collection, primarily a by-product of the Reference Antarctic Data for Environmental Research (READER) project (SCAR PACA READER Project 2000, Turner et al. 2003), provided a ready-made, quality-controlled data set of 6-hourly observations of temperature, pressure (both sea level and station pressure), wind speed and direction along with u and v components of the wind. Portions

of the BAS dataset were based on data collected originally at the National Climatic Data Center (NCDC). The BAS database however, lacked surface weather observations including those of fog. Hence, observations of fog came from a decoded NCDC database used by the USAP's Long Term Ecological Research (LTER) project. This database offered two sets of partially decoded McMurdo observations: one with semi-coded observations of several fields from 1956 to 1966 and a second with all fields of information decoded from 1973 to mid-1998. This database was not quality controlled, and had observations at 6-hourly, 3-hourly and off-synoptic hours. The 6-hourly observations of fog were selected from this collection and merged with the BAS dataset. Observational data from mid-1998 to the end of 2004 (and in some cases through 2007) came from the archives at the Antarctic Meteorological Research Center (AMRC) at the University of Wisconsin-Madison. This database of McMurdo Station observations and nearby airfield observations, which are posted to the Global Telecommunications System (via satellite broadcast received through the University of Wisconsin's Space Science and Engineering Center (SSEC) Data Center), provided the last collection of data needed to complete a greater than 30-year climatology record. This dataset was also not initially quality controlled, and was matched to the BAS dataset in temporal space – having only 6-hourly observations. One additional dataset was employed in the analysis: a set of monthly spreadsheets of raw observations from Mac Weather. This data provided additional details regarding fog events and occurrence reported at the station and nearby airfields.

Quality control checks were done on the combined dataset from 1998 through 2004 (with some variables updated through 2007). 1998 was used to verify that statistics in this project matched those computed by the READER project. Much of the quality control efforts focused on

the removing bad data. Primarily pressure observations required checking because these values were often in error due to poorly coded data or a reversal in the coding of the station pressure and sea level pressure. Used as an independent dataset, the monthly spreadsheets of observations direct from Mac Weather were spot-checked. Some errors were found and corrected in the datasets analyzed.

A choice was made to use only 6-hourly observations. During the winter season from early March until late August or September, McMurdo Station only takes 6-hourly observations. 3-hourly observations are taken during the rest of the year. It is felt that the use of the 3-hourly observations during the austral summer would skew the climatology results over the annual cycle presented here. The READER project also followed this model. Using 6-hourly observations is the minimum standard for best climatology practice (WMO 1983).

There are some periods during the record that lack observations from any source. In particular, it appears that, there are no observations available from McMurdo Station for much of the austral summer in 1998. Additionally, during the mid-1970s, some winter months had few observations available (e.g., as few as 15 observations for an entire month). While this is the exception, not the rule, these imperfections are a part of this data set. Similar issues exist with nearby airfield observation when operations were conducted at each airfield. There are examples of airfield observations being limited due to the closing of the airfields due to fog.

One important finding during the quality control of the 1998 to 2004 data was the change in method used by the McMurdo Weather Office to compute sea level pressure. Prior to 1998, sea level pressure was computed using the U.S. Standard Atmosphere as the basis for the computation (Cayette personal communication, 2003). After mid-1998, the method was changed

to using a computed R-value with the surface temperature and table provided by the US Naval Detachment/Air Force Combat Climatology Center (AFCCC) at NCDC (AFCCC 2002). Although the R-value method calls for the computation to be done on sites that are only 15 meters in elevation or less, McMurdo Station, at an elevation of 34 meters, utilizes this method regardless. The data used in this analysis have been kept as reported, and not altered or adjusted. No attempt was made to recalculate the sea level pressure in a consistent manner. As a result of this finding, the station pressure was primarily chosen for analysis.

3. Fog Types

As documented by the weather observers and forecasters, several types of fog impact the Ross Island region of the Antarctic. Fog event types are typically classified as:

- Advection fog events, typical for the summer season

- "Camp," "station" or "ice" fog events, typical during mid- to late-winter season

- Radiation fog, which is anecdotally noted as rare for the region

- "Inversion" fog, which is the operational terminology for frontal fog

These types of fogs are primarily diabatic in nature with the exception of the frontal fog, which is more likely to be adiabatic. It is possible that some of the events that take place in this region could be other types of fog such as mixing fog or perhaps upslope fog, given the dramatic varying terrain found in the area. In contrast, these types of fog are adiabatic in nature. This section provides a descriptive introduction to each type of fog known to occur in the Ross Island

and McMurdo Sound region based on forecaster handbook information (NSFA 1990, ATS 1999, SPAWAR 2007a and 2007b) and interviews with forecasters (Cayette personal communications, 2001, 2002, 2007; Clogston personal communications, 2007).

a. Advection Fog

Advection fog is one of the more common fog types. Anecdotal evidence indicates that this type of fog occurs with winds from the sea advecting moisture over the ice, which in turn cools the air, and forms fog. It is most likely to occur from late December with a peak in March. Forecasters have noted three avenues for the moisture advection. One is from the north of Ross Island, over McMurdo Sound toward McMurdo Station and the airfields. A second also from the northeast of Ross Island, near Cape Crozier on the eastern tip of Ross Island, come toward Windless Bight and then on to the airfields and McMurdo Station. The third is from the Ross Sea over the Ross Ice Shelf to the southeast of Ross Island, and then moves into the Ross Island region impacting the airfields and McMurdo Station.

This type of situation is the basis for the U.S. Navy forecaster's handbook guideline for using the Ferrell AWS as an early warning site for forecasting fog at the McMurdo airfields. Unfortunately, due to the nature of the movement of the Ross Ice Shelf, Ferrell AWS has moved approximately 19 kilometers over the last 28 years (Weidner personal communications, 2008). In January of 2007 a new AWS named Lorne was installed to maintain a line of Wisconsin AWS stations to monitor weather systems moving toward McMurdo Station and the airfields. Mac Weather has installed its own seasonally deployed AWS sites inside the Wisconsin AWS

network (Stringer and Newell 2000). The Mac Weather AWS fog network is designed for in-situ observations of fog. The seasonal network is not used in this study due to the small number observations available as a consequence of limited observing periods and highly variable durations of AWS deployment.

b. Radiation Fog

Although not the most common type of fog, radiation fog, or radiation-advection fog, is a fog that can challenge forecasters. The advection of moisture over McMurdo Sound and over the McMurdo area airfields in this situation does not lead to immediate fog. However, forecasters suspect the pooling of moisture over the colder snow and ice surface leads to the possibility of fog formation in the region via radiational cooling of the moist air over the ice surface. Key features forecasters look for include small dewpoint, depressions, high relative humidity, and no cloud ceilings less than 7,000 feet.

c. "Station," "Camp" or Ice Fog

"Station," "camp," or "ice" fog is a common fog type anecdotally reported during the austral winter typically when temperatures are below -30°C. One trigger for this type of fog is thought to be the increase in ice condensation nuclei found in the exhaust generated by heavy equipment, trucks and aircraft. Since the start of the USAP, there has been a winter fly-in to McMurdo (known as WINFLY) in the late August or early September time frame. This coincides with the

secondary peak in fog occurrence at McMurdo Station (see Chapter 3). It is not known at this time if this is coincidental or not. Since this study is focused on the primary operational field (austral summer) season, known as Main Body, which runs from October to March, ice fog is not the focus of this dissertation. Currently, no known studies on ice fog have been conducted in the McMurdo area.

d. "Inversion" or Frontal Fog

McMurdo Station's marine location on the Antarctic coast does experience impacts from frontal systems, including the development of polar low systems that are very common in this part of the Antarctic (Carrasco and Bromwich 1996, Carrasco et al. 2003). Although commonly referred to as "inversion" fog in operational circles, frontal fog occurs with frontal systems and small shortwave systems that bring snowfall to the region. Souders and Renard describe this fog type best with a reference to historic Antarctic forecaster's handbook (Sounder and Renard 1984):

> "…fog occurs in conjunction with falling snow at McMurdo. Both parameters occur for several hours, producing a rapid reduction in visibility to values below airport minimums. Initially, the snow produces saturation of the layer of air below the surface inversion. As the inversion weakens or disappears, the fog dissipates due to vertical mixing (Sallee and Snell 1970)"

e. Other Fog Types

Upslope Fog: The Ross Island region of the Antarctic is in a region of dramatically varying topography. Ross Island hosts four mountain peaks, including 3794-meter high Mt. Erebus, the world's southern most active volcano (Kyle et al. 2003). Across from McMurdo Station are the

Transantarctic Mountains and specifically the Royal Society Range. Yet, despite these features, anecdotally there is no evidence that McMurdo Station itself or the McMurdo airfields are impacted with upslope fog, especially given their locations relative to the topography. Upslope fog, very low and thin stratus cloud formations have little operational impact for the most part (with the exception of helicopter flight operations to the Mt. Erebus huts) and are limited to near the sides of the island and Transantarctic Mountain regions. This fog type is not the focus of this study, due to its limited impact on the majority of operations and limited surface observation.

Mixing Fog: One type of fog that is not discussed in any prior anecdotal reports is mixing fog. The Ross Island is a meeting point for different air mass types – marine polar to the north, continental polar/Antarctic to the south and west. Hence, it is reasonable to test for the possibility of mixing fog. In the last several years, the calving of tabular icebergs (e.g. Lazzara et al. 1999) has offered the opportunity to set up monitoring via the placement of AWS instruments on these icebergs. This provides the opportunity to have multiple observations from the marine environment to the north of Ross Island that has not ever been available before. Hence, a sample case was tested for the possibility of mixing fog using the surface AWS observations to the south and east of Ross Island, and the AWS observations to the north. The method employed a simple technique of grouping the AWS sites together by region, to determine average temperature and relative humidity characteristics of the regions before the onset of the fog event. The number of hours in advance of the event was determined based on the speed of the wind flow that would advect these air masses into the McMurdo area. Then the two air

masses were "mixed" by simple averaging of the temperature and moisture characteristics. The new "mixed" air mass is then checked to see if its characteristics of temperature and relative humidity are such that fog is likely to form. The results for the sample case reveal only marginal results – with only a slight likelihood that the newly mixed air mass would be saturated enough to form fog.

4. Boundary Layer Structure of Fog

Moderate to high-resolution radiosonde observations can reveal the structure of the boundary layer. Radiosonde observations launched from McMurdo Station, with data reports every 10 seconds of flight or more recently upgraded to every 3 seconds of flight, are used to illustrate the structure of temperature, moisture and wind in the lowest 1.0 to 1.5 kilometers (km) of the atmosphere. The wind information is analyzed with a 1-2-1 smoothing. Figure 9 is a sample profile launched close to a fog occurrence at McMurdo Station and is an example of the boundary layer structure found in a majority of the fog events analyzed. The typical profiles may reveal a surface or friction layer close to the ground (not in all cases), a fog layer in the core of the boundary layer, an inversion at the top of the fog layer (which also marks the top of the boundary layer), and the lowest portion of the free atmosphere. Fog is difficult to capture via radiosonde observations that are widely spaced every 12 hours (or more in the case of missing observations). This results in radiosonde observations only providing snap shots of fog structure in the vertical during a particular stage of evolution.

The surface or friction layer is often thin in most cases and not well resolved by the radiosonde observations. Additionally, the McMurdo Weather Office practice is to assign the lowest level of the radiosonde report from the surface measurement made at the McMurdo Weather building and not by the radiosonde itself. Since that measurement is not always matched in time and is usually at a slightly different location, in most of the analysis here, this lowest observation level has been often been removed. This example seen in Figure 9 does not have this removed, hence a surface layer between the lowest two observation points can be envisioned, although for this case, the radiosonde was launched between surface reports of fog and the surface layer may be mixed out given the wind speeds on the order of 10 meters per second (ms^{-1}).

In the example, the fog layer (~100 to 250 meters) is marked with a moist layer of air as compared to air aloft that is drier. This layer is also somewhat cooler than the air aloft. Both dewpoint and temperature have a slight decrease from the bottom to the top of the layer. Winds within this layer, in this sample, reveal an increase of the wind with height through the fog layer to the bottom of the inversion layer, where the wind becomes geostrophic at the level of the free atmosphere (Stull 1988). Wind directions are primarily from the east, which is commonly the case for fog occurrences. In the inversion layer (between ~250 to ~350 meters), temperatures increase from the bottom to the top of the layer, while the layer becomes increasingly drier from the bottom to the top of the layer. This gives the profile a classic "goal post" shape between the temperature and dewpoint (Croft et al. 1997). In this particular example, wind speeds decrease some with increasing height as winds switch toward the southeast. Above the inversion layer is the free atmosphere (above ~350 meters) with different air mass characteristics.

McMurdo Radiosonde 17 January 2004 12 UTC
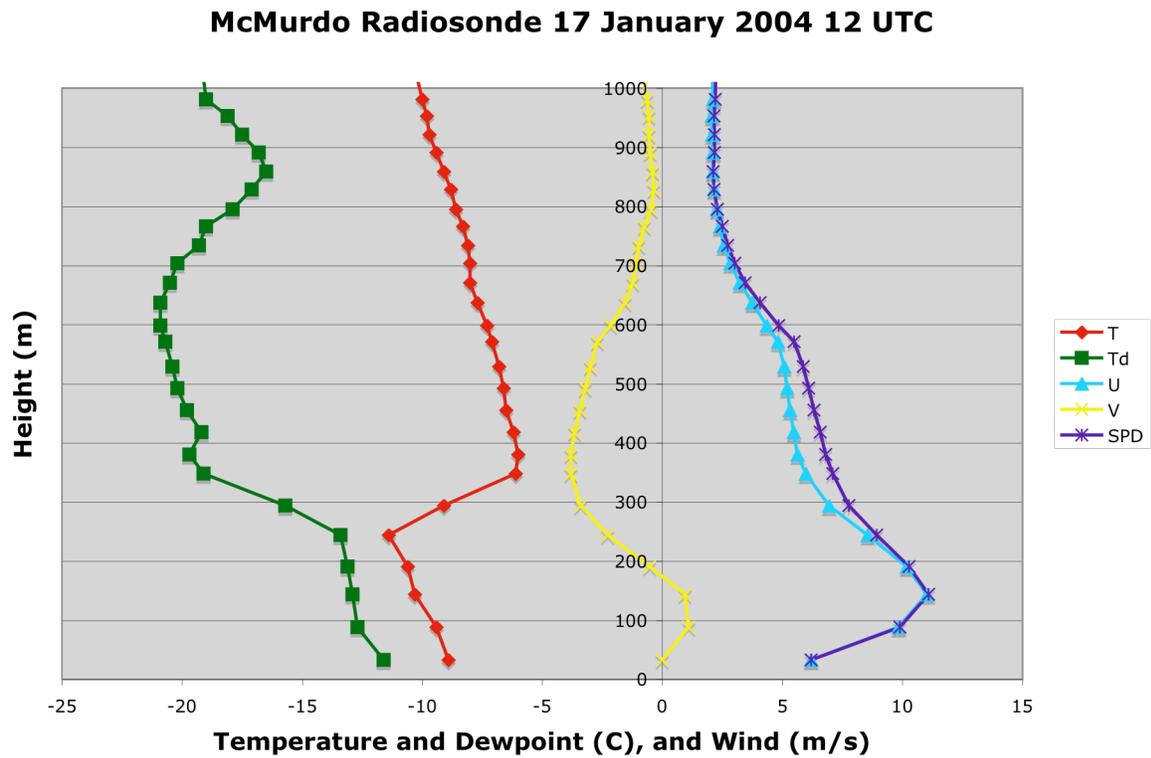
Figure 9. A sample radiosonde from 12 UTC on 17 January 2004 captures the boundary structure temporally close to a fog event at McMurdo Station, Antarctica.

5. Collection of Fog Particles

The physical characteristics of fog are important for remote sensing applications. This section describes an attempt to make in situ measurements of fog particle properties.

a. Method

The physical properties of Antarctic fog particle sizes, shapes and concentrations have not been measured. During the 2002-2003 Antarctic field-season, a simple fog collection effort was attempted. This is the first such information ever obtained in the Antarctic. The method employed to facilitate collection during a fog event in the McMurdo Station area was a set of petri dishes filled with DC-200 fluid or Silicon oil (donated from Chemcentral Corporation of New Berlin, Wisconsin), placed out in the open during an event. Fog particles fall into the petri dish (by wind and/or gravity) and are captured and collected in the fluid. The viscosity of the fluid is fairly close to that of water (1.5 centistokes, water is approximately 1.0 centistokes), which preserves the particle's shape and size. The DC 200 fluid was stored in a -20°C freezer in an attempt to ensure that the fluid does not melt any possible frozen or ice fog particles. The particles were then studied at the Crary Science and Engineering Center (CSEC) at McMurdo Station, where microscopes are available to make measurements and take photographs. An invert microscope was utilized to view the samples collected in the petri dishes.

b. Results

Personnel were deployed during the 2002-2003 field season, during the months of typical maximum fog occurrence (See Chapter 3 for details). Unfortunately, conditions were such that only two fog events took place during deployment (24 Jan 2003 and 3 Feb 2003). Sampling was attempted during both these events along the side and atop Observation Hill, located next to McMurdo Station.

The first event took place on 24 January 2003 at approximately 1 UTC (2 p.m. local time). At Williams Field, approximately 10 km from McMurdo, fog in the area with reduced visibility was reported during this brief event (Table 1). This case is an example of how the prevailing visibility was greater than the definition of fog (1 km or less), which is not uncommon. At the same time, fog was rapidly developing around McMurdo Station itself. Due to the rapid development of the event, it was decided to attempt to collect fog at nearby Observation Hill, rather than miss the opportunity while attempting to travel to Williams Field.

Table 1. A listing of weather observations from Williams Field Antarctica, roughly 10 km from McMurdo Station, showing the short duration of this fog event.

Time UTC	T [C]	Td [C]	Dir [deg	Spd mps]	AltSet [hPa]	Vis [km]	Weather	Clouds [coverage/m×100]
23:55	2	0	080	3	999.0	11.3		5/002
00:55	2	0	090	3	999.0	4.8	F	8/001
01:55	2	0	090	5	999.3	11.3		5/001
02:20	2	-1	090	5	999.0	11.3		5/002

During the first fog event on 24 January 2003, the first sample was taken at a location approximately two-thirds of the way up Observation Hill at 1:30 UTC for 5 minutes. A second and third sample were taken at 1:45 UTC for 5 minutes and 2:07 UTC for 20 minutes, respectively.   After this, the fog event quickly ended. The second event took place on 3 February 2003, however this event came with strong enough winds that prevented this collection system from working - the petri dish nearly lifted away with the wind in the one attempt made during the event.

An initial review of 24 January 2003 weather observations from the AWS network around the McMurdo Station and Ross Island region (Figure 10) confirms the weather conditions during these two events with high relative humidity reports and fog in the observations from the nearby airfield (Table 1). This fog event impacted aviation operations during the hour it occurred, by delaying the landing of a C-141 aircraft at Pegasus Field.
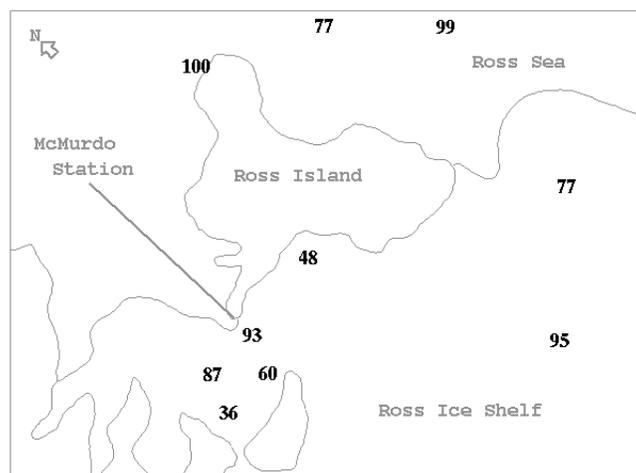
Figure 10. A plot of relative humidity from the AWS network shows high relative humidity (percent) measurements in the Ross Island region during the fog event of 24 January 2003 at 1 UTC.

Of the three samples taken during the first fog event, an examination under the microscope revealed that only the first of the three samples held fog particles, and in this case they were indeed liquid droplets. Only three droplets in total were found in this sample. Figure 11 shows the two droplets found in this sample as seen under the microscope at 60X power. Measurements and calibration of the microscope using a micrometer estimate that each division (minor) in these images is approximately 2.5 to 3.8 microns (μm). Thus, these diameters are droplets approximately 7.5 to as much as 10 μm in size. This is not an unexpected droplet size for fog (Brown and Kunkel 1985, Pruppacher and Klett 1997). It also nearly matches aircraft observations of stratus clouds in the Ross Island area that revealed mean droplet diameters in the range of 9.24 to 13.5 μm (Saxena and Ruggiero 1985).
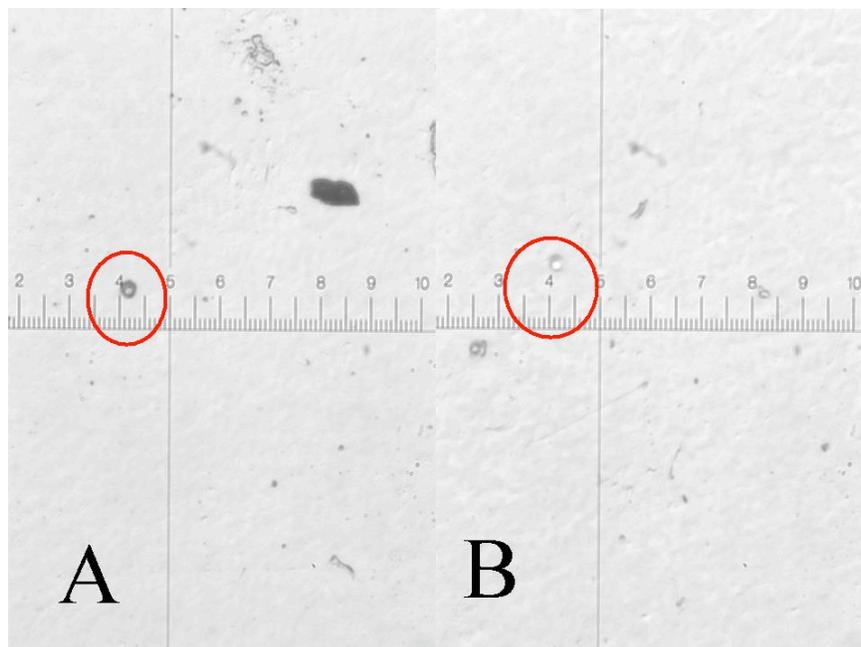
Figure 11. This figure shows two of the fog particles found in a sample taken during the first fog event on 24 January 2003. The fog droplets are circled in red, and the scale in each figure has one subdivision equal to approximately 2.5 to 3.8 μm.

Although the second fog event on 3 February 2003 did not produce any samples due to the strong wind, the situation did offer some key information. This fog event came with both high winds and a light rime ice on any feature above the ground, including buildings, rocks, and antenna towers. This rime ice confirms that this fog is indeed in liquid form rather than frozen (temperatures were in the range of -4°C). This helps to reinforce that in the austral summer, liquid fogs are perhaps more likely than ice fogs which are reported to be found in the Ross Island area during the austral winter (ATS 1999, Cayette 1998 and 1999, SPAWAR 2007a).

c. Discussion

The fog that was collected in this fieldwork was in the maturing phase of the fog evolution, at sizes not unusual for fog droplets, as studied in the middle latitudes (i.e. Brown and Kunkel 1985, Pruppacher and Klett 1997) and at the low end of the range for fog droplet sizes in the Arctic (Nilsson and Bigg 1996). As noted in the introduction, a fogbow (Figure 1) was documented by Scott's team, which would indicate that larger droplet sizes could be possible and larger than this fieldwork measured, as fogbows have known to have droplet sizes on the order of 50 μm or larger (Nilsson and Bigg 1996). This may reflect the nature of fog away from the coastal region, as noted Figure 1 was drawn on the "Great Barrier" – up on the Ross Ice Shelf away from McMurdo Station. Analysis of METAR surface observations over the last decade from the airfields in the McMurdo area reveal that fogbows have not been reported during fog occurrences, nor have any fogbows come to the attention of on-station weather staff (Clogston

personal communications, 2007). Influences by the marine environment as well as anthropogenic impacts in the Ross Island area may indeed affect fog physical characteristics as prior electron microscope studies have shown in the Arctic (Ohtake 1977). Studies of stratus clouds from aircraft in the Ross Island region reveal the cloud condensation nuclei are marine in source including sodium and chloride from sea salt, and biogenic potassium and calcium from phytoplankton (Saxena and Curtin 1983). The remaining nuclei found were silicates whose source is likely from the few areas of exposed volcanic rock in the region, which in turn is suspected to be the ice nuclei for austral wintertime ice fog, under the right conditions (Ohtake 1977, Saxena and Curtin 1983, Pruppacher and Klett 1997). Additionally, the human activity in the region, with McMurdo Station as a major hub of the USAP, most assuredly adds anthropogenic pollutants into the atmosphere that may additionally keep fog droplet sizes small.

The fog collection conducted here is a simple method, and limited to being done at the ground. Depending on the in situ site of the collection and the stage of fog development, methods such as this might possibly only collect the larger particles that would more likely be found at the lower portions of a fog layer, taking into consideration settling of fog droplets due to gravity. Any mixing that might occur in the fog will also skew these results (in the vicinity of Observatory Hill, mechanical turbulence is very possible). Hence, this sample is likely not completely representative of the entire fog layer. Modern ground based fog particle collectors (Collett et al. 1998; Collett personal communications, 2007) and airborne cloud particle collectors (Heymsfield personal communications, 2004; and Lachlan-Cope personal communications, 2007) have been developed in recent years that would provide more complete sampling of fog, including the sizes and distribution. More direct observations of fog physical

properties are clearly needed to gain additional documentation and understanding of fog's microphysical characteristics.

Chapter 3: Observational Analysis of Fog

An important step to understanding fog in Antarctica is a climatological description of its occurrence, which does not currently exist. This chapter describes the fog and its climatology around McMurdo Station. The chapter explores the relationships between fog and other meteorological variables.

The following section characterizes the fog climatology for McMurdo Station, Antarctica from 1 January 1973 0 UTC through 31 December 2004 18 UTC (with some analysis extended to include observations through 31 July 2007 18 UTC). Included in this analysis (1973 through 2004) are 41,096 observations of which 721 (1.8 percent of the total) are observations of fog. First, fog climatology and characteristics are outlined. Next, standard meteorological parameters during fog occurrences are contrasted to non-fog occurrences and/or compared to all observations. Finally, comparisons of fog occurrence to sea ice concentration, El Niño and Antarctic Oscillation are investigated.

1. Fog Climatology and Characteristics

In reviewing the fog occurrences at McMurdo Station, a classification of fog days was done to quantify the fog occurrences for this analysis. A fog day is defined as when at least one hour of the day has a report of fog (including current weather or past weather). Figures 12, 13, and 14 show the fog days as a histogram (quantified by months) over the years as well as organized by

month. Unlike the analysis with meteorological variables in the following sections, the data used for this analysis did employ all observations including all 3-hourly observations, when available. The analysis was primarily conducted using McMurdo Station observations due to the more complete nature of the data set: The nearby airfields have a limited observational data set due to operational constraints that do not have these airfields open all of time, but only during a portion of the austral summer, operational field season.

a. Fog Seasons

Over the time period studied, McMurdo has had periods of significant fog – as much as 17 days in a single month (Figure 12). The 1990s have much fewer fog events per month. Additionally, there are some periods of poor data quantity, especially the mid-1970s during the austral winter. However, the data are otherwise reasonably complete and does not distract from the verification in the variability of fog anecdotally reported on fog (Cayette 1999, ATS 1999, SPAWAR 2007a). Figure 13 shows the same information for the same period of time, but in this case shown by months of the year. The figure reveals two clear seasons for fog: the late winter peaking in September, and another season in middle of summer, peaking in January. Minimums are found in early winter in May-June as well as in spring in November. The only break in the progression occurs in February, with an unexpected decrease in fog events as compared to January and March. One likely reason may be due to February having the highest snowfall at McMurdo Station (Figure 15) as reported as a part of NCDC's International Station Meteorological Climate Summary (ISMCS) climatology dataset. Figure 13 clarifies the current

thinking on fog seasons, as McMurdo forecasting manuals report the peak in fog in March (SPAWAR 2007a), when this analysis reveals January to be the peak month for fog.
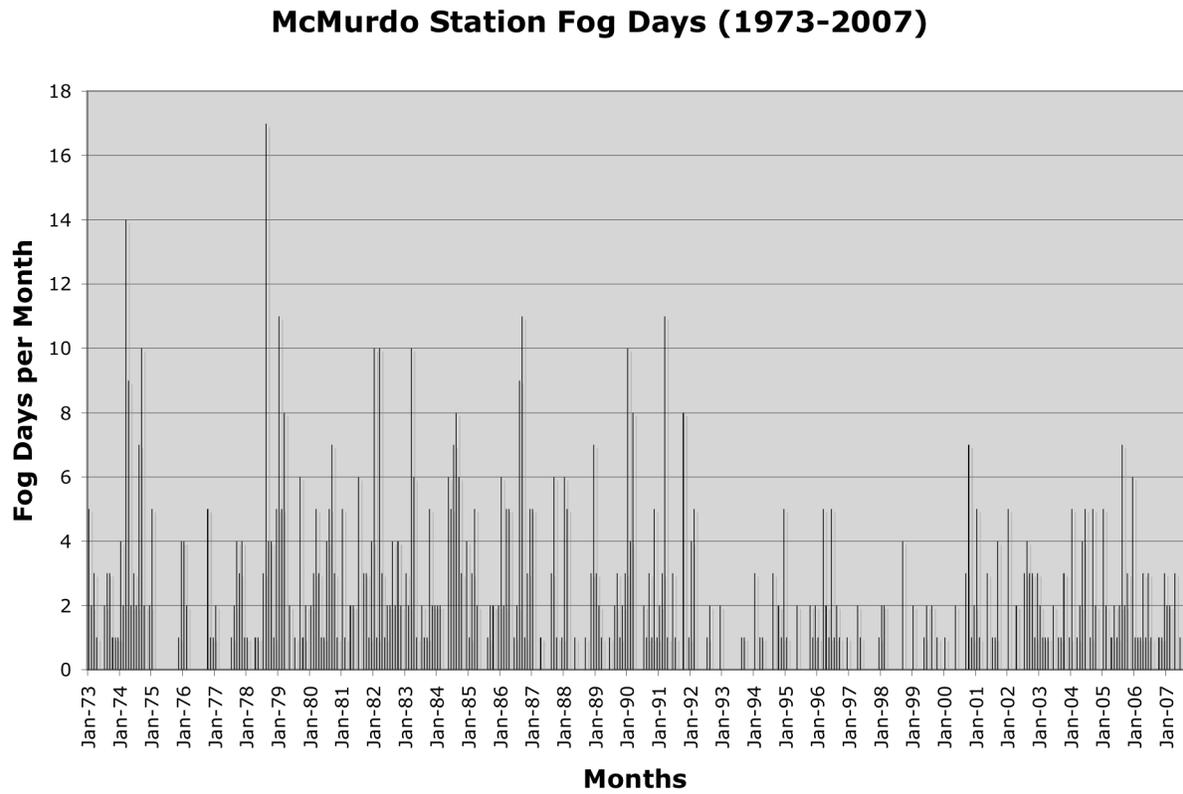
Figure 12. A histogram showing the number of fog days per month from January 1973 through July 2007 at McMurdo Station.

Fog Days By Month
Including all observations from 1973-2007
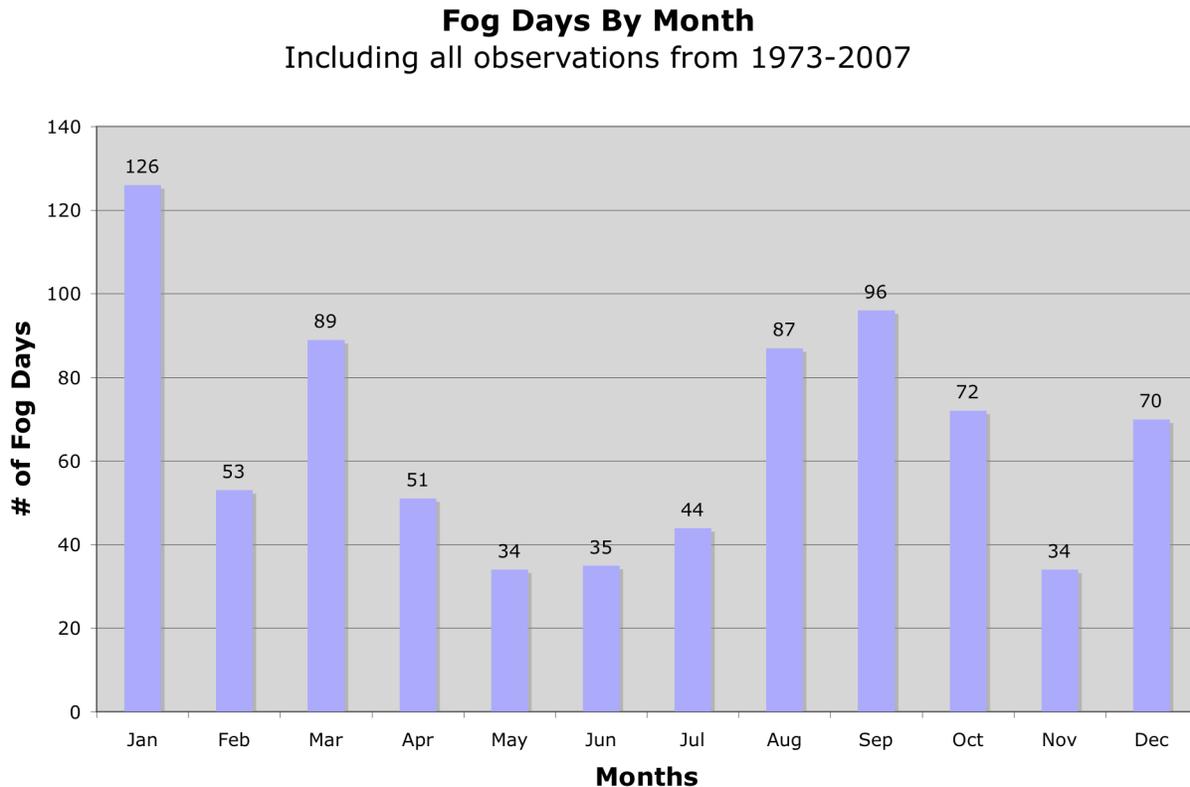
Figure 13. A summary of all fog observations (includes 3- and 6-hourly observations) by month from January 1973 through July 2007.

To verify the robustness of the seasonality of fog, the information in Figure 13 was broken down into three approximate decades; 1973-1983, 1984-1994, and 1995-2007. Figure 14 shows these results. The first two decades clearly reflect the same pattern seen in the full data record as shown in Figure 13. The most recent decade, while having approximately the same pattern, does have a few differences in the March through June timeframe, where there is an inverse behavior of increasing fog during this period rather than decreasing.
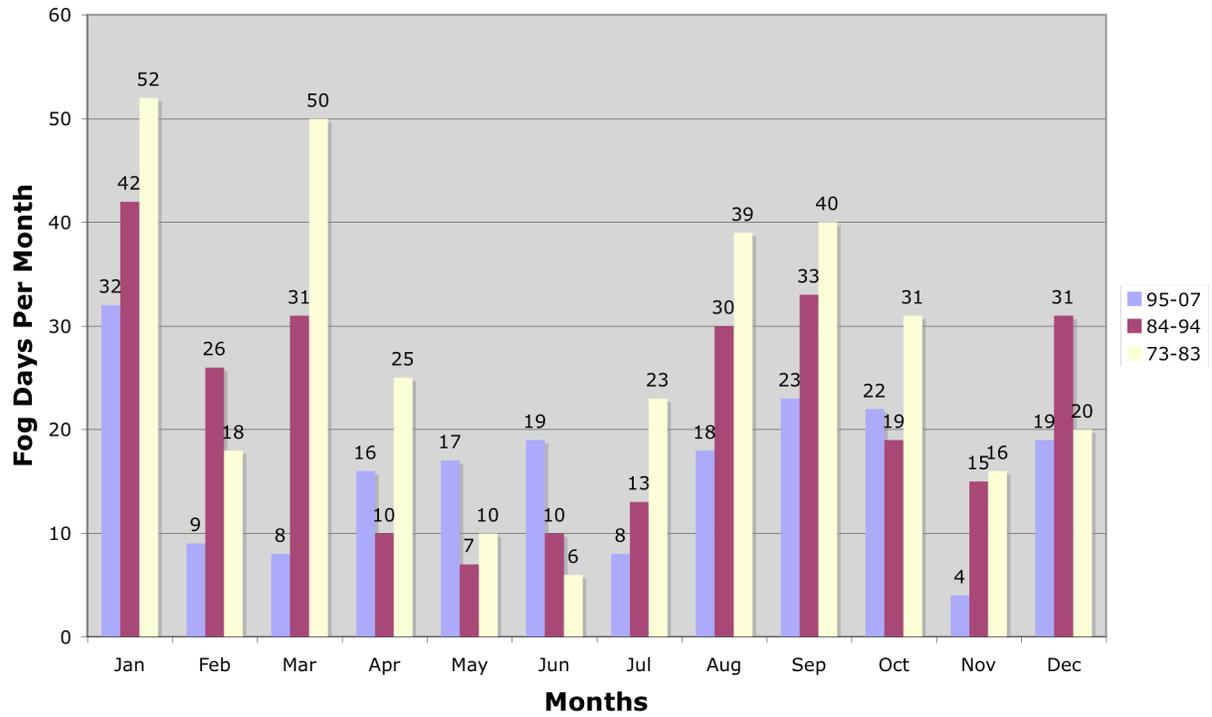
Figure 14. The same fog days by month as shown in Figure 13 but here the information is broken down by decade.

McMurdo Station Mean Snowfall (1956–1987)
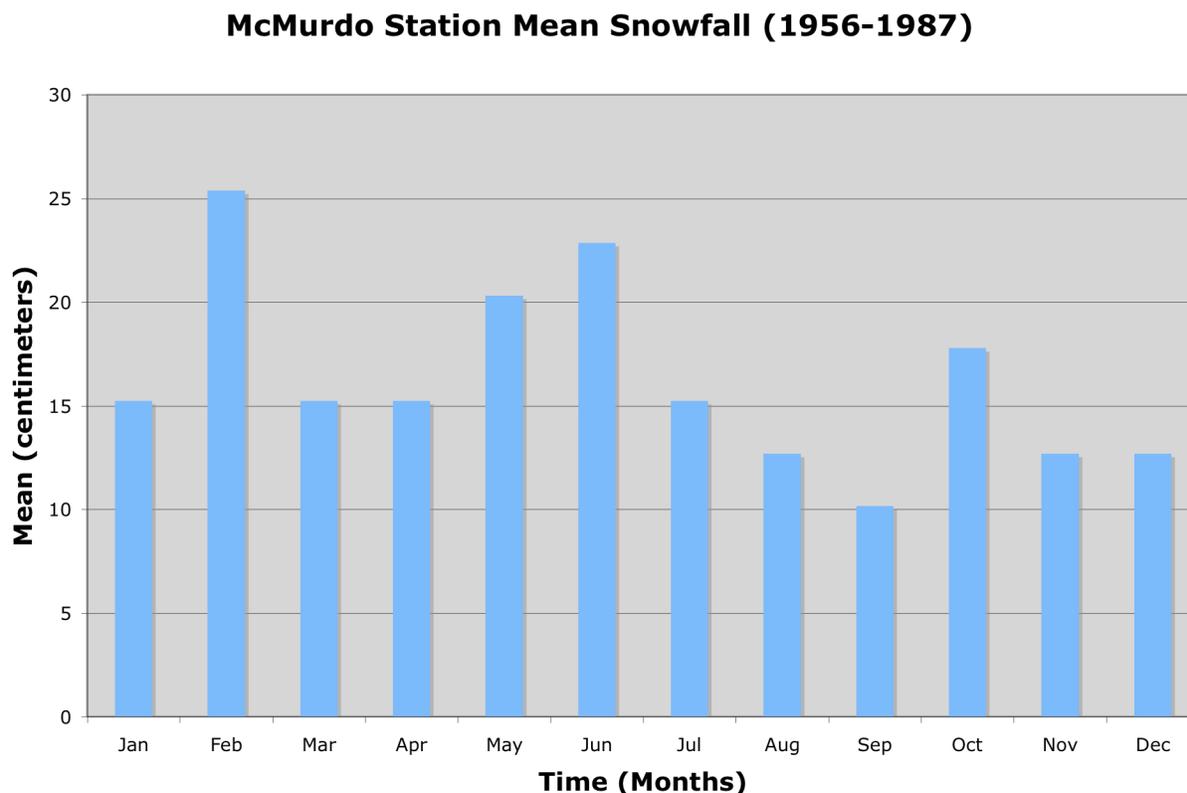
Figure 15. The mean monthly snowfall at McMurdo Station Antarctic from the NCDC International Station Meteorological Climate Summary.

b. WMO Fog Types

The different present weather fog types as reported by McMurdo Station are shown in Figure 16 (and in this case using only the 6-hourly observations). Table 2 offers a review of the WMO definitions of the different types and codes used for fog as shown in Figure 16 (NOAA 1988, SPAWAR 2007b). Other than light fog (type number 10), the majority of the observations during the time period studied are fog in the distance at the time of the observation but not at the

station during the past hour (type number 40). This turns out to be consistent when considering

fog occurrences at the airfields in the Ross Island area, as reviewed in the next section of this

chapter.

Table 2. The listing of WMO International Codes on present weather for fog types with description of each code (NOAA 1988, SPAWAR 2007b).

WMO Fog Type Code	Description
4	Fog (Code for Past Weather only)
10	Light fog
11	Patches of shallow fog at station not deeper than 6 feet on land
12	More or less continuous shallow fog at station, not deeper than 6 feet on land
28	Fog during past hour, but not a time of observation
40	Fog at distance at time of observation, but not at station during past hour.
41	Fog in patches
42	Fog, sky discernable, has become thinner during past hour
43	Fog, sky not discernable, has become thinner during past hour
44	Fog, sky discernable, no appreciable change during past hour
45	Fog, sky not discernable, no appreciable change during past hour
46	Fog, sky discernable, has begun or become thicker during past hour
47	Fog, sky not discernable, has begun or become thicker during past hour
48	Fog, depositing rime, sky discernable
49	Fog, depositing rime, sky not discernable

McMurdo Station Fog Reports by WMO Type (1973-2004)
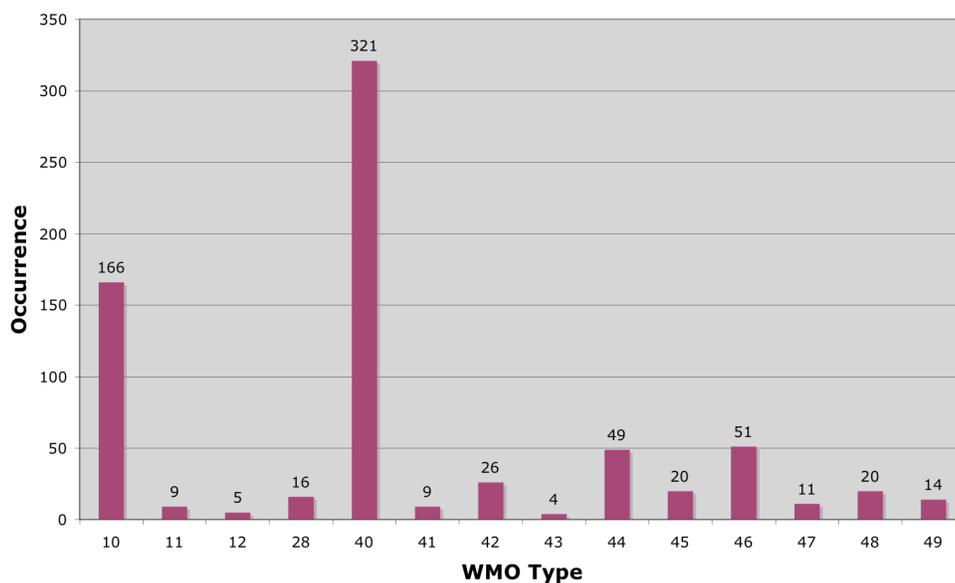
a.

WMO Fog Types by Decade
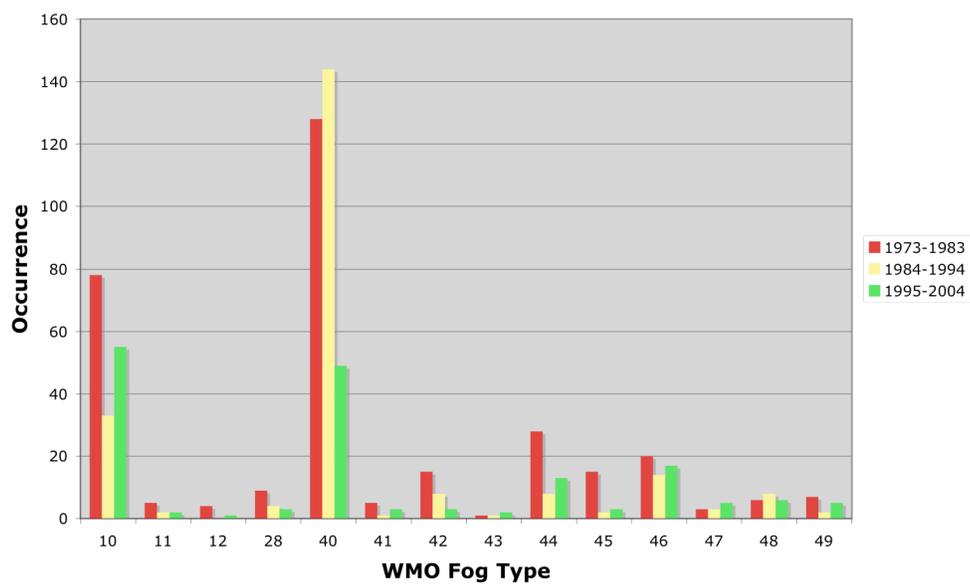
b.

Figure 16. a.The number of reports of fog used in this analysis is shown here broken down by WMO classification. b. Same as part a, displayed by decade.

c. Fog at McMurdo Station vs. McMurdo Area Airfields

A comparison of fog at McMurdo Station has been made with observations from nearby airfields, such as Williams Field, Pegasus Field and the Ice Runway during the operational field season. Over this period, the USAP operates no more then two airfields at a time (Scheuermann personal communication, 2003). In making this comparison of three airfields with McMurdo Station, no duplicate data was used in the analysis when more than one airfield was actively observing and reporting fog. Observations taken during the season when one or more of the airfields are open show that McMurdo Station has a comparatively smaller number of fog occurrences (Figure 17). McMurdo Station has nearly 4 times fewer fog events than the airfields experience. Hence, the general climatology of fog as depicted at McMurdo is a subset of events that occur in the Ross Island and McMurdo Sound region of Antarctica. Unfortunately, observations from the airfields are spotty in nature due to the logistic operational schedule of the USAP. Hence, with observations only available during the operational field season, and only when the airfields are open during that time frame, not enough consistent observations are available to use these stations as the basis for a balanced climatological study. A brief review of reports from Williams Field from 1998 through the first part of 2007 (Figure 18) shows fog occurrence at this airfield reflects the same peak in fog in January, and less in February and December over the decade.
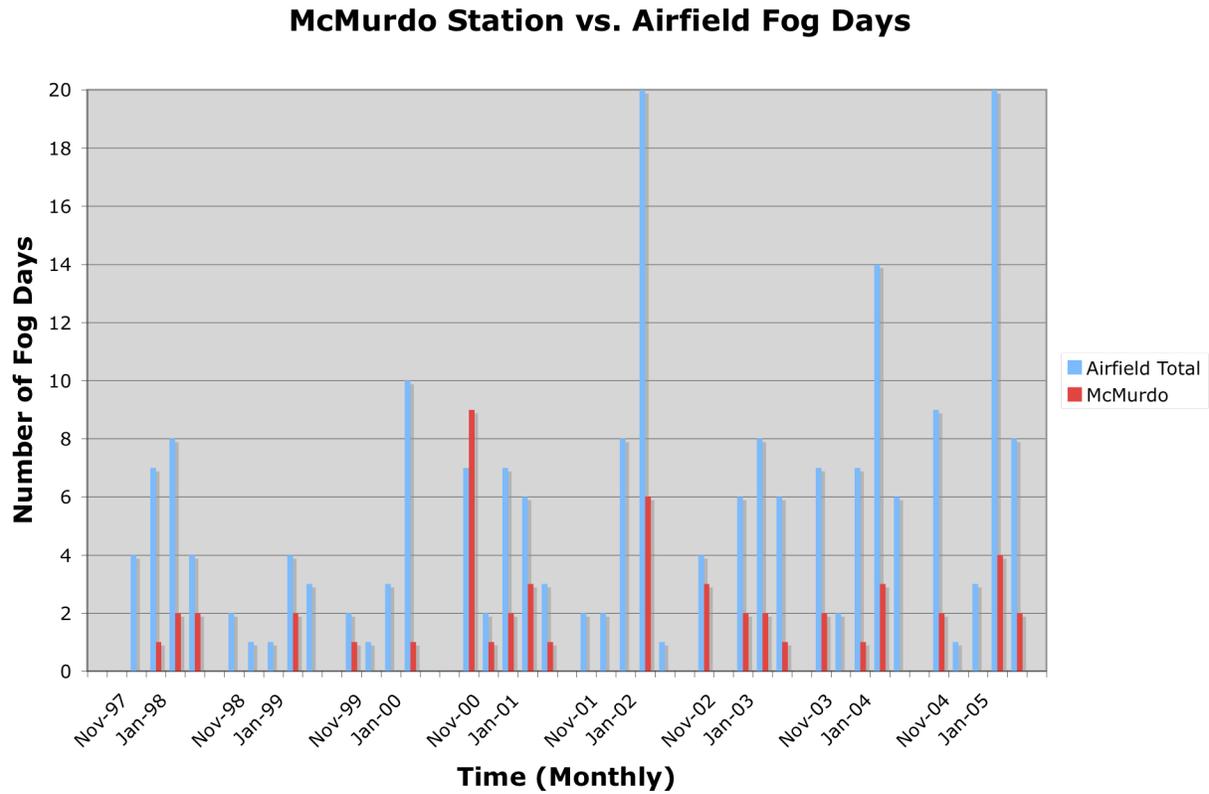
Figure 17. McMurdo Station experiences only approximately 25 percent of the fog events in the McMurdo Sound Basin, when comparing with fog occurrences at the three nearby airfields

Fog Days by Month 1998-2007
Williams Field, Antarctica
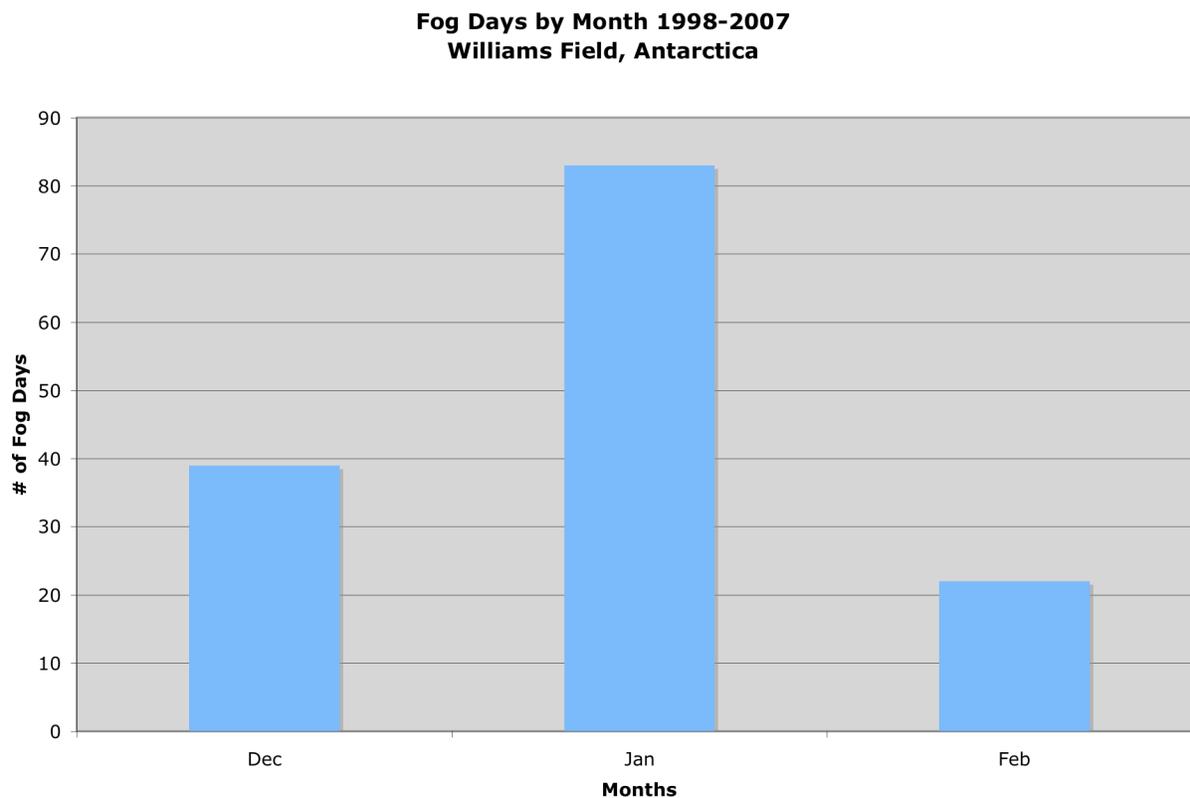
Figure 18. Number of fog days as reported at Williams Field, Antarctica from 1998 through 2007.

d. Fog Trends

As discussed briefly in the first portion of this section, fog at McMurdo Station appears to have some trends over the years. Figure 19 is a plot of the yearly averages with a trend line added for the period 1973 through 2007. Fog seems to be decreasing since the early 1970s at McMurdo Station; however, there is some indication of an increase since the low point of the 1990s. For the early period, 1973 to 1989, the average number of fog days is on the order of 2.5 days with a

standard deviation of 2.8. Meanwhile for the later period, 1990 to 2007, the average number of

fog days is on the order of 1.4 days with a standard deviation of 1.9. Hence there is a noteworthy

decrease in fog over the study period. The end of this chapter reviews tests for other relationships

between fog and other environmental influences such as sea ice and El Nino. A brief

investigation of trends of standard meteorological variables such as temperature and pressure

(not shown) does not indicate any connection.

Yearly Average Fog Days Per Month 1973-2007
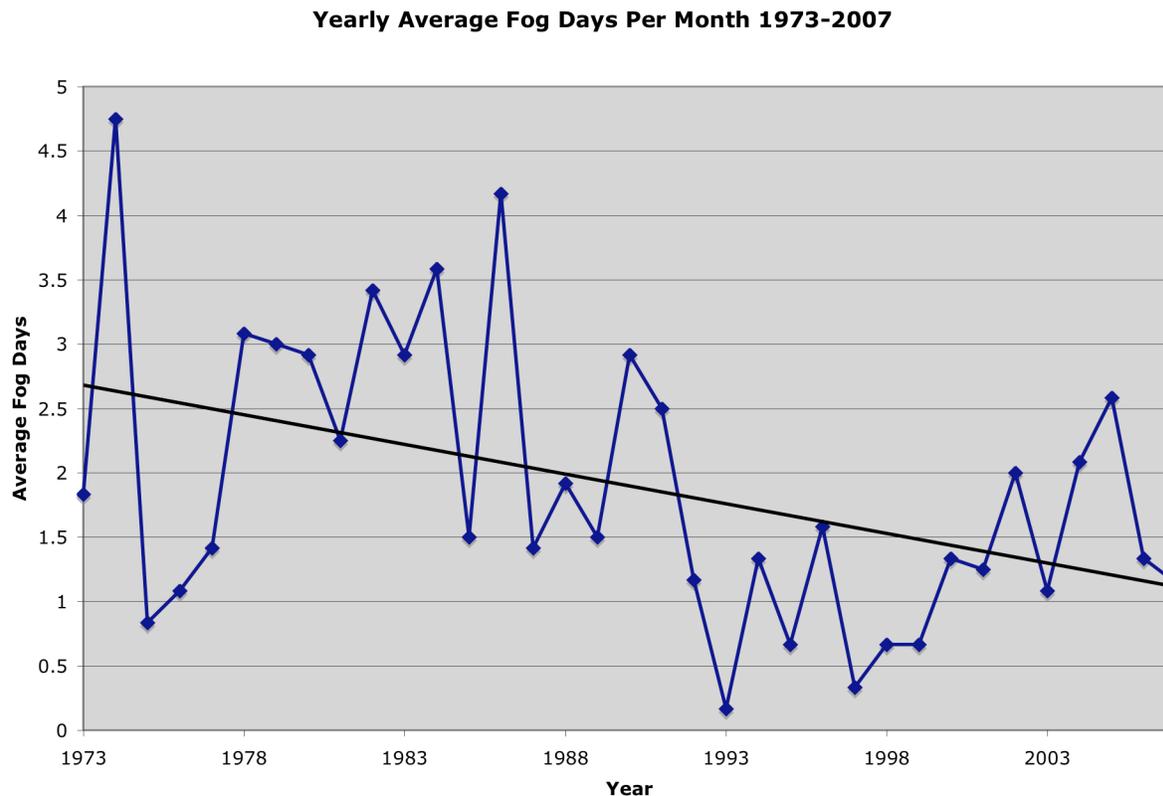
Figure 19. The yearly average fog days per month, and its trend for McMurdo Station from January 1973 through July 2007 showing there is an overall decrease in fog during this period, from nearly averaging 2.5 days of fog per month to just over 1 day of fog per month.

e. Fog Duration and Time of Day

Time of Day: As noted above, McMurdo Station does not have a classic diurnal cycle during the austral summer. However, it does have some subtle variability which may explain the approximately 50% greater occurrence of fog during the local morning hours (18 to 0 UTC ~ 6 am to 12 noon local) than the local evening hours (6 to 12 UTC ~ 6 pm to 12 midnight local) (See Figure 20a). Even though the sun is up all of the time, the elevation of the sun does change throughout the local day. This clarifies the current anecdotal documentation on fog, which states that peak for formation is between 12 and 20 UTC (SPAWAR 2007a). Figure 20b presents the same information broken down by decade. It reflects the apparent downward trend in fog, as well as a shift in the time of day the minimum fog occurs from 6 to 12 UTC.

a.
b.
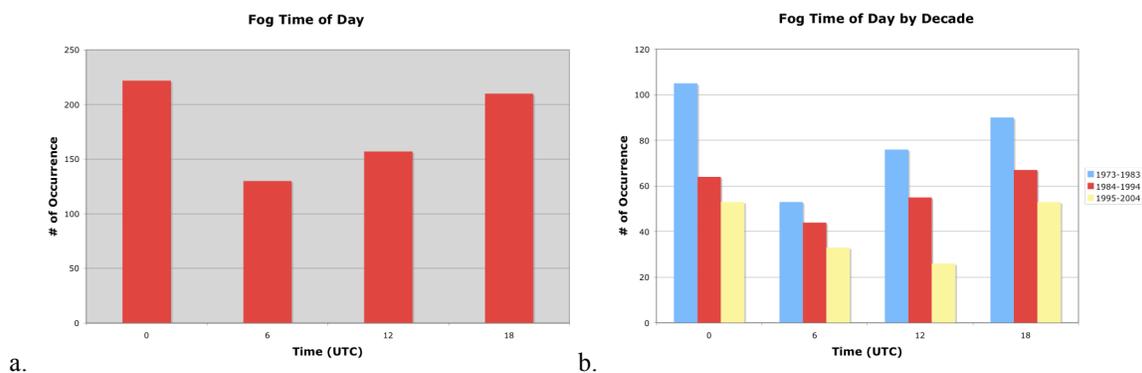
Figure 20. a. McMurdo Station experiences fog at any time of day, but increasingly sees more fog during the local morning hours (0 UTC ~ 12 noon local time) b. Same information as in part a, displayed by decades, which reveals the downward trend in fog and shift of minimum fog from 6 to 12 UTC.

Duration: Determining the climatology of fog duration poses a challenge when reviewing synoptic observations. From the 6-hourly set only, and considering the use of both current weather and past weather observational fields, the duration of fog can only be estimated in blocks of 6-hour intervals (Figure 21). In this analysis, fogs at McMurdo Station are increasingly more likely to be 6 hours or less in duration. Despite this, the analysis shows two events with an approximate 30-hour duration during the analysis period, providing an approximate upper limit on continuous fog events. More detailed recordings of fog duration, in hours, from McMurdo Station are now available since 1999 (Cayette 1999, SPAWAR 2007b). Figure 22 plots these reports and shows similar characteristics to Figure 21; however, it provides much more detail on the duration of fogs at the station. A majority of these fogs lasted about 3 hours in length or less, with the possibility of some fogs lasting up to as much as 30 hours or more, which corresponds with the synoptic observation data.

Estimated Duration of Fog Occurrences: 1973-2004
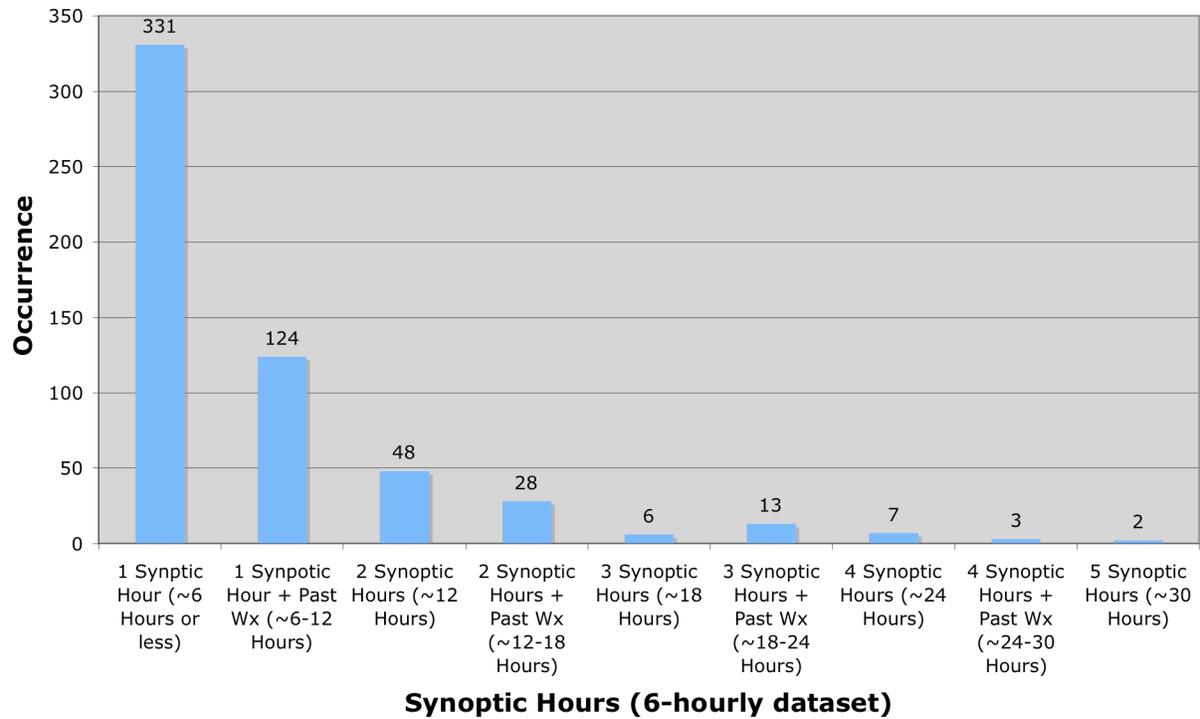
Figure 21. An estimate of the duration of fog events from 6 hourly synoptic observations. Note that both current and past weather fields were used.

Duration of Fog Occurrence: 2000-2007
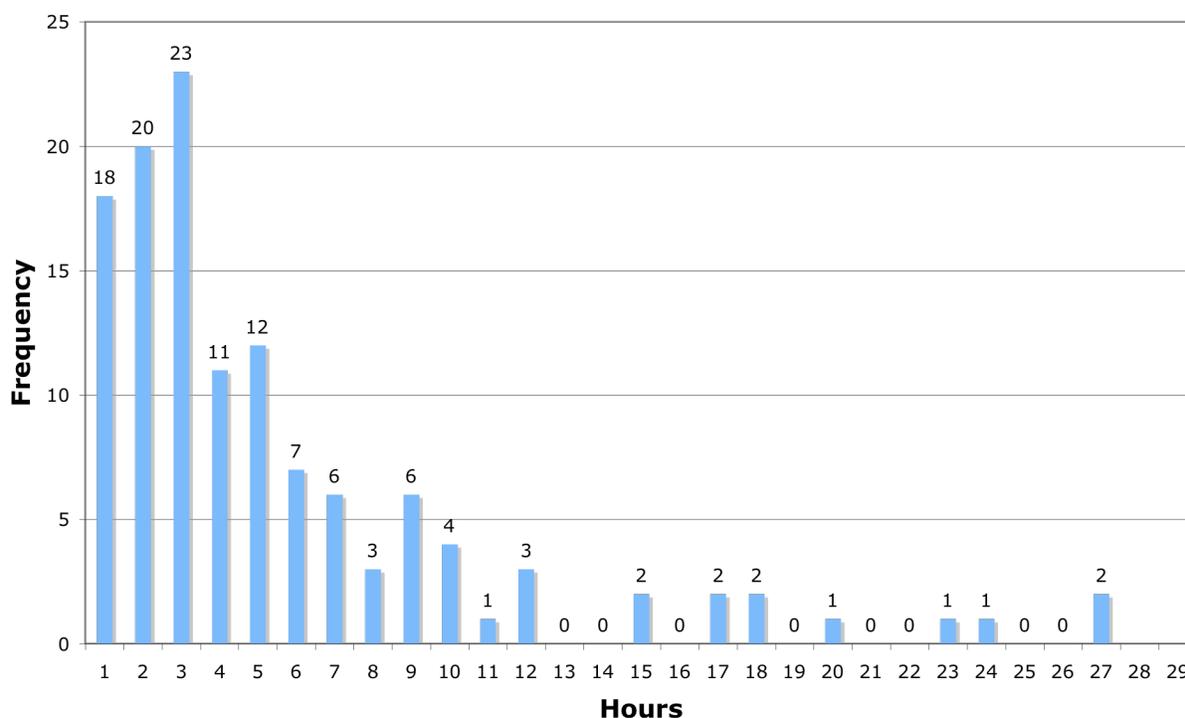
Figure 22. A more detailed histogram of fog duration made from Mac Weather observation logs from January 2000 to July 2007.

2. Fog and Meteorological Parameters

a. Fog and Temperature

McMurdo Station, Antarctica has an average temperature of -16.7°C over the period studied (1973-2004), over all months, with a mode of -20°C and a median of -17.2°C. Figure 23 shows the variation of monthly mean temperature as well as the range of minima and maxima on a monthly basis over the time period. McMurdo's highest maximum temperature during this

studied time period is 10.6°C occurring on 21 December 1987 at 6 UTC. The lowest minimum temperature during this same timeframe is -47.8°C taking place on 4 August 1975 at 0 UTC. The data revealed a standard deviation of 9.98°C for the year. As a note, McMurdo Station's temperatures do reflect the kernlose or coreless winter, where the temperatures curve is "flat" during the winter months (Wendler and Kodama 1993, Stearns et al. 1993).

McMurdo Station Monthly Means and Extremes of Temperature (1973-2004)
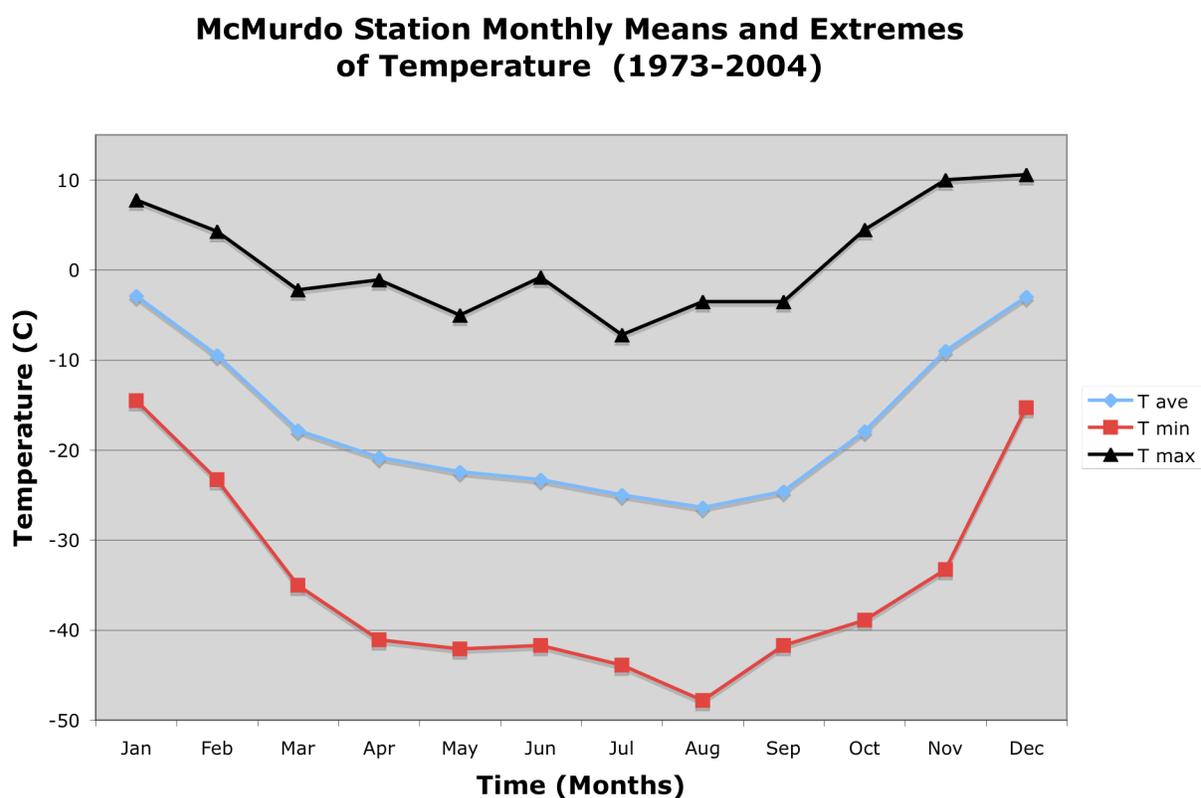
Figure 23. The monthly temperature means and extremes for McMurdo Station, Antarctica over the years 1973 though 2004.

The average temperature at which fog occurs is -19.1°C, over all months with a mode of -25.6°C and median of -20.9°C. The minimum temperature at which fog has been recorded during the studied time frame is -47.2°C on 4 August 1978 at 12 UTC and the maximum temperature at which fog has been reported during this same period is 4.4°C on 26 December 1984 at 6 UTC. The standard deviation over the annual cycle of temperatures during fog occurrences is 11.4°C.

A seasonal analysis of temperature and fog occurrence grouped the four core summer months of November, December, January and February (NDJF) together as well as the five core winter months of May, June, July, August, and September (MJJAS). Results during the NDJF period reflect the annual results with a cooler average temperature of -6.5°C during fog occurrence verses -5.9°C for all observations. Maximum temperatures between all observations and fog-only observations showed the same results noted in the annual observations with 10.6°C for all NDJF observations vs. 4.4°C for fog-only observations during NDJF. All other measures (standard deviation, variance, median, etc.) nearly matched between fog-only observations and all observations, with the minor exception of the mode with -5°C for all observations as compared to -3.3°C for fog-only observations during this austral summer season.

A comparison of all observations, all non-fog observations, and all fog observations indicates that temperatures during fog occurrences are on average colder than the mean (Figure 24). This corresponds with the expectation that in foggy conditions the air is saturated and is much closer to the dewpoint temperature. The temperature trend tracks very closely with the average of all observations. In comparing fog occurrence minimum and maximum temperatures with all observations of extremes (Figure 25) the minimum temperatures during fog occurrences

are comparable to minimum temperatures over all observations, while there is a difference in maximum temperatures between fog occurrences and all observations.

Figures 26 and 27 shows the distribution of temperatures in non-fog and fog situations. While McMurdo's temperature distribution is skewed toward colder austral wintertime temperatures in the case of non-fog observations, there is a more bi-modal distribution found with fog-only observations. The two modes found in Figure 27 reflect the two seasons for fog – one in late austral winter, and one in mid-austral summer. Figure 28 depicts this situation with the seasons separated, with winter as April through September, and summer as October through March. This figure supports the anecdotal evidence of ice fogs in the winter period, while Chapter 2 notes that summer fogs at this time can be liquid.

McMurdo Station Monthly Average Temperature 1973-2004
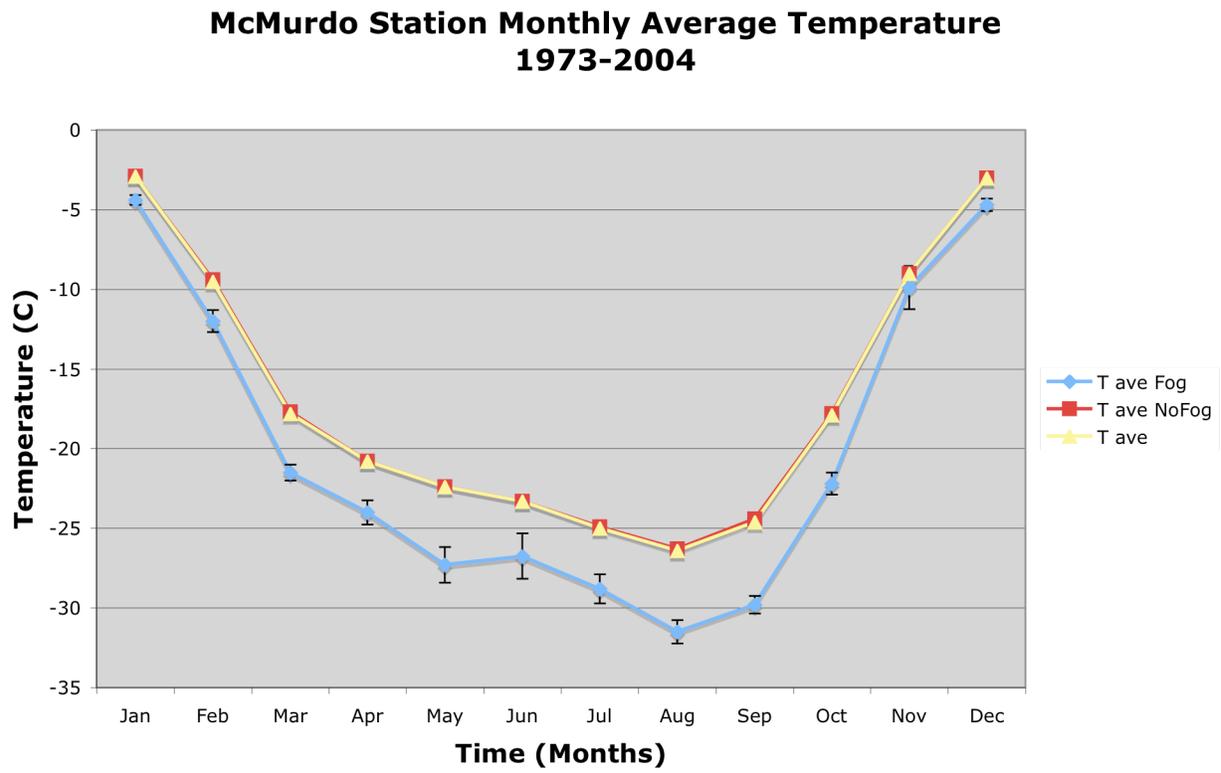
Figure 24. The monthly temperature means for McMurdo Station, Antarctica from 1973 through 2004 separated into temperature means over all observations, over non-fog observations and fog-only observations. Standard error is plotted as error bars.

McMurdo Station Temperature Extremes During Fog Occurrence vs. All Observations (1973-2004)
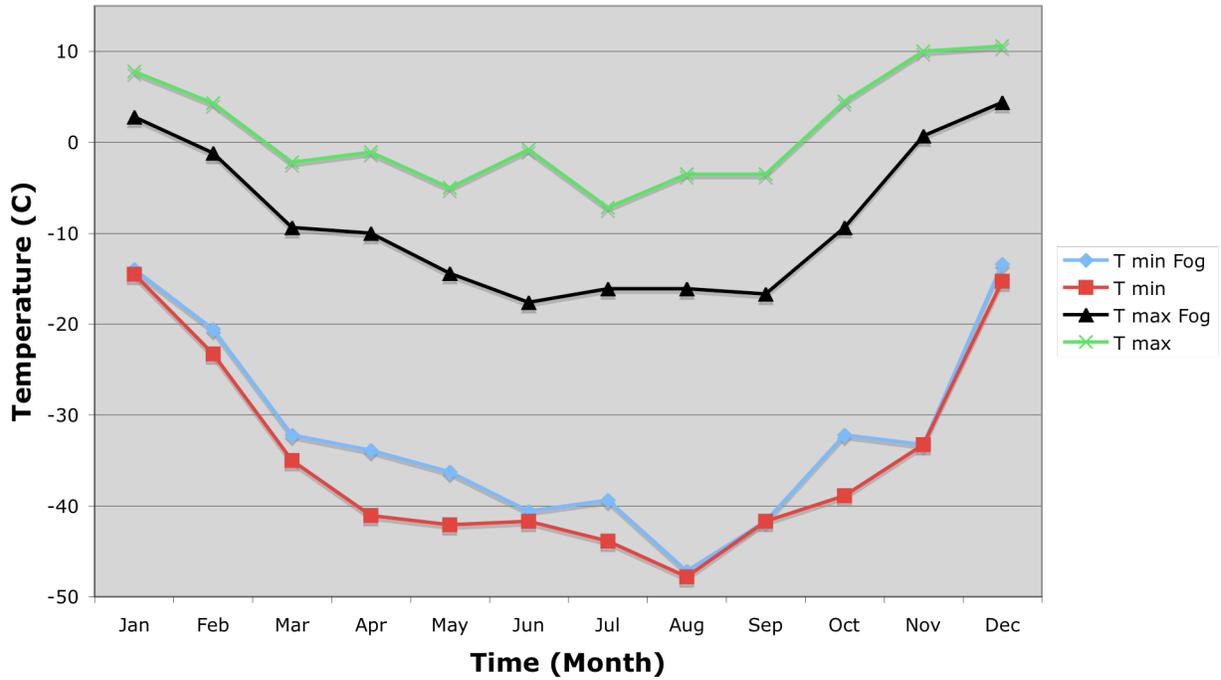
Figure 25. The monthly temperature extremes for McMurdo Station, from 1973 through 2004 for minima and maxima over all observations and fog-only observations.

Temperature Distribution - No Fog 1973-2004
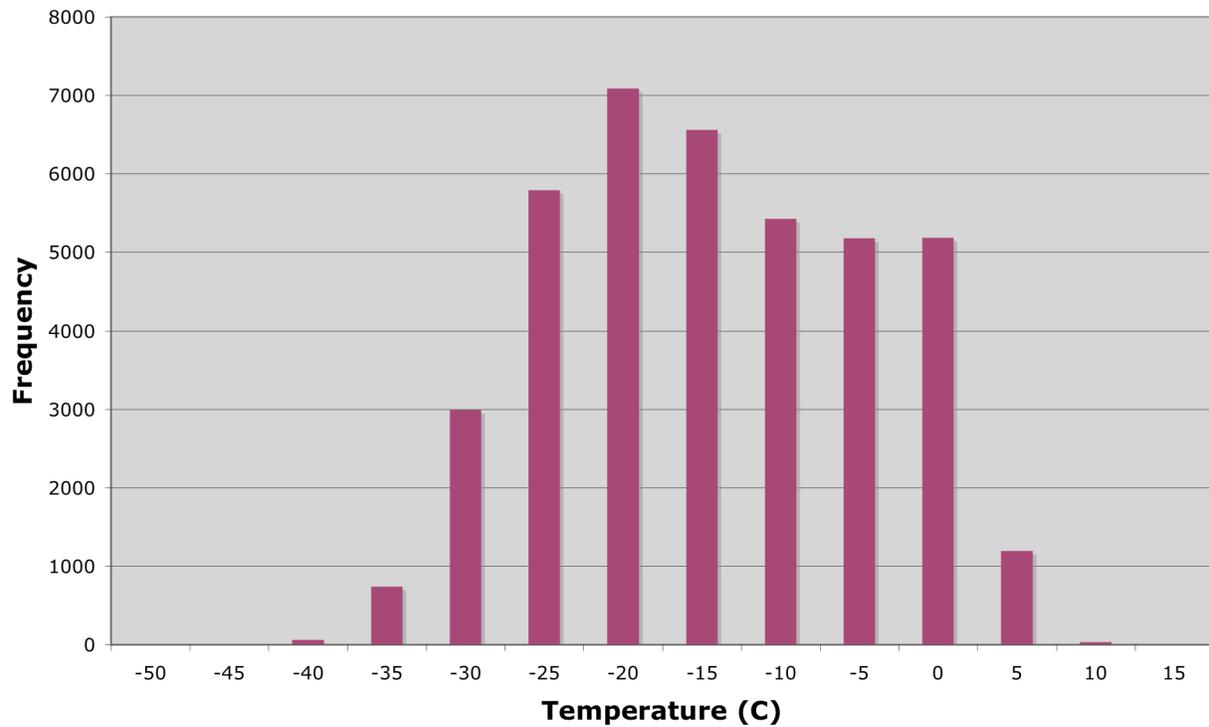
Figure 26. Temperature distribution at McMurdo Station, Antarctica excluding fog occurrences shows a skewed distribution toward colder temperatures.

Temperature Distribution - Fog only 1973-2004
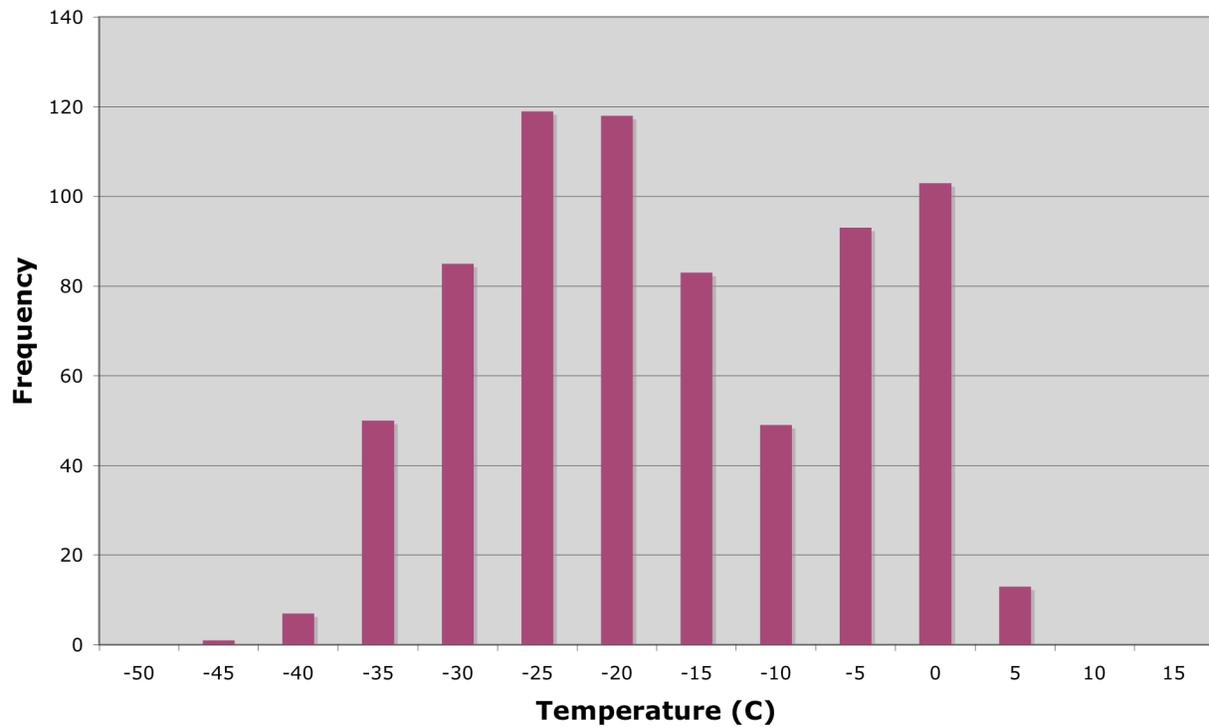
Figure 27. The temperature distribution at McMurdo Station during fog occurrence showing a bimodal distribution, reflecting the two peak seasons of fog, late austral winter and mid-austral summer.

Distribution of Temperatures During Fog (1973-2004)

■ Freq Summer ■ Freq Winter
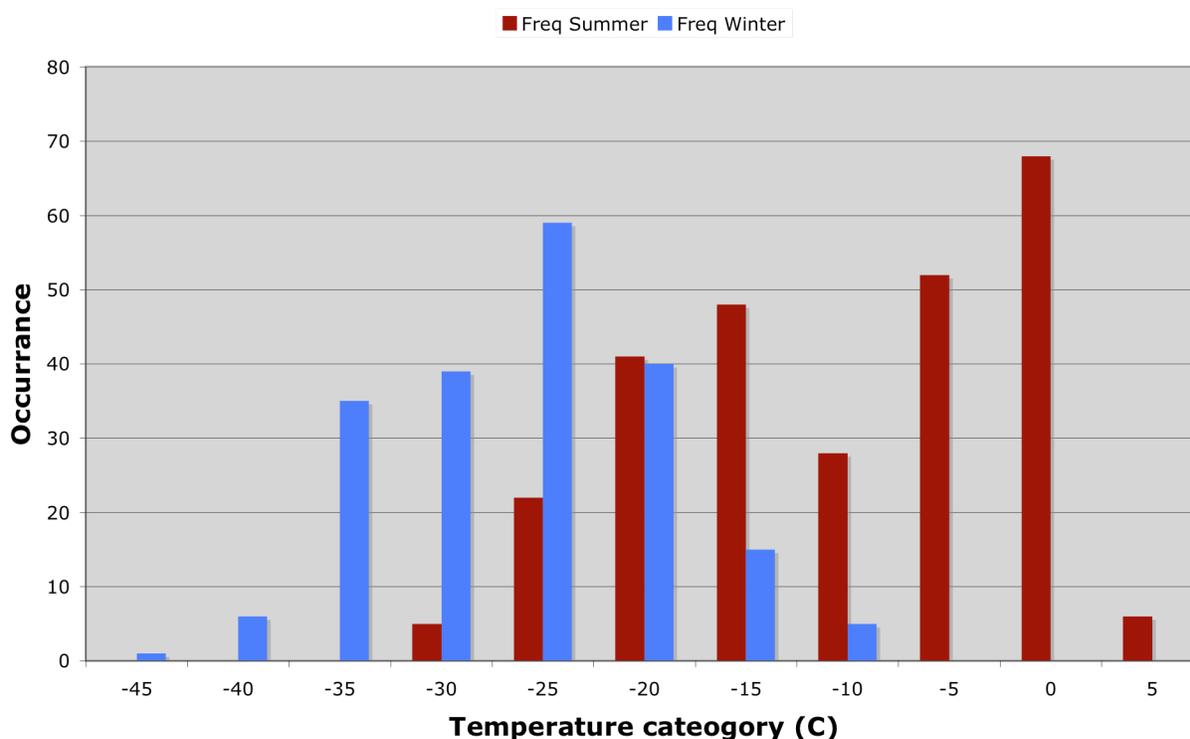
Figure 28. The temperature distribution during fog is divided between two seasons - winter (April-September) and summer (October-March).

b. Fog and Atmospheric Pressure

McMurdo Station's station pressure average, mode and median are all 986.1 hectopascals (hPa) during the study period. The extreme maximum, 1035.2 hPa, occurred on 9 August 1974 at 0 UTC, while the extreme minimum is 937.5 hPa on 19 July 1993 at 18 UTC. The standard deviation is 10.7 hPa over the annual cycle. Figure 29 depicts the monthly means and extremes for each month.

McMurdo Station Station Pressure Monthly Means and Extremes (1973-2004)
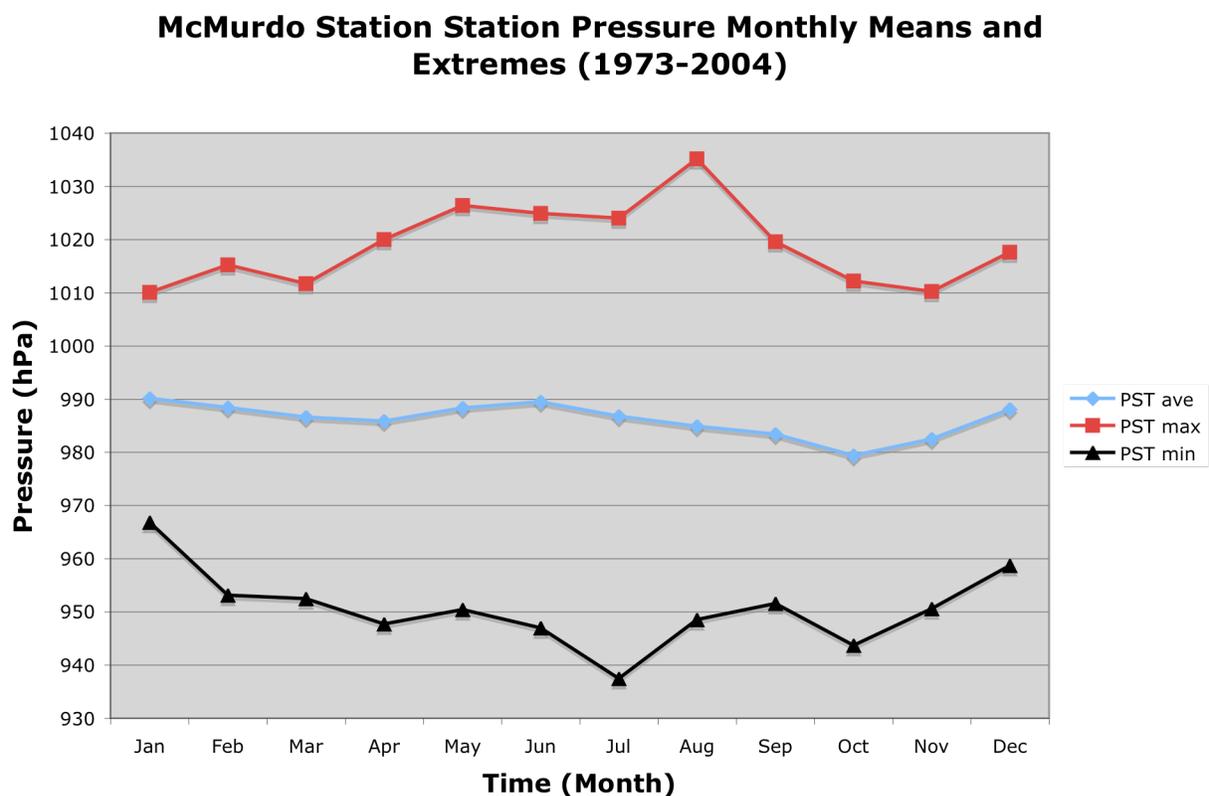
Figure 29 McMurdo Station monthly means and extremes of station pressure of all observations from 1973 through 2004.

In reviewing fog occurrence and station pressure, the averages are practically identical with the average for all observations at 986.3 hPa while for fog only observations at 986.1 hPa. This is reflected in a comparison of the month-to-month averages as seen in Figure 30. In agreement with anecdotal evidence (Cayette personal communications, 2002; SPAWAR 2007b), fog occurs at average pressure conditions primarily (Figure 31). Additional analysis below further illustrates this forecaster rule of thumb.

**McMurdo Station Monthly Average Sea Level Pressure
(1973-2004)**
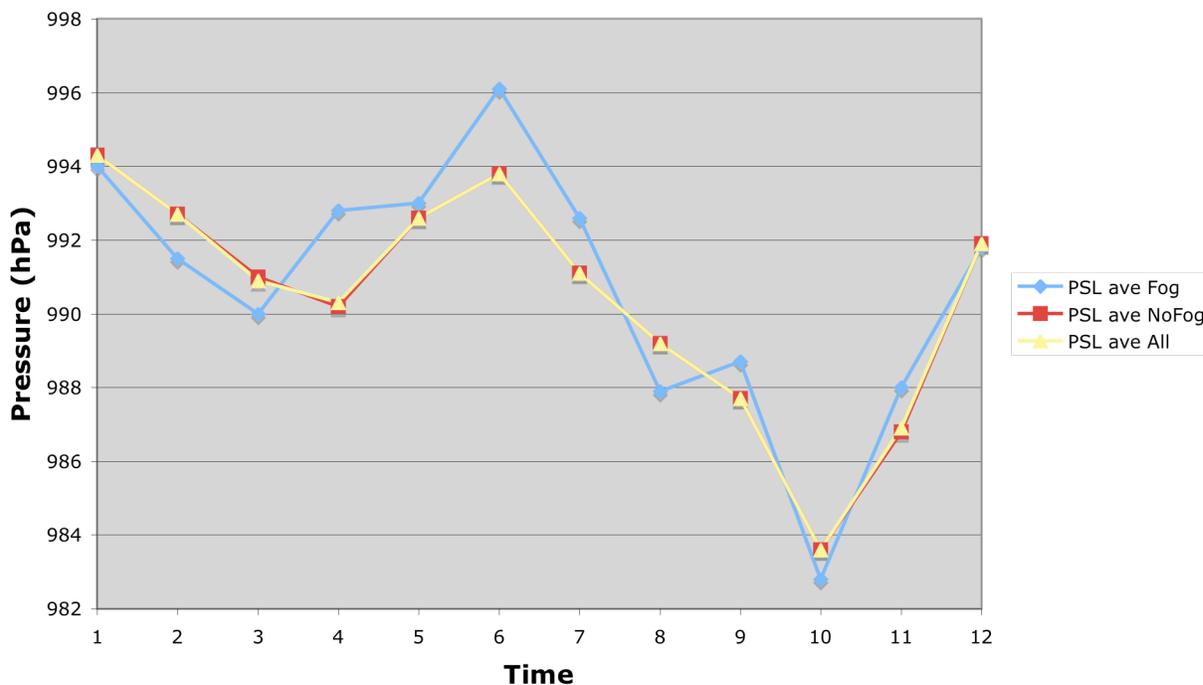
Figure 30. Station pressure means showing the close relations between means over all observations, fog-only and no-fog observations at McMurdo Station.

Seasonal analysis of station pressure and fog occurrence was conducted in the same way as with temperature, discussed in the prior section. Results during the NDJF period had the average station pressure for fog at 988.2 hPa while all observations averaged a very similar station pressure of 987.3 hPa. In this same season, maximum station pressure during fog observations was 1007.8 hPa, while all observations had a maximum at 1017.6 hPa. During the NDJF season, minimum pressure during fog occurrence observation is 962.7 hPa, while it is 950.6 hPa for all observations. Results during the MJJAS season have a similar behavior: Average station pressure is 986.5 hPa for all observations, while it is 985.8 hPa for fog-only

observations, Maximum station pressure is 1035.2 hPa for all observations, while it is 1009.8 hPa for fog-only observations, Minimum station pressure is 937.5 hPa for all observations, while it is 954.3 hPa for fog-only observations. Other measures such as median values, track very closely together when comparing all observations vs. fog-only observations (for NDJF, 987.6 hPa vs. 988.3 hPa respectively and for MJJAS, 986.1 hPa vs. 985.1 hPa, respectively). However, some differences are noted with mode values for all observations vs. fog-only observation (for NDJF, 988.1 hPa vs. 992.5 hPa, respectively and for MJJAS, 981 hPa vs. 988.8 hPa). A similar situation is noted with standard deviation of station pressure between the seasons. There is some agreement between all observations and fog-only observations for standard deviation (for NDJF, 8.9 hPa vs. 7.3 hPa and for MJJAS, 11.9 hPa vs. 10.8 hPa).

In Figure 32, the distribution of station pressure in fog occurrence can be seen to mimic the behavior of the non-fog occurrence observations. A similar normal distribution is seen in both datasets, with station pressures during fog not as broad a distribution. This also points to how the fog nearly matches the long-term climatology, and how fog primarily occurs at average station pressures and not at the extremes.

McMurdo Station Means and Extremes of Station Pressure 1973-2004
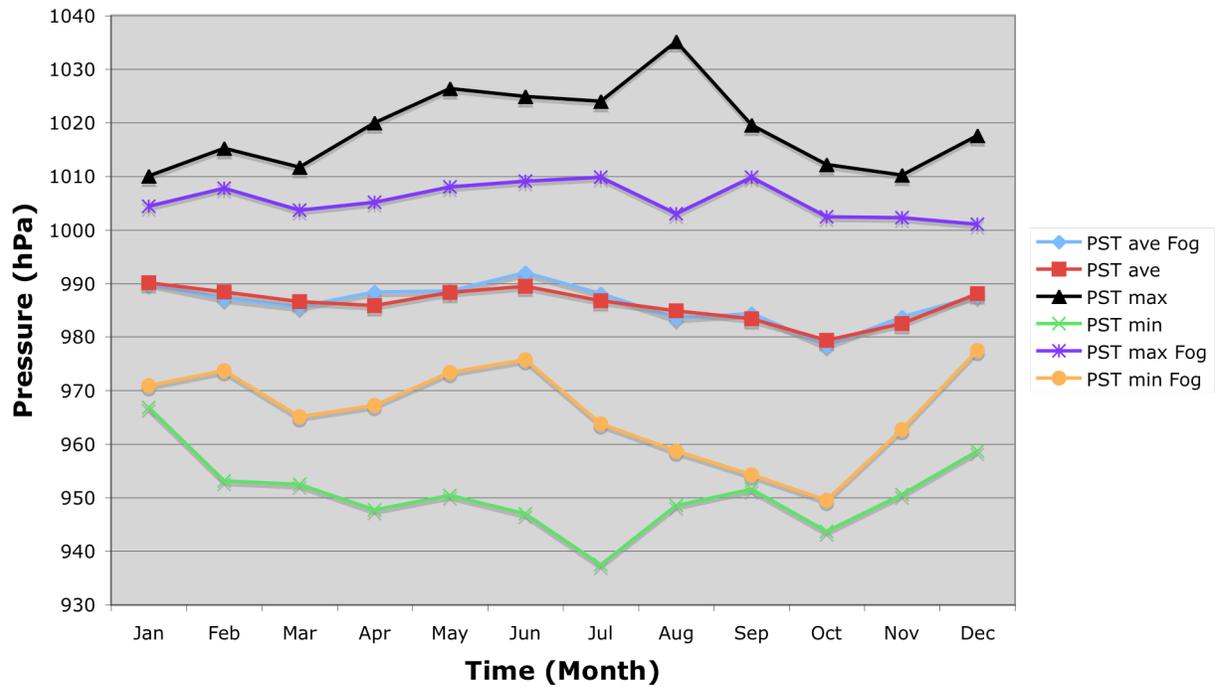
Figure 31. McMurdo Station extremes for Station Pressure for all observations and fog only occurrence observations. Standard deviation is shown as error bars on the mean curves.

**McMurdo Station Pressure Distribution with No Fog
(1973-2004)**
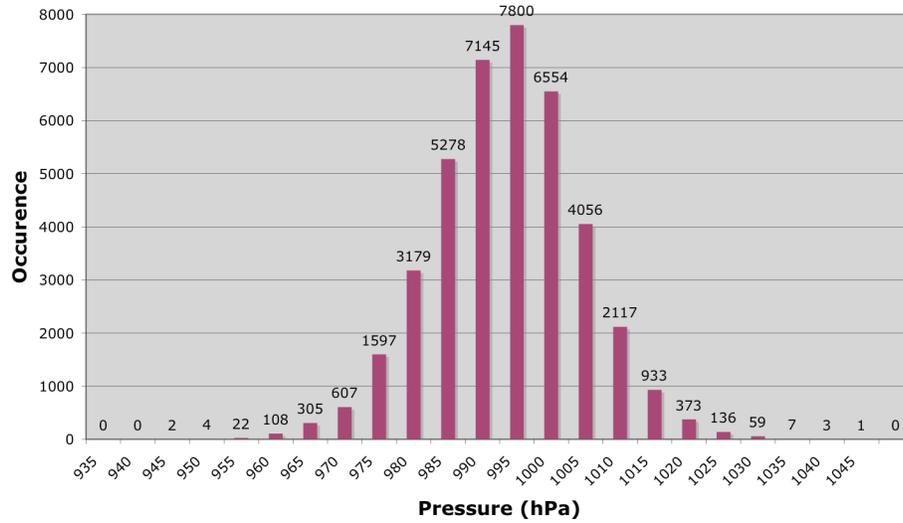
a.

McMurdo Station Pressure during Fog (1973-2004)
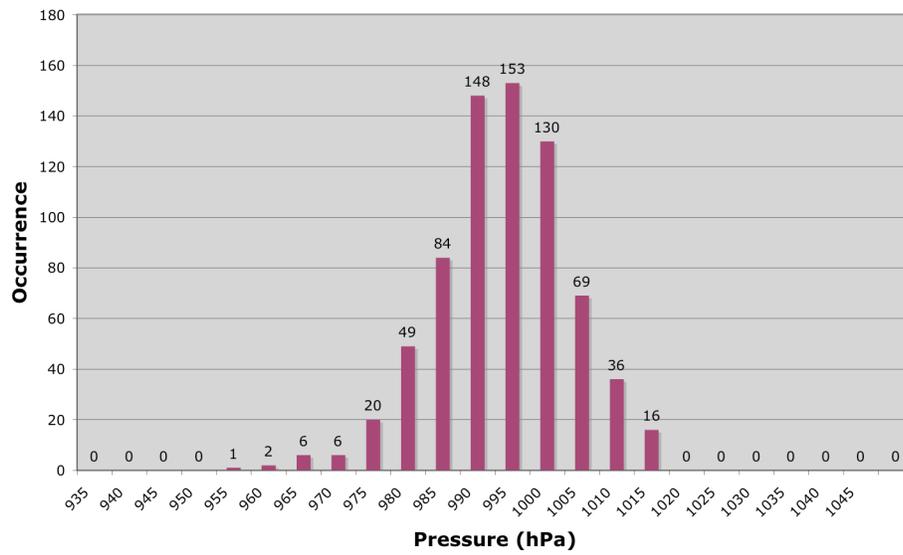
b.

Figure 32. a. The distribution of station pressure observations depicted during non-fog occurrence and b. fog occurrence at McMurdo Station.

c. Fog and Wind

McMurdo Station experiences a preferred wind direction with a large percentage of the winds coming from the east as seen in the wind rose in Figure 33. Some of this direction is due to topographic influences of Ross Island on the wind (Schwerdtfeger 1984, Seefeldt et al. 2003). Wind observations at the station have an average speed of 10.1 knots (Figure 34). The maximum wind speed observation made at the station during the study period is 112.3 knots recorded on 27 February 1998 at 0 UTC. Computation of the resultant wind speed (the magnitude of the average wind vector) is 6.8 knots with a direction of 82.4° and a constancy (the ratio of the resultant wind speed to the average wind speed) of 0.67. Reflecting this result, the average u-component is -6.8 knots and v-component is 0.9 knots.
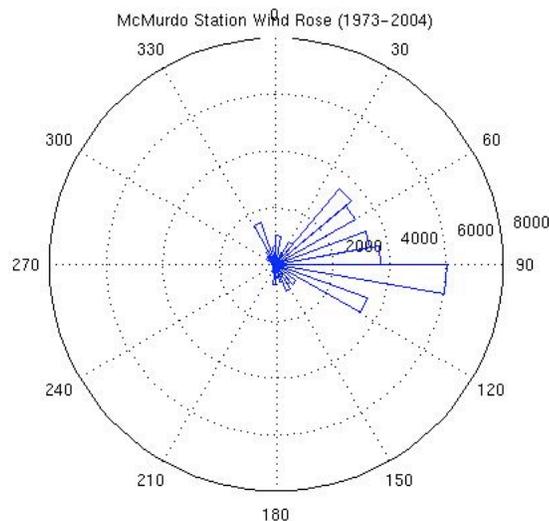
Figure 33. A wind rose for McMurdo Station, Antarctica using all observations shows the easterly nature of the winds at the station (calm winds reported as 0 knots and 0 degrees are not included). This display has 10-degree bins for the wind direction and the circular rings are in 2000 observation increments.

**McMurdo Station Mean, Maximum and Resultant
Wind Speed (1973-2004)**
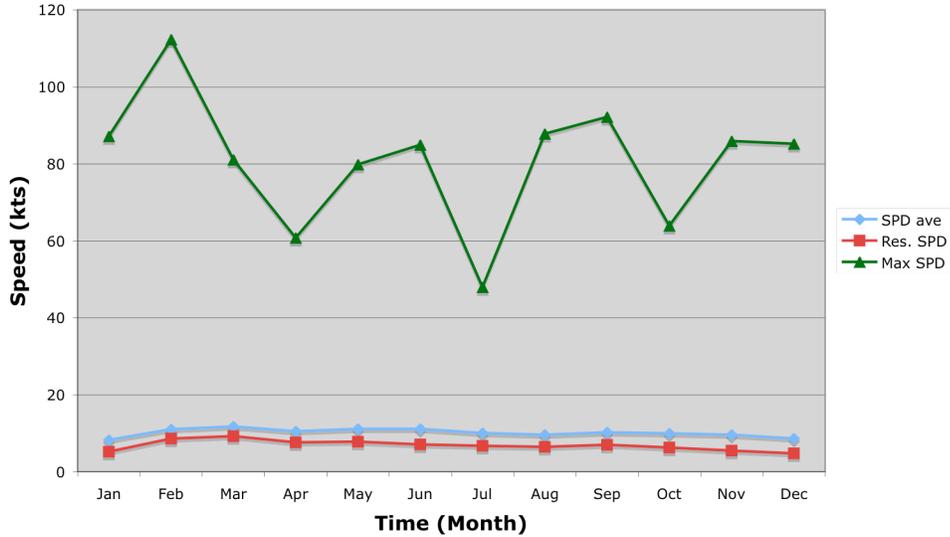
a.

**McMurdo Station Mean and Resultant Wind Speed
(1973-2004)**
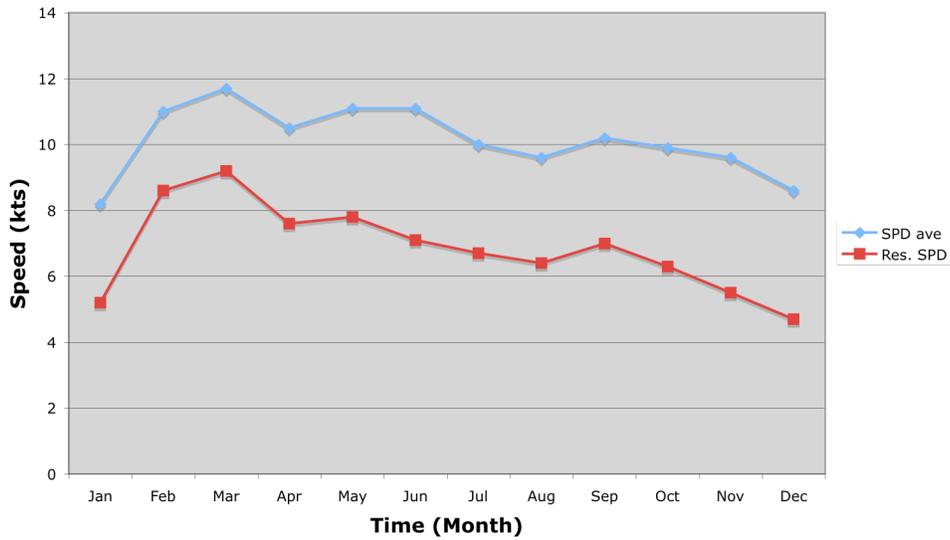
b.

**Figure 34 a. Wind speed averages, resultant wind speed and maximum wind speed on a
month-by-month basis for McMurdo with standard error shown as error bars on the mean
speed curve.   b. Wind speed average and resultant wind speed only month by month.**

Wind speed distributions shown in Figures 35 and 36 point to the similarities between fog and non-fog periods. One difference is the relative increased frequency of calm wind speeds reported during fog situations than non-fog situations. During fog occurrences, wind directions are extremely close to that of McMurdo's general climatology, as can be further seen in Figures 37 and 38. Additionally, the resultant wind is about 80° with a resultant average speed of 7.6 knots (kts) along with the scalar average mean speed of 9.3 kts. These parameters are fairly close to McMurdo's general wind climatology. The constancy for fog occurrence wind direction is 0.81, which reveals how fogs are much more likely to be from the east. All other statistics including modes, medians, standard deviation, and minimum speeds were all very similar between all observations and fog-only observations.

Wind Speed Distribution - No Fog 1973-2004
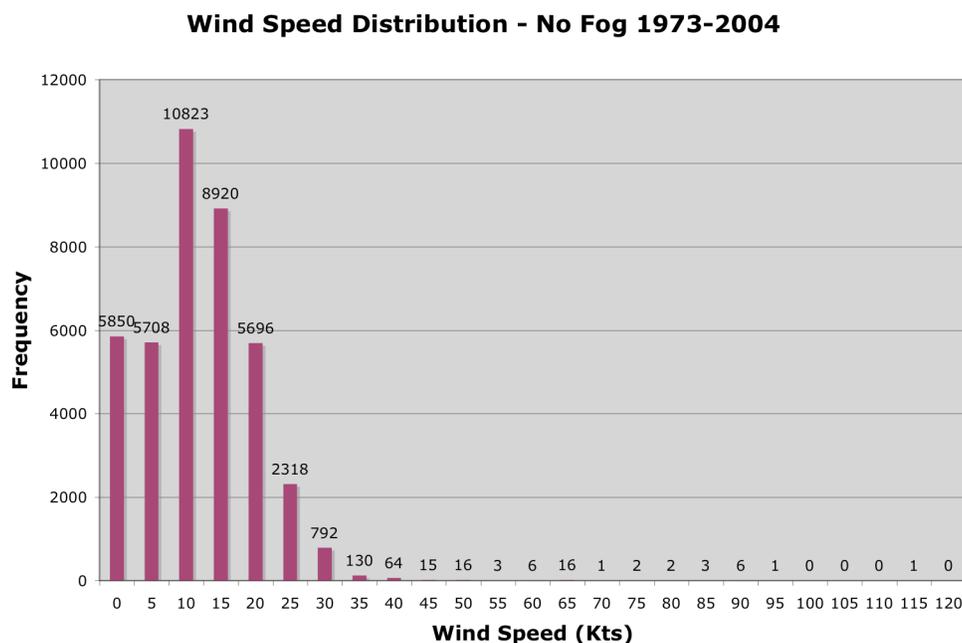
Figure 35. Wind speed distribution for non-fog situations with speeds in 5-knot bins.
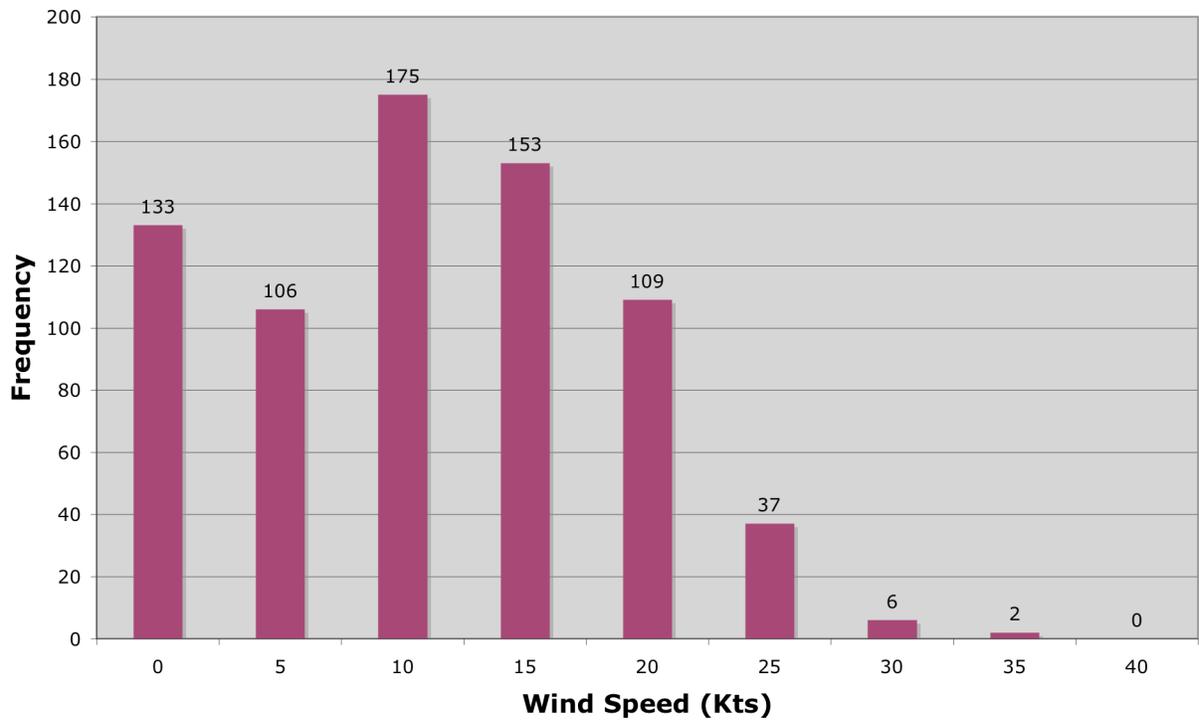
Figure 36. Wind speed distribution for fog only occurrences.

Wind Direction Distribution - Fog only 1973-2004
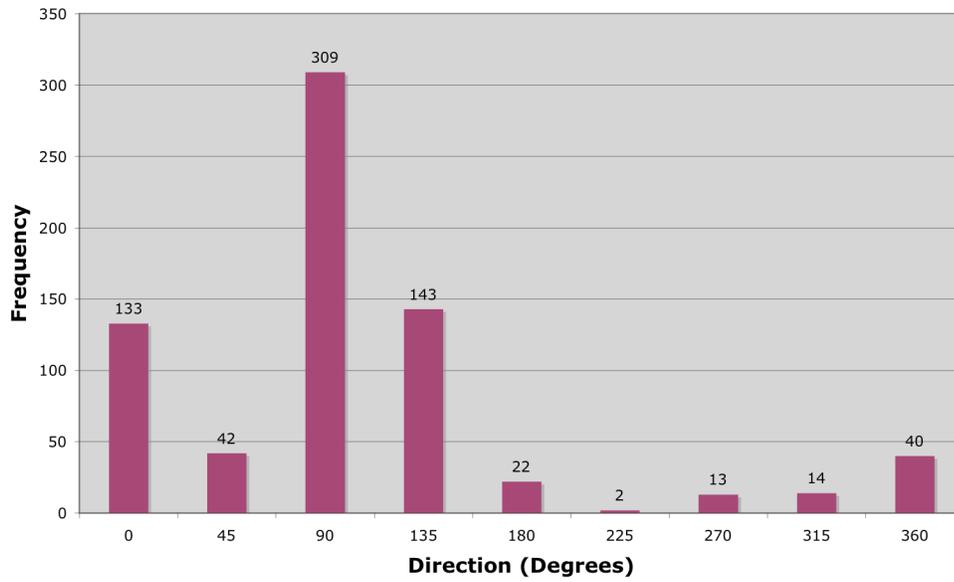
a.

Wind Direction Distribution - No Fog 1973-2004
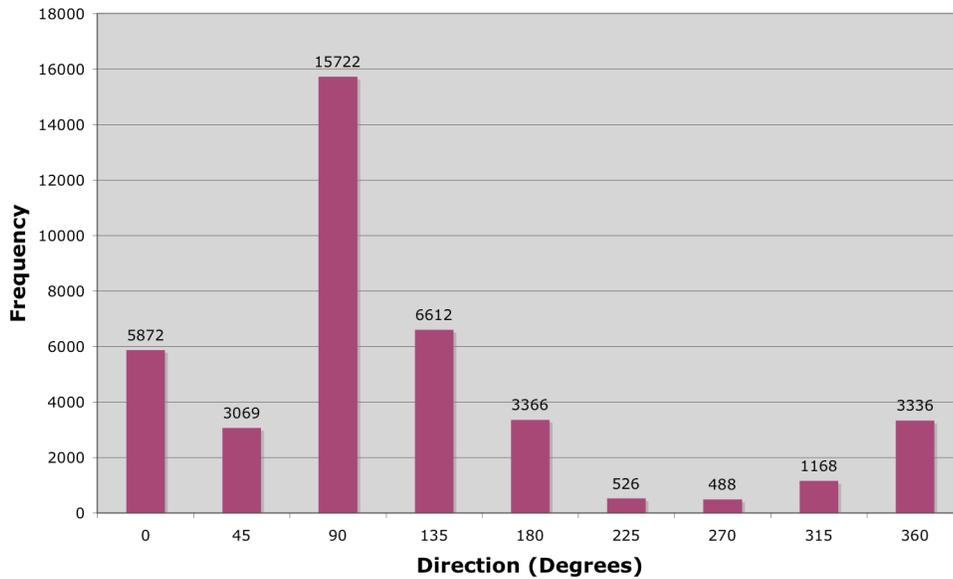
b.

Figure 37. Wind direction distribution in 45-degree bins for fog (a) and non-fog (b) situations showing the extreme similarity between the two and a peak in occurrence of winds from the east.
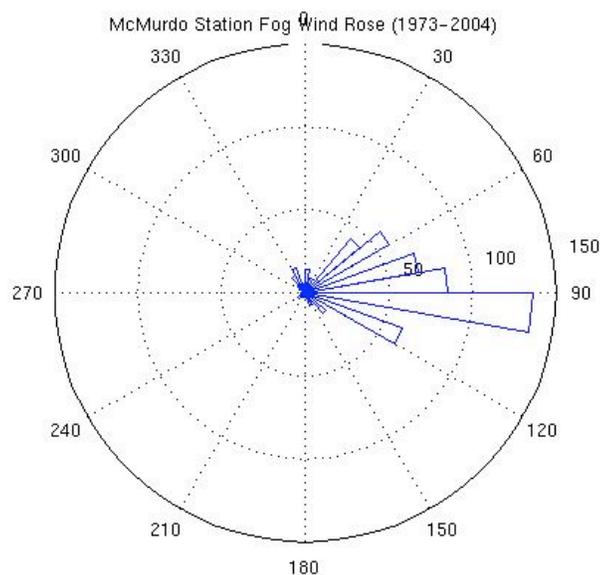
Figure 38. A wind rose for McMurdo Station during fog-event occurrences shows the very easterly component to the wind.

In comparing seasons, there is a consistency of the wind statistics between the two seasons for all observations. During NDJF, average speeds are 9.3 kts, while for MJJAS they are 10.4 knots. For resultant wind direction and speed, they are 82° at 5.9 kts during NDJF vs. 82° at 6.9 kts during MJJAS. However, fog-only observations did have a few small differences between seasons. The wind speed average during fog occurrence in MJJAS was 7.8 kts, which is somewhat less than NDJF at 9.2 kts. This reflects how there is more wind associated with fogs in the summer due to the advective nature of summer fogs. Winter fogs (not the focus of this study) are currently anecdotally known to be station or camp fog, which implies it is not advective in nature. Wind constancy is on the order of 0.82 in MJJAS as compared to 0.75 in NDJF. Other statistics of fog only observations such as resultant wind direction and speed show greater similarity: MJJAS at 76° at 6.4 kts, while NDJF has 80° at 6.9 kts. All other statistics

including modes, medians, and standard deviations all have values relatively close to each other between the fog-only observations and all observations in each of the seasons. One important note is that wind speeds from the analysis of McMurdo observations may indeed reflect the influence of topography on the observations. At McMurdo, weather from the east has wind that is funneled in the pass between Observation Hill and Crater Hill. Local effects of topography have been noted in boundary layer test studies at Williams Field, when northerly wind flow impacted observations (Liu and Bromwich 1993).

d. Dew point, Visibility and Clouds

Measurement and observation of moisture variables in the McMurdo region offer some limited insights into the behavior of fog. Meteorological observations of visibility, dew point, and cloud characteristics from the three airfields (Williams Field, Ice Runway and Pegasus Field) and McMurdo Station over the last decade (1997-2007) are briefly discussed in this section. Emphasis is placed on the observations made during the later half of the last decade as they offer the best quantity and quality of observations, especially with regard to dew point measurements. As an additional note, this section's analysis includes fog and mist (where visibilities are less than 11 km but greater than 1 km) observations combined, unless otherwise noted.

Dew point: Measurement of moisture meteorological variables as they relate to fog is sensitive to the population of measurements. During the first portion of the decade analyzed (1997-2007), there is missing data, with few or no dew point measurements available from the

airfields. Hence, clear conclusions are difficult to ascertain. The distribution of dew points reported during fog and mist are found to have a similar behavior to dew points over all observations, with some exceptions. At Williams Field, dew points during fog and mist are skewed toward warmer values as compared with the distribution of all dew point observations (Figure 39). The opposite appears to be the case at the Ice Runway, with fog and mist reports skewed more toward colder temperatures. These behaviors are likely reflections of the times of year that these sites operate. Williams Field is open in the warmer months of December, January, and February while the Ice Runway is open in the cooler months of October and November. Pegasus Field observations during fog and mist mirror the distribution over all observations (its operating season has shifted over the years from early and late season to include more of the austral summer). McMurdo's observations are based only on fog (hence, do not include mist) and additionally have year round observations included in the analysis. The result is a broader range of dew point temperatures in the distribution, likely due the year-round observations. During fog at McMurdo, there is a more bimodal distribution found in the dew point temperatures. This seems to reflect the two seasons for fog: one during austral summer and one in the late austral winter/early spring.

Dewpoint Distribution during Fog and Mist 1997-2007

a.
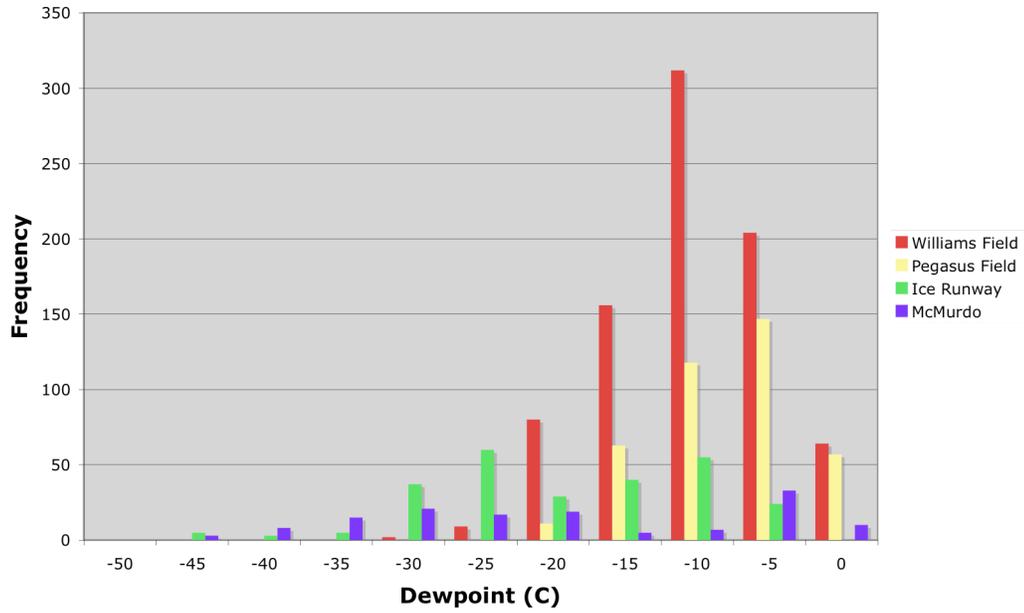
Dewpoint Distribution All Observations 1997-2007
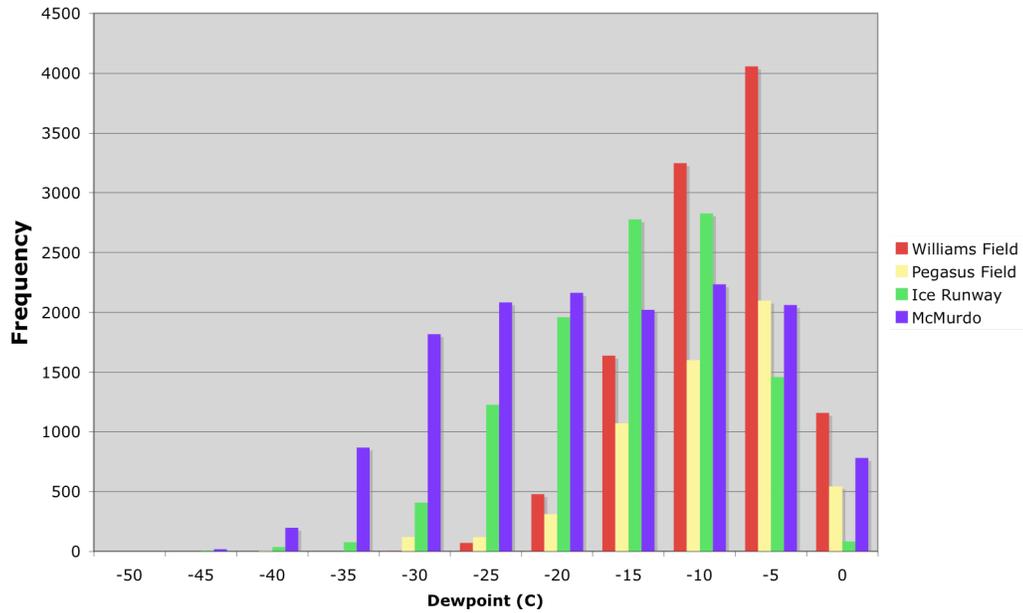
b.

Figure 39. a. Dew point distribution during fog and mist in categories of 5°C (McMurdo Station are during fog only) b. Dew point distributions of all observations.

Visibility: As shown in Figure 40 and Table 3 visibility reports are on average much greater on

average than the accepted modern definition of fog of 1 km (Baliles 1959, AMS 2000). There

are several reasons for this result. The first is that visibility is reported as a prevailing visibility

taking into account all sectors of view. This implies fog is occurring in sectors, and not the

whole field of view for a large amount of the time fog is observed. An example of this is noted

in the decoded METAR data in case discussed in Chapter 2 (Table 1). Additionally, the

observers are instructed to code the visibility based on the WMO code (ww) fog type

(SPAWAR, 2007b):

> "The visibility restriction on ww = 10 shall be 1000 meters or more. The
> specification refers only to water droplets and ice crystals. For ww = 11 or 12 to
> be reported, the apparent visibility shall be less than 1000 meters. For ww = 28,
> visibility shall have been less than 1000 meters. A visibility restriction 'less than
> 1000 meters shall be applied to ww = 42-49. In the case of ww = 40 or 41, the
> apparent visibility in the fog or ice fog patch or bank shall be less than 1000
> meters. 40-47 shall be used when the obstructions to vision consist
> predominantly of water droplets or ice crystals, and 48 or 49 when the
> obstructions consist predominantly of water droplets.' When referring to
> precipitation, the phrase 'at the station' in the ww table shall mean 'at the point
> where the observation is normally taken.'"

The second reason is that many of the observations, especially from McMurdo Station, report

fog in the distance, when it is not actually at the station. A third is due to the inclusion of both

fog and mist in this analysis for the airfields: mist observations are reported with visibilities

greater than 1 km. Mist is very often associated with fog occurrence. One finding from this

analysis is that visibility on average is worse at Williams Field during fog (approximately 4.4

km) than the other observing sites (McMurdo: 5.9 km, Ice Runway: 5.2 km, and Pegasus Field:

5.6 km). Another finding reveals the changes in visibility reporting practice over the years. In

about mid-2001, the observers stopped reporting visibilities above 11 km at all sites. Visibilities from the 1970s through the 1990s were reported up to 80 miles at McMurdo, and then it went down to 60, 40, etc. over the years of reporting. It is unclear if this change in reporting is due to better distance measurement to landmarks in the region or due to changes in standard observing practice of reporting visibilities no higher than 11 km. It is suspected to be a combination of both.

A climatology study of visibility at McMurdo Station and Williams Field was conducted over the years 1966 through 1983 (Souders and Renard 1984). This study focused on visibility as it impacted aircraft operations, finding that blowing snow was by far the biggest impact, followed by snow (precipitation) and then fog. One finding from Souders and Renard study is that February has fog and falling snow occurring together for the largest percentage of time (62%) (Souder and Renard 1984): This situation leads to overall less fog due to the vertical mixing. The earlier study overlaps the present analysis, which had a finding of an increase in fog. This can be seen in Figure 19, in the 1970s and early 1980s portion of the graph. Since that time, fog has decreased.

Visibilities in the McMurdo Sound Area During Fog/Mist: 1997-2007
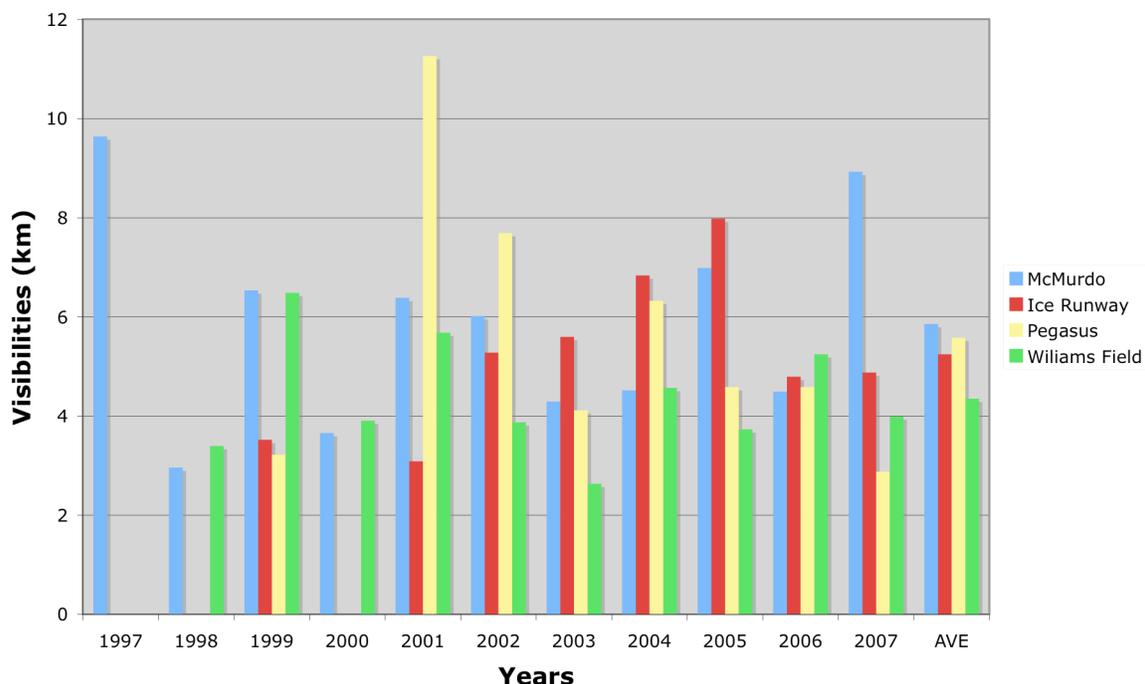
Figure 40. Annual average visibilities during fog and mist at the airfields and just fog at McMurdo Station over the last decade.

Table 3. Table of average visibilities (in miles) during fog and mist at the airfields and just fog at McMurdo Station revealing how visibilities (km) are on average worse at Williams Field during these events when compared to the other airfields.

Years	McMurdo Station	Ice Runway	Pegasus Field	Williams Field
1997	9.6	NA	NA	NA
1998	3.0	NA	NA	3.4
1999	6.5	3.5	3.2	6.5
2000	3.7	NA	NA	3.9
2001	6.4	3.1	11.3	5.7
2002	6.0	5.3	7.7	3.9
2003	4.3	5.6	4.1	2.6
2004	4.5	6.8	6.3	4.6
2005	7.0	8.0	4.6	3.7
2006	4.5	4.8	4.6	5.2
2007	9.0	4.9	2.9	4.0
AVE	5.9	5.2	5.6	4.4

Clouds: Clouds are very often reported during fog, on the order of three quarters of the time for

single level clouds, and more than a third of the time for multiple decks. Also, just 6 out of 10

fogs will be reported with a cloud ceiling (Table 4). Clouds heights are variable, but are reported

most often at heights of one to two thousand feet or less. Cloud heights are reported at other

levels, however, less often at increasing heights. The exception to this is a spike of frequency of

clouds reported at the airfields at 15,000 feet, and less so at 9,000 feet. McMurdo has roughly

the same frequency spikes, but with the inverse occurrence between the two heights. Coverage

of these clouds is overwhelmingly reported as scattered in coverage for the first and/or second

non-ceiling cloud decks when these clouds are present, while the cloud ceiling deck is most

often reported as broken or even overcast.

Table 4. Percentages for cloud coverage reported during fog and mist. CIGH and CA are reported if there is a cloud ceiling, CC1 and CAI1 are the first non-ceiling clouds decks, and CC2 and CAI2 are the second non-ceiling cloud deck.

	Ice Runway			Williams Field			Pegasus Field			McMurdo Station		
Years	CIGH	CC1	CC2	CIGH	CC1	CC2	CIGH	CC1	CC2	CA	CAI1	CAI2
2001	100%	50%	NA	47%	83%	31%	NA	100%	67%	86%	62%	5%
2002	67%	100%	56%	77%	51%	30%	73%	81%	46%	61%	47%	0%
2003	56%	98%	77%	96%	30%	9%	88%	69%	28%	100%	63%	5%
2004	36%	100%	67%	75%	81%	38%	62%	79%	61%	94%	39%	17%
2005	52%	100%	67%	47%	90%	60%	83%	91%	54%	85%	65%	25%
2006	60%	100%	50%	48%	90%	49%	55%	89%	58%	83%	50%	0%
2007	62%	100%	54%	73%	60%	41%	84%	49%	32%	95%	53%	11%
AVE	62%	93%	62%	66%	69%	37%	74%	80%	49%	86%	54%	9%

McMurdo Station Clouds during Fog 1997-2007
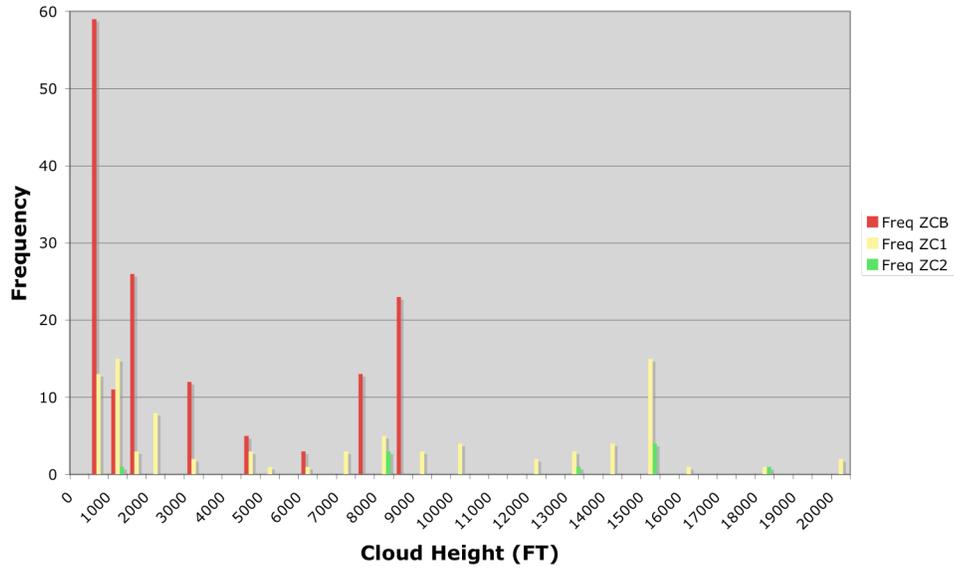
a.

Williams Field Clouds during Fog and Mist 1998-2007
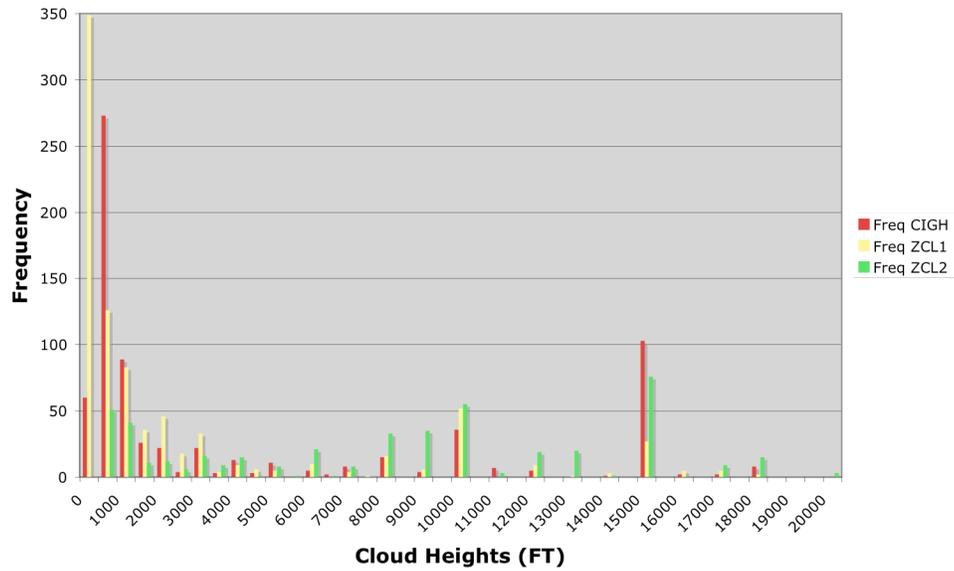
b.

Figure 41. a. Frequency of cloud heights reported during fog and mist at McMurdo Sound sites and b. Williams Field.

e. Summary

In reviewing the findings, McMurdo Station has ranges of temperatures, pressures and winds as expected for this location in the Antarctic region in the polar easterly wind regime. Fog tends to occur at lower temperatures on average, but this might be expected as the surface is always snow covered and lower temperatures favor saturation conditions. Fog occurrences at the station are indeed embedded in this climatological flow pattern. However, McMurdo Station proper only sees a fraction of the fog events when compared with nearby airfields. A summary of the highlights of McMurdo Station climatology is outlined in Table 5 and Table 6.

Table 5. A summary of key climatological values are shown here for all observations from McMurdo Station from 00 UTC 1 January 1973 through 18 UTC 31 December 2004.

Variable	Value	Date (if applicable)
Maximum Temperature	10.6 °C	06 UTC December 21, 1987
Minimum Temperature	−47.8 °C	00 UTC August 4, 1975
Maximum Station Pressure	1035.2 hPa	00 UTC August 9, 1974
Minimum Station Pressure	937.5 hPa	18 UTC July 19, 1993
Maximum Wind Speed	112.3 knots	00 UTC February 27, 1998
Average Temperature	−16.7 °C	
Average Station Pressure	986.1 hPa	
Average Wind Speed	10.1 knots	
Resultant Wind Speed	6.8 knots	
Resultant Wind Direction	82 degrees (East)	
Constancy	0.67	

Table 6. A summary of key climatological values are shown here for fog-only observations from McMurdo Station from 00 UTC 1 January 1973 through 18 UTC 31 December 2004.

Variable	Value	Date (if applicable)
Maximum Temperature	4.4 °C	06 UTC December 26, 1984
Minimum Temperature	−47.2 °C	12 UTC August 4, 1978
Maximum Station Pressure	1009.8 hPa	06 UTC July 29, 1980 12 UTC July 29, 1980 18 UTC September 12, 1980
Minimum Station Pressure	949.5 hPa	00 UTC October 9, 1993
Maximum Wind Speed	33.1 knots	18 UTC February 18, 1992
Average Temperature	−19.1 °C	
Average Station Pressure	986.3 hPa	
Average Wind Speed	9.4 knots	
Resultant Wind Speed	7.6 knots	
Resultant Wind Direction	80 degrees (East)	
Constancy	0.81	

3. Fog, Sea Ice, and Icebergs

With the open ocean very close to McMurdo Station, it is a nearby moisture source potentially aiding in fog development. When the ocean is capped by annual sea ice or by icebergs, it could possibly limit the availability of moisture for fog events, and in turn should reduce fog occurrence and perhaps duration. In mid-2001 the large tabular icebergs C-16 and B-15 moved into the north side of Ross Island (Falconer and Pyne 2004; Knuth personal communications, 2004). With the icebergs located in this position, annual sea ice was able to cover much of the McMurdo Sound, and remain longer into the summer season. This situation occurred until early 2006. During the period 2001 through 2006, the icebergs essentially "shaded" the McMurdo Sound region, allowing it to increase with annual and multi-year sea ice. As seen in Figures 42 and 43, it appears that despite the period of extended capping on the ocean of McMurdo Sound,

fog occurrences were slightly higher than before. Supporting sea ice edge observations courtesy of the US Coast Guard icebreakers Polar Star and Polar Sea roughly verify the extent of the sea ice during this period via its informal first sighting of the sea ice edge observations (Figure 43). Reasons for this may include that the moisture sources for fogs in McMurdo are not exclusively from the nearby open ocean and instead are from more remote sources. Another possibility is that leads and ice-free ocean that is just beyond the capped sea ice and tabular iceberg edge are enough of a local or regional source. Additionally, the icebergs and sea ice provide additional cold surface that can cool the surface layer of air to the condensation point, helping to initiate fog.

Fog Days Before and After Sea Ice/Iceberg Impact
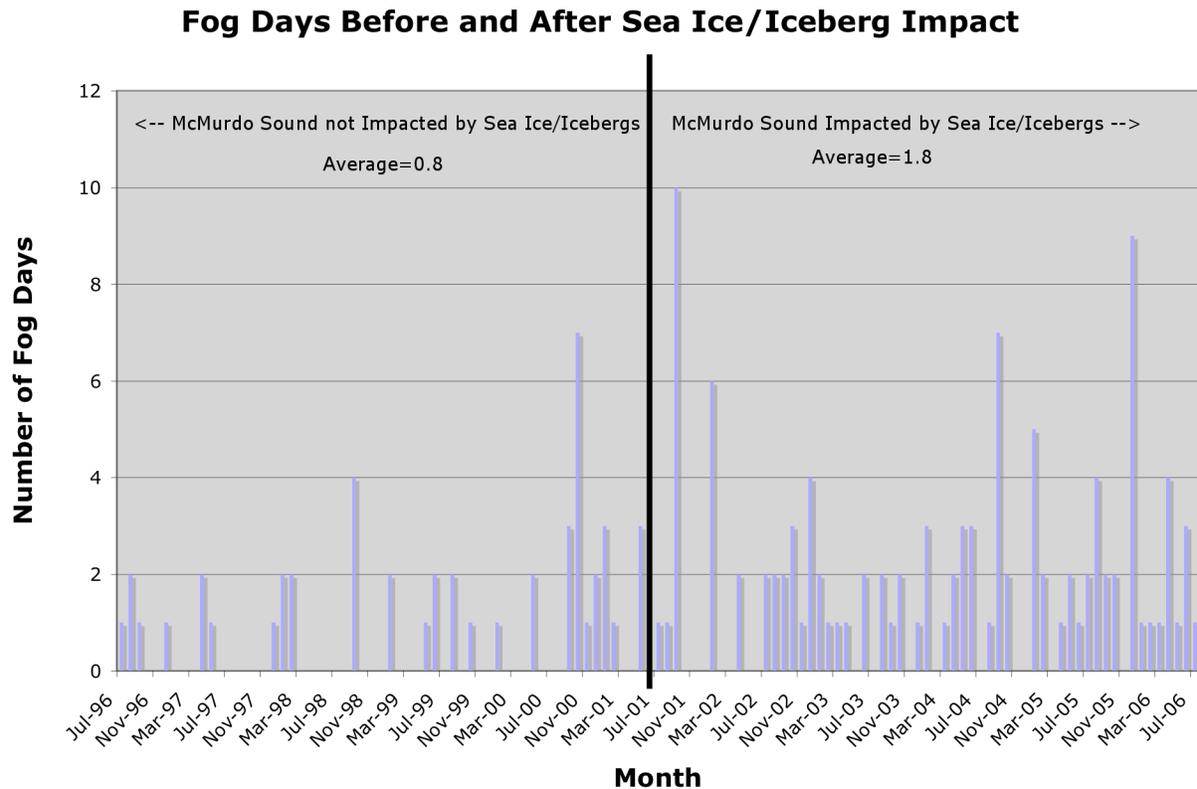
Figure 42. This figure depicts the last 12 years of fog events plotted as a histogram by month. The more recent half shows how there are more events since McMurdo Sound came under the influence of B-15A and C-16 Icebergs and increased sea ice, pointing toward possible impact of the icebergs on fog events at McMurdo Station.

Fog Days Before and After Sea Ice/Iceberg Impact with USCG Sea First Ice Edge Contact
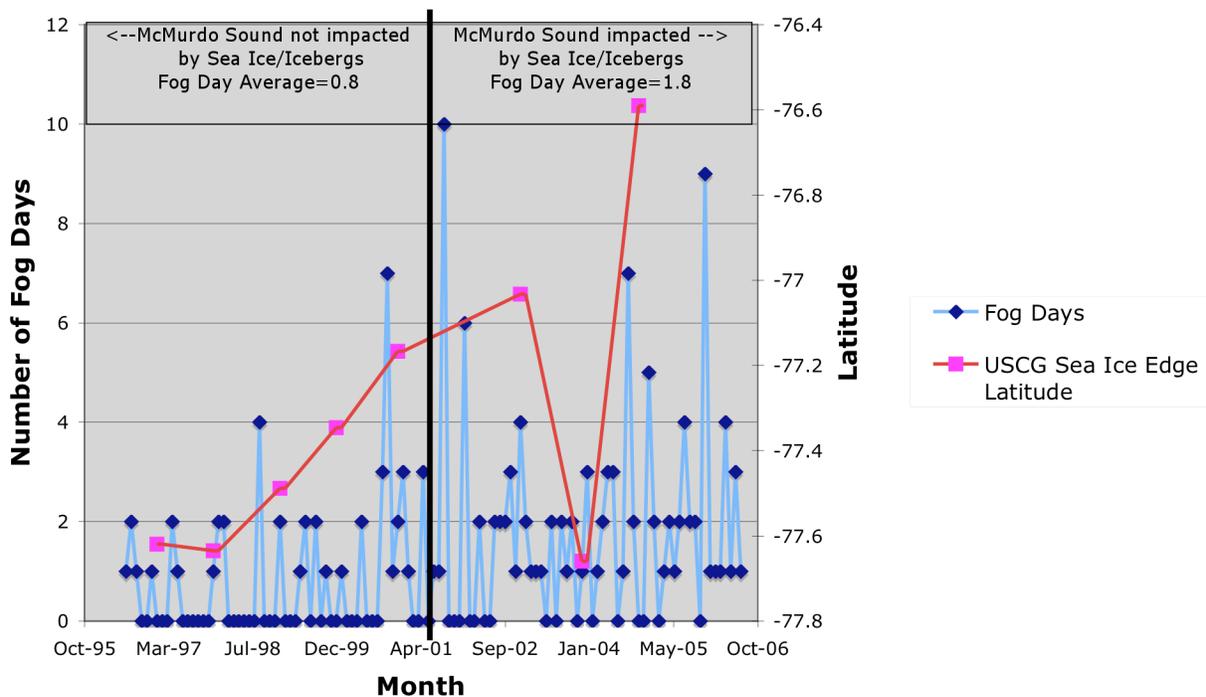
Figure 43. **Same figure as Figure 42 with an overlay of the USCG Icebreaker ice edge reported locations.**

To better answer this question, an analysis was undertaken to compare sea ice concentration with fog days reported from McMurdo Station. Sea ice concentration analysis data from the National Centers for Environmental Prediction's (NCEP) Ocean Modeling Branch (OMB) were used in the analysis covering the period October 1997 to March 2006. The basis for the NCEP OMB ice concentration analysis (ICA) is from microwave satellite observations from the Special Sensor Microwave Imager (SSM/I) on board the Defense Meteorological Satellite Program (DMSP) satellite series (Grumbine 1996). Four regions around the Ross Sea and Ross Island regions were selected to compare ICA to fog days. To make the comparison,

daily ICA gridded fields were averaged over the four regions selected: Eastern Ross Sea, Western Ross Sea (as well as an average of the two), McMurdo Sound and Lewis Bay (Figure 44). Then monthly averages were created from daily regional averages, and then correlated with fog day occurrence.
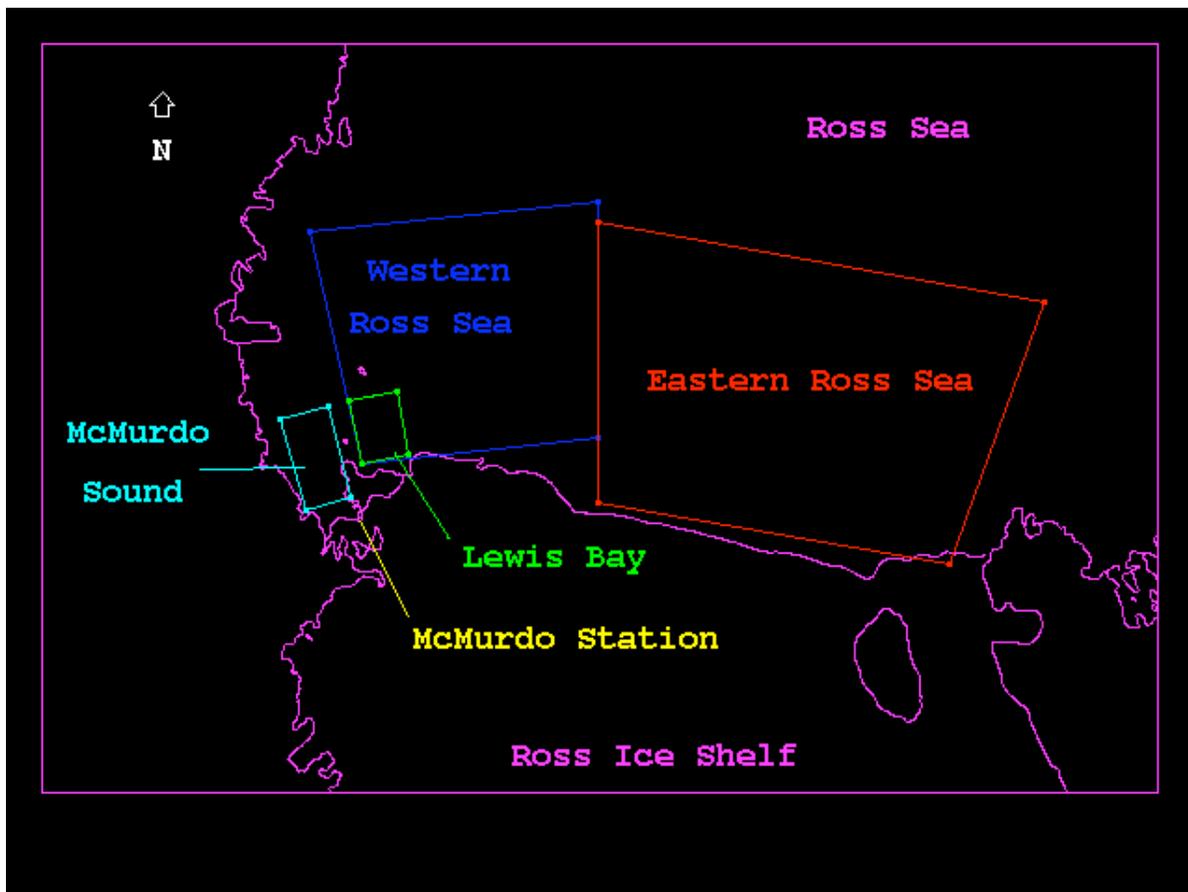
Figure 44. The four regions selected for comparing fog days to NCEP sea ice concentration.

The results of the comparative correlations are seen in Table 7, including correlations over the full year, the broader austral summer months of October through March, and the narrower austral summer months of November through February. None of the regions showed

any relationship other than a weak correlation with the Lewis Bay region and with McMurdo Sound in austral summer. It is to be expected that the strong annual cycle in sea ice concentration would not lead to a high correlation as fog in the McMurdo area does not have the same annual cycle characteristics as sea ice (Figure 45). It is interesting to note the consistency of the weak correlation in the Lewis Bay region, regardless of time period. This low correlation challenges the currently accepted anecdotal evidence (Cayette personal communications, 2002; SPAWAR 2007a) that open water in Lewis Bay to the North of Ross Island is directly related to fog occurrence at McMurdo and the nearby airfields. With small negative correlations in the greater Ross Sea, and small positive correlations in McMurdo Sound and Lewis Bay, it appears that open water in the core summer months of November through February is only weakly related to fog formation in the McMurdo Station region of Antarctica.

Table 7. Correlations of NCEP ICA to fog days are denoted over the full year, a broad summer austral period of October through March (ONDJFM), and a narrow austral summer period (NDJF).

	Eastern Ross Sea	Western Ross Sea	Ross Sea (Average)	McMurdo Sound	Lewis Bay
All Year	0.01	-0.04	-0.03	0.01	0.22
ONDJFM	-0.06	-0.13	-0.10	0.07	0.25
NDJF	-0.23	-0.25	-0.25	0.36	0.26

Fog Days and Sea Ice Seasons (1997-2006)
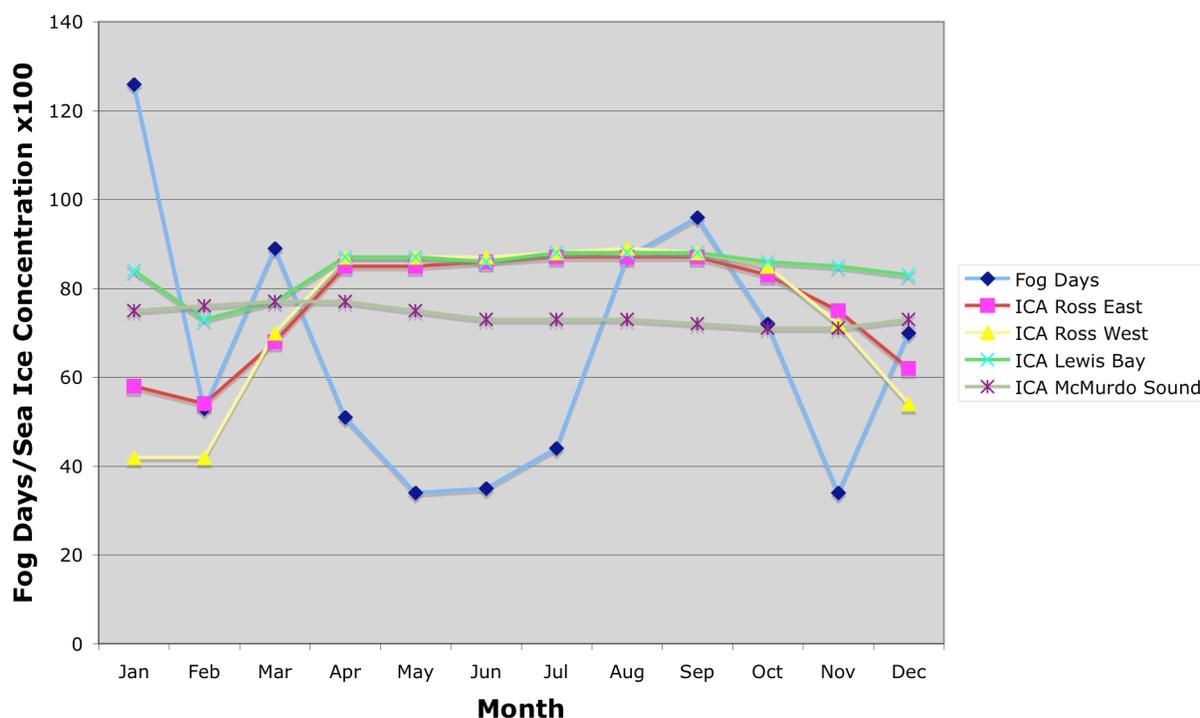
Figure 45. Fog days and sea ice do not share the same seasonal characteristics.

4. Fog and Climate Indices

The variability of fog seen in the 30-year climatology of fog days by month (Figure 12), leads to a question of relationship of fog occurrence at McMurdo Station to other large scale climate circulation forcing such as the El Niño Southern Oscillation (ENSO) and the Antarctic Oscillation (AAO) (also known as Southern Annual Mode). Motivation for this comparison is not uncommon. An analogous example is the effort to relate fog in the Los Angeles basin to climate indices (Witiw et al. 2002, Witiw and LaDochy 2004; LaDochy and Witiw 2007). An analysis has been done to assess if any relationship might exist. Three indices were chosen for

evaluation based on two climate phenomena: Nino 3.4 and Southern Oscillation Index (SOI) to represent the ENSO phenomena and Antarctic Oscillation index to represent AAO. As with the sea ice, correlations were computed between the monthly value of the climate indices and the fog day series over the 1973 through 2007 period. Due to the delay in impact often noted with these climate phenomena, three lags were selected to determine correlations: 0 month or no lag, 3 month lag and 6 month lag. The results, as outlined in Table 8, reveal that there is no clear relationship between the climate phenomena at any lag. Large-scale climate circulation forcing does not appear to drive the observed variability of fog in the McMurdo area.

Table 8. Correlations of fog days with climate indices.

Lag (months)	Nino 3.4	SOI	AAO	AAO (Dec to May)
0	0.01	0.03	0.02	0.03
3	-0.04	0.08	-0.07	-0.07
6	-0.09	0.04	-0.04	0.04

5. Discussion

Fog has two seasons in the Ross Island region of Antarctica: midsummer and late winter/early spring. Additionally, fog occurs more frequently at the nearby airfields compared to McMurdo Station proper, but this does not change the fog seasons that the area experiences. Yet, it does confirm the majority of observations of fog taken from McMurdo are occurring over the

McMurdo Sound area – where the airfields are located. Most fogs are on the order of one to three hours, however, longer duration fog events have occurred up to 30 hours.

In comparing fog to meteorological variables, maximum and average temperatures during fog are cooler when compared to non-fog observations, but no other significant relationships distinguish fog occurrence. An analysis of sea-ice concentrations as compared to fog provides evidence that fog is not strongly correlated with open water in the Ross Sea, McMurdo Sound or Lewis Bay. The low correlation between fog and Lewis Bay ice concentrations brings some doubt to the current thinking as documented by forecasters that open water in Lewis Bay is associated with fog. The trend in fog also has no relationship to any large scale circulations/climate indices as seen in the analysis with ENSO or AAO. The trend in fog over the last 30 years is declining. This trend does not match the trends in other meteorological variables over the same time period.

Chapter 4: Monitoring Fog from Satellite

With McMurdo Station suffering from one to four days with fog each month on average, to as much as four times that number for the nearby airfields, the ability to depict and monitor fog, as well as forecast its evolution, is critical for aviation safety, aviation and other logistics in the region. Recently, web cameras have been installed in the McMurdo region with an aim of aiding the forecasting of fog (Figure 46). While web cameras are very helpful with monitoring fog from the confines of the McMurdo area and nearby airfields, it will not be able to assist with fog formation out of sight of the camera. In these cases, satellite observations will be an important tool used to depict and monitor fog events. This chapter reviews the known means for monitoring fog/low cloud via satellite, and introduces a new method for depiction in Antarctica using a modern imaging spectrometer from a polar orbiting satellite: Moderate-Resolution Imaging Spectroradiometer (MODIS) via principal component analysis.

a.   b.   c.

Figure 46. Capture of a fog event over Williams Field by a web camera from 2 February 2006. (*Courtesy of SPAWAR/Mac Weather*)

A partial technical description of the MODIS sensor is described in Appendix A. This sensor system is on board the Terra and Aqua satellites – NASA's two lead spacecraft in the Mission To Planet Earth (MTPE) Earth Observing System (EOS). MODIS brings significant improvements in the spectral and spatial resolution over previous sensors such as the Advanced Very High Resolution Radiometer (AVHRR) and is inspiration for the next generation of sensors such as the Visible/Infrared Imager/Radiomenter Suite (VIIRS) (See Appendix A).

1. Current Depiction Methods

a. Single Channel Applications

One of the early applications of satellite observations was for observing fog. Early polar orbiting (including Very High Resolution Radiometer (VHRR) – the predecessor to the AVHRR sensor) and geostationary satellite platforms used the visible channel (typically near 0.67 μm wavelength) for fog monitoring (Bader et al. 1995). These early observations were not often able to exploit the single infrared channel for this kind of information, since fog has similar temperatures as its surroundings (Bader et al. 1995). Hence, fogged in regions were unable to be detected clearly as compared to clear fog-free regions nearby, especially at night. Later as other spectral channels became available, other single channels were applied, such as 3.9 or 3.7 μm. Used alone, this channel can reveal low clouds and fog due to emission differences from the clear-sky environment. This channel use is primarily exploited in two-channel methods, described in the next section. As with AVHRR, the MODIS sensor can be used to detect fog in the visible (0.64 μm) and shortwave infrared (3.9 μm) range that are very much like those the

AVHRR offers. MODIS in the visible bands offers higher spatial resolution, up to 250 meters (See Figure 47), as compared to the 1 km on AVHRR.
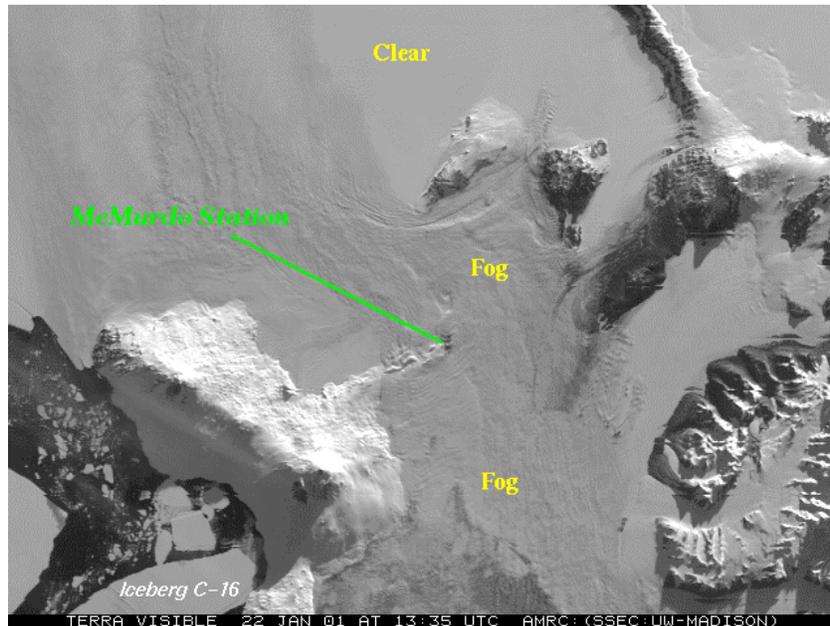
Figure 47. Fog seen filling McMurdo Sound from the Terra satellite with 250-meter resolution visible channel.

b. Two Channel Detection

In the mid-1980s the first bi-spectral or two channel applications for fog were developed for satellite data. Using the AVHRR on the National Oceanic and Atmospheric Administration (NOAA) satellite series, Eyre et al. (1984) exploited spectral differences in fog signatures in the 3.9 μm and 11 μm wavelengths. This technique was targeted for detecting fog at night, when the visible sensors of the satellite were not available (Eyre et al. 1984) and solar reflectance in 3.9 μm is zero. The method consisted of an amplified temperature difference between the two infrared channels. Its power is in the shortwave infrared channel (3.9 μm) as there is an

emissivity difference between the two channels in the presence of fog and low clouds, with more emission in the infrared window channel than in the shortwave infrared channel. This method received its first test as documented in Turner et al. (1986), which was a critical application of Eyre's work over England.

Ellrod applied Eyre's bi-spectral method to the Geostationary Operational Environmental Satellite (GOES) (Ellrod 1991, 1994 and 1995). Before the close of the decade, this method would become operationally used in the U.S. National Weather Service. Figure 48 is an example of this method applied to AVHRR data over the Antarctic. Lee et al. (1997) critically reviewed fog detection methods with GOES-8 and -9 data. They concluded that the bi-spectral method and single visible channel methods for fog detection are both important, and each should be used at a specific time of day for the best results: bi-spectral at night, and reflectance at day and sunset/sunrise times.

The landmark work by Eyre and applications by Ellrod face challenges when applied in the Antarctic. Such methods may highlight fog, but not in all cases. Since the critical use of the two-channel application is at night, the method does not work well during the austral summer, when there is likely both a peak fog occurrence, and nearly 24 hours of sunlight. There will be some periods when this method will be partially effective (Figure 48a), but it will be greatly dependent on the solar impact to the 3.9 μm channel. Also, the same method may highlight other features, including high clouds, seen in Figure 48b.
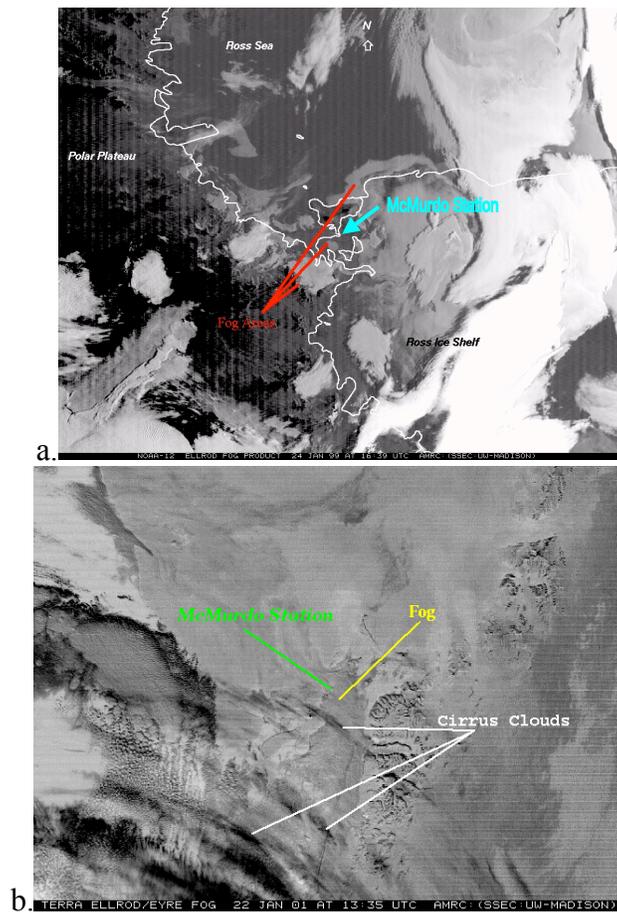
Figure 48. a. A sample AVHRR bi-spectral fog product image over Ross Island Antarctic just hours before a fog event strikes Williams Field, near McMurdo Station, Antarctica. This image follows methods outlined by Erye et al. (1984) and Ellrod (1994), with manual contrast stretch enhancement. b. The Eyre/Ellrod dual channel method applied using MODIS observations, with contrast stretch, shows the impact the cirrus clouds have on this example and the inability for this case to do well.

c. Multi-Channel Detection

With the availability of additional spectral channels on the MODIS sensor, it is possible to consider other spectral channels applied toward the detection of fog. There are a few approaches that can be considered including spectral band color combinations - some with differential

spectral band color combinations. Spectral test schemes are also reviewed here. The final section reviews a method that is inspired from these combinations and uses principal components of the satellite observations themselves to aid in depicting fog.

i. Spectral Band Color Combinations

One method of combining multiple spectral channels is the use of a "three channel combination" via colorizing three selected channels individually through the colors of red, green and blue (RGB). The result of running the brightness count values through these colors and then combining them may automatically enhance the features inherent in each of the single channels. The 8-bits per channel of brightness counts is combined into a 24-bit display (Figure 49). One additional channel to use in the combination on Figure 49 is the 1.6 μm channel (band 6 on the MODIS sensor), which offers the ability to provide discrimination assistance against the snow/ice background during daylight hours. Unfortunately, this channel is not available on the MODIS instrument onboard the Aqua satellite as that channel deteriorated before launch (Baum, personal communications 2001). Alternative channels that offer similar abilities include the 1.24 μm channel (band 5), and 2.11 μm channel (band 7). One example of a channel that is not as effective in this portion of the near-infrared band is the 1.38 μm channel (band 26), where high thin cirrus clouds are enhanced over the fog below.

Beyond using the RGB method on individual channels, it is also worth considering the same application applied toward algebraic combinations of channels such as brightness temperature differences between two channels. An additional possibility is the combination of some single channels with the difference of other channels. One such example is an RGB combination of 0.64-μm (red), 1.6-μm (green), and 11-μm brightness count difference with the 1.6-μm channel (blue) (Figure 50). This combination has some capability to provide an enhanced view of the fog although there is impact from katabatic-scoured ice surface in this combination.
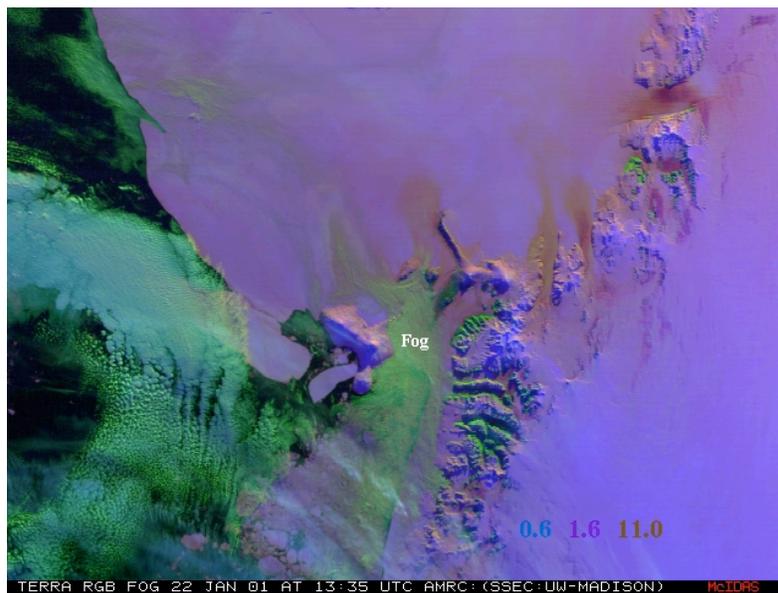
Figure 49. An RGB three channel color combination of the visible 0.6 μm, 1.6 μm and infrared 11.0 μm channels. Each channel is automatically contrast stretched before combining. The fog area can be seen in the green tinged cloud region labeled. Notice katabatic flow regions and other land features are also enhanced.
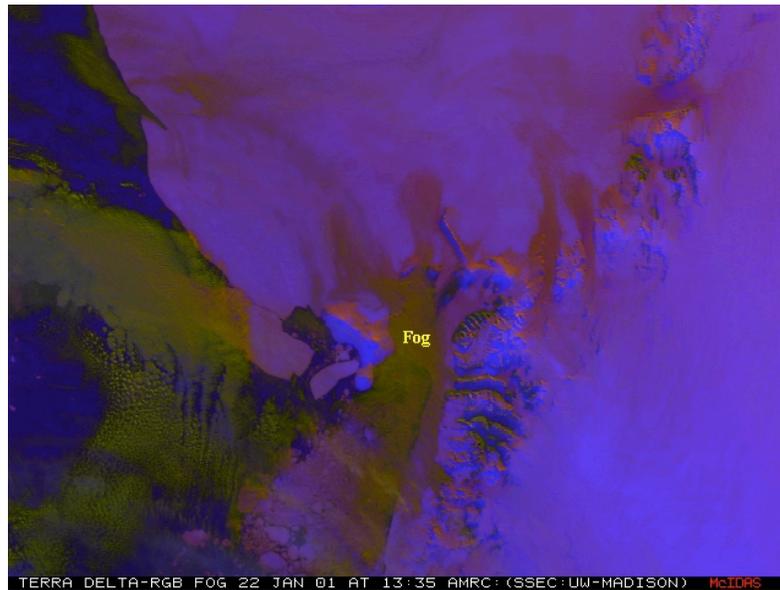
Figure 50. An RGB combination of 0.6 μm, 1.6 μm and the difference between the 11 μm and 1.6 μm channels.

ii. Spectral Test Methods

Significant effort has been put into the detection of or "masking" for clouds in satellite imagery (i.e. Ackerman et al. 1998). Hence, one method for detecting fog is to consider detecting clouds/no clouds as a starting point and use the results as a basis for isolating suspected fog areas. Efforts related to this type of method have been under investigation in Europe using both the Meteosat Second Generation satellite in geostationary orbit and Terra and Aqua satellite's MODIS sensor in polar-orbit (Bendix et al. 2003, Bendix et al. 2004, Bendix et al. 2005, Cermak 2006, Cermak and Bendix 2007). The technique, named the Satellite-based Operational Fog Observation Scheme (SOFOS), is a decision tree method to identify low stratus and fog areas. This method was primarily tested and developed over mountains in central Europe. The SOFOS procedure (Cermak and Bendix 2007) starts with a general cloud mask (using the infrared

window and shortwave infrared channels). This results in areas identified as clouds and areas as non-clouds. It is then followed by specific checks to remove ice clouds and snow as well as search for small droplet clouds. Next, the spatially coherent areas and clusters of fog/low cloud, which are left after these checks, are individually tagged. From here, a fog/low cloud altitude test is done on each identified cluster by comparing elevations from digital elevation model (DEM) altitude information and cloud altitude estimated via threshold using an assumed temperature gradient compared with the infrared window channel temperature differences between the cloud edge and the adjacent clear area. If identified as a low cloud, a spatial homogeneity test is performed to make the final determination if it is indeed stratus or fog. An estimation of the cloud base height is made using a cloud microphysics model that has inputs of liquid water path (LWP), cloud top height and corrected cloud top temperature and the solution is iterative based on agreement of observed LWP and modeled LWP. If the resultant cloud base of the cloud layer is below the DEM, the identified area is indeed listed as fog, otherwise it is labeled as stratus.

In the Antarctic, this method faces challenges due to the influence of the snow/ice background on the initial cloud mask, and retrieval of the LWP. An example cloud mask product is shown in Figure 51, matching the same fog case analyzed in the above sections. Part a of the figure shows the prior version of the MODIS cloud mask fails to detect the cloud/fog over the ice in the southern portion of McMurdo Sound. The current updated version of the cloud mask improves its ability in the region. However, it is not clear that other checks, especially the need for other ancillary data such as the estimate of LWP would enable SOFOS to work well over the ice. An additional challenge is the lack of sufficient communications bandwidth to Antarctic

stations. With limited communications, it may not be possible to deliver all of the required

ancillary information (such as routine model output data values) to use this method in real-time.
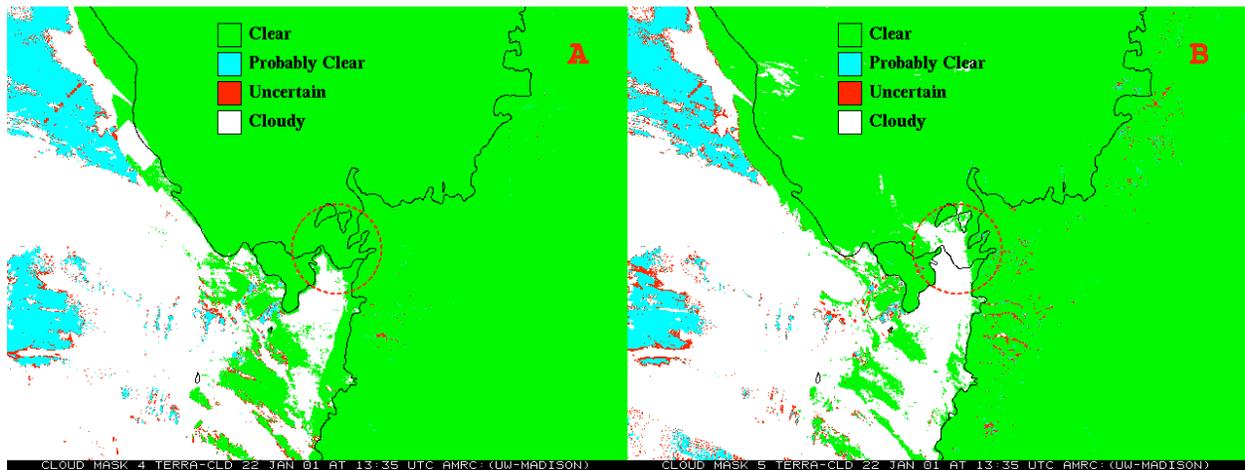
Figure 51. a. The standard cloud mask shown from the same fog example case 22 January 2001 at 13:35 UTC. The results show that the standard cloud mask method does not properly classify scenes over the ice/land areas and marks them incorrectly clear. b. Improved methods are able to determine there is cloud in McMurdo Sound over the ice.

2. Principal Component Analysis Method

Principal Component (PC) Analysis (PCA) provides another means for depicting features in the

satellite imagery (Hillger 1992, 1994, 1996). This section describes the method, and offers one

of the first attempts to apply this method for depicting Antarctic fog/low clouds. PCA is often

performed on a dataset to reduce the redundancy in it – as is the case with the MODIS multi-

spectral observations. It is also used to bring out features in the dataset, which is the objective

here.

a. Method

The Hillger approach (Hillger 1996) takes multiple spectral channels of a sample satellite observation, and determines the principal component "images" (PCI) for a given number of input channels. It was originally applied toward imager and especially the multi-channel sounder on the GOES satellite series. The first PCI depicts the features from the original observation that explain the most variance of the data and the features that are most common in the input channels. Similarly, the second PCI depicts the features from the observation that explain the second most variance of the data, and typically the differences between the input channels (Hillger 1996). Higher order PCs usually depict noise and other differences between the input channels. In its application here, the PCA provides information on variance spatially and spectrally, and does not offer the additional temporal variance that most Empirical Orthogonal Function (EOF) analyses accomplish. The procedure for generating PC of any data set uses the following outline (Anton 1987; Smith 2002; Hillger personal communications, 2007). The example here will be given with reference to a single field-of-view three channel multi-spectral satellite observation.

1. Calculate a single covariance matrix using each spectral channel (ch):

$$\text{cov}(ch_1, ch_2) = \frac{\sum_{i=1}^{n}(ch_1 - \overline{ch_1})(ch_2 - \overline{ch_2})}{(n-1)}$$

$$\text{cov}(ch_2, ch_3) = \frac{\sum_{i=1}^{n}(ch_2 - \overline{ch_2})(ch_3 - \overline{ch_3})}{(n-1)}$$

$$\mathrm{cov}(ch_1, ch_3) = \frac{\sum_{i=1}^{n}(ch_1 - \overline{ch_1})(ch_3 - \overline{ch_3})}{(n-1)}$$

etc.

The subscripts 1, 2, and 3 refer to the input channels of the satellite observations. All of the combinations of covariances for the three channels are computed, hence in this case, 9 combinations. These covariances are done between each of the channels that are included in the PCA, as well the variances of the channels (found along the diagonal below)) and used to create a covariance matrix (A):

$$A = \begin{vmatrix} \mathrm{cov}(ch_1, ch_1) & \mathrm{cov}(ch_1, ch_2) & \mathrm{cov}(ch_1, ch_3) \\ \mathrm{cov}(ch_2, ch_1) & \mathrm{cov}(ch_2, ch_2) & \mathrm{cov}(ch_2, ch_3) \\ \mathrm{cov}(ch_3, ch_1) & \mathrm{cov}(ch_3, ch_2) & \mathrm{cov}(ch_3, ch_3) \end{vmatrix}$$

2. Find the eigenvalues (λ) of the covariance matrix (A):

$$\det(\lambda I - A) = 0$$

where I is the identity matrix, and det is the determinant.

3. Find the eigenvectors (x) paired with each eigenvalue (λ):

$$(\lambda I - A)x = 0$$

4. From the matched pairs of eigenvectors and eigenvalues, reorder the eigenvectors (x) by the eigenvalues (λ) ordering them from highest to lowest value. The reordered eigenvectors (x) form the eigenvector matrix (E).

$$E = \begin{vmatrix} e_{11} & e_{12} & e_{13} \\ e_{21} & e_{22} & e_{23} \\ e_{31} & e_{32} & e_{33} \end{vmatrix}$$

5. Create the PCI for each channel using the transpose of the feature vector times the original data of each channel. Hillger's application of PCA utilizes the formula:

$$PCI = E \times CH$$

Where CH is the input channel data from the satellite observations, E is the eigenvector matrix and PCI is the resultant principal component imagery. A more specific formulation is a linear combination of the input channels of data from the satellite. The following is the case for 3 satellite channels:

$$\begin{vmatrix} pci1 \\ pci2 \\ pci3 \end{vmatrix} = \begin{vmatrix} e_{11} & e_{12} & e_{13} \\ e_{21} & e_{22} & e_{23} \\ e_{31} & e_{32} & e_{33} \end{vmatrix} \times \begin{vmatrix} ch_1 \\ ch_2 \\ ch_3 \end{vmatrix}$$

$$pci1 = (e_{11} \times ch_1) + (e_{12} \times ch_2) + (e_{13} \times ch_3)$$
$$pci2 = (e_{21} \times ch_1) + (e_{22} \times ch_2) + (e_{23} \times ch_3)$$
$$pci3 = (e_{31} \times ch_1) + (e_{32} \times ch_2) + (e_{33} \times ch_3)$$

The above method describes how the 3 input channels of observations are transformed into PC images. PCI1 image shows the commonalities among the input observation channels. PCI2 and PCI3 reveal differences between the input observation channels.

b. Example PC Imagery and Analysis

Using the same example fog event discussed in the prior sections, Figure 52 shows the first, second and third PCI created from using only three input channels from MODIS. For comparison, Figure 53 shows the input imagery used in making the PCI shown in Figure 52. The images in Figure 52 are the result of the PC analysis and are not a specific channel or band of the MODIS observations. The input observations offer a variety of strong features that come through in the PCA. Clearly seen in the first principal component in Figure 52, the ice surface has a strong representation along with other features found in the infrared window imagery seen in Figure 53c. In contrast, the second principal component focuses on the visible portions of the spectrum (much like what is seen in Figure 53a) while the third is a mix of information from the channels – nearly matching some of the prior example enhancement methods for fog and low clouds.
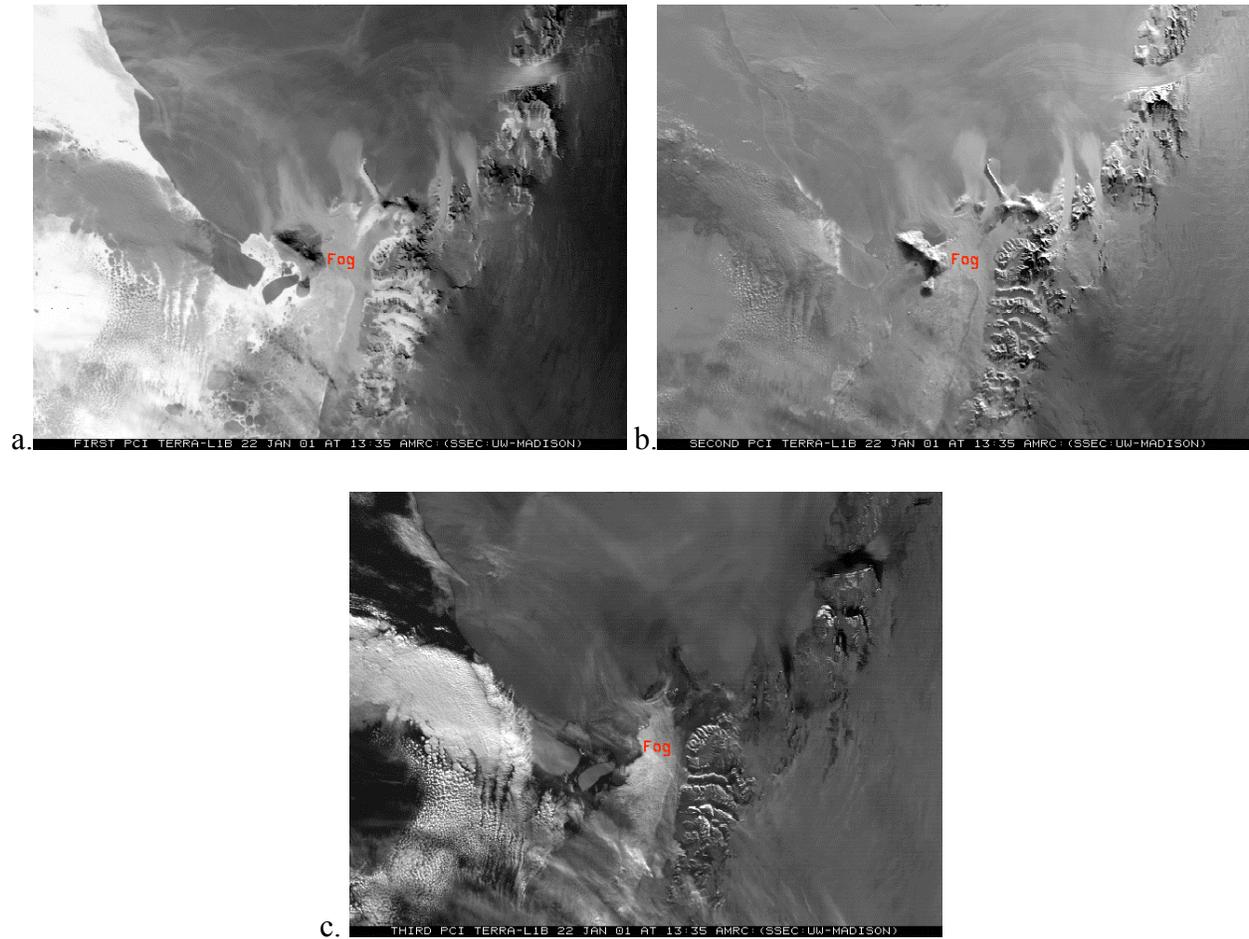
Figure 52. The first (a), second (b), and third (c) PC images generated from three channels from MODIS. The area with fog is labeled in each of the displays.
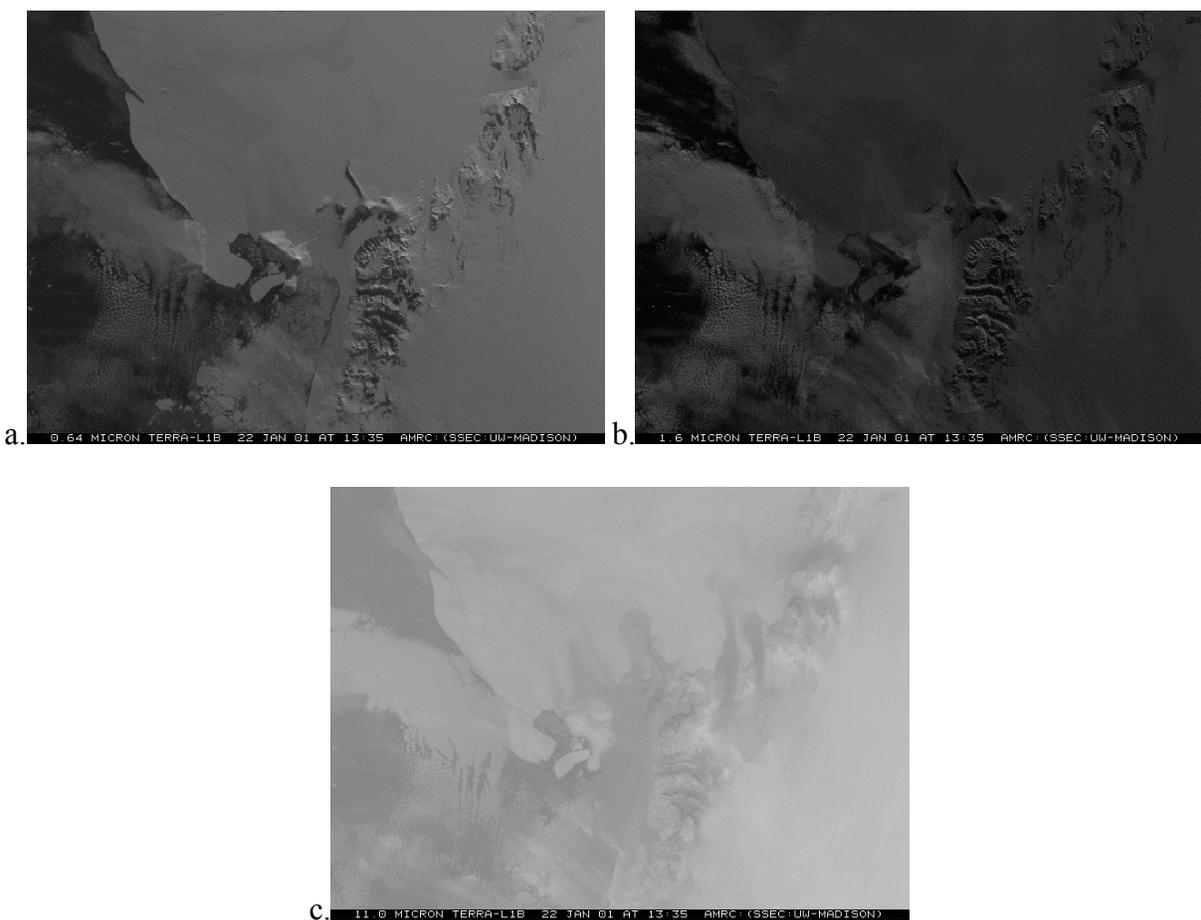
Figure 53. These are the three input channels to the PCI shown in Figure 52: a) 0.64 μm, b) 1.6 μm, and c) 11.0 μm. All images are not enhanced or contrast stretched.

In addition to the PC imagery itself, two graphical displays Figure 54 highlight the level of contribution of each spectral band used in individual PCI components and the amount of variance explained by each PCI component. These are PCI transformation vectors (Hillger 1996) and the figure offers two views of this information: from the PCI point of view and from the spectral band point of view.

In Figure 54a, the left vertical axis denotes the three principal components and on the opposing right axis is the percentage of the explained variance by the corresponding PC. The

curves in the figure represent the different spectral channels or bands that went into the PCA. On the horizontal axis is the level of contribution by each of the spectral channels or bands, which is scaled from negative one to positive one. The importance is the level of contribution – the absolute value – rather than the sign. This style of graph offers several characteristics of the PCA. For example, the level of explained variance that corresponds to each principal component is readily apparent. In Figure 54a, the first PC has 83.0 percent of the variance explained, 10.3 percent for the second PC, and 6.72 for the third. Reading across the first PCI, the visible spectral channel (band one) offers a fairly large negative contribution to this PC, the near-infrared channel (band 6) offers no contribution, and lastly the infrared window channel (band 31) offers a maximum positive contribution. As can be seen in the original data, much of this PCI is an additive of the emission from the infrared window channel and the reflection from the visible channel. In fact, if the brightness counts of this figure are inverted, it closely resembles the original infrared window seen in figure 53c, with enhancements from the reflected visible information.

In Figure 54a, the right vertical axis and horizontal axis remains the same as in Figure 54a, however, the left axis is now the contributing spectral channels or bands and the curves are the PCIs. This is the same information, but now displayed with respect to the input data. With this alternative view, the values of the explained variance on the horizontal axis are representative of where each PCI gets its contributions. In the case of the curve labeled 1 for the first PCI, the maximum positive contribution in that PC is from band 31, with no contribution from band 6 and a large negative contribution from band 1. In following this interpretation for the third PCI, the curved labeled 3 in Figure 54b shows how this PCI has a maximum positive

contribution from band 6, no contribution from band 1, and a nearly no contribution from band 31. This PCI "enhances" the depiction of the fog as labeled in Figure 52, as well as the other cloud areas. In Figure 54b, the vertical axis labeling of the explained variance notes how much of the variance in the analysis source is from the corresponding spectral channel on the left side of the graph. Hence, band 1 (visible), 40.3 percent (%) of the explained variance in the analysis originates from this spectral channel. The infrared window channel contributes to 52.5% of the explained variance in this analysis, while the near infrared channel offers 7.3% of the explained variance. In this example case, the infrared window and visible channels are dominant. The near infrared channel offers a small but important contribution as the differences that come out of the PCA help to better depict the clouds and fog.
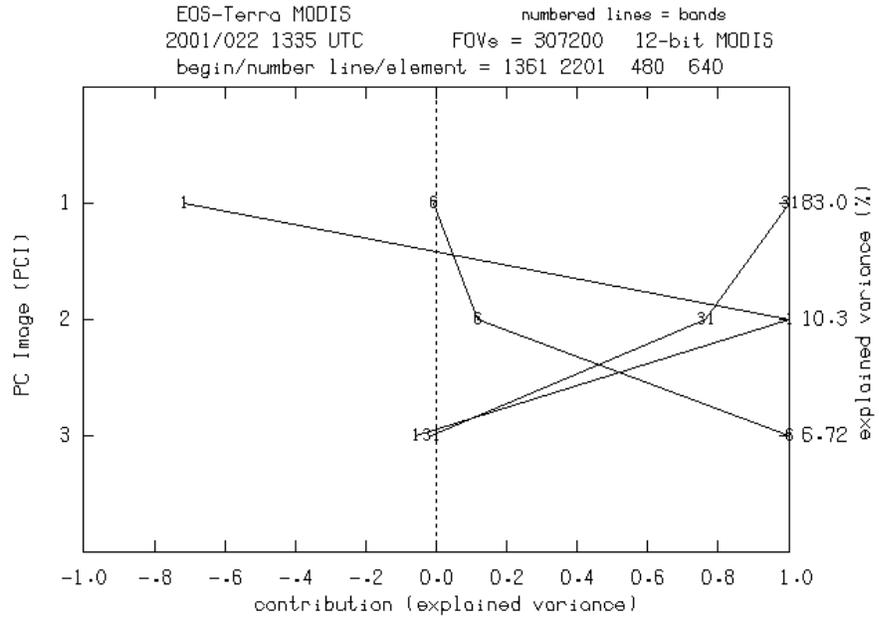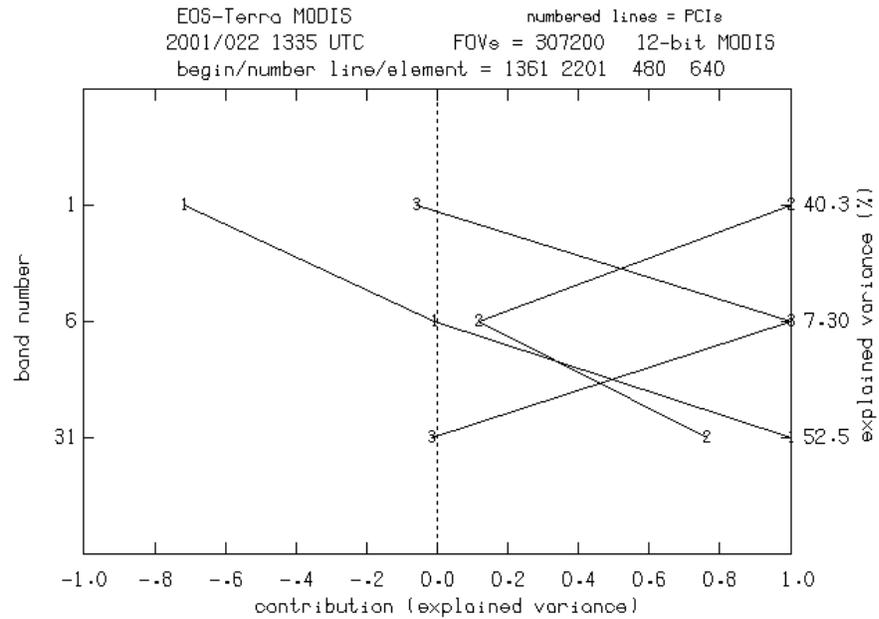
Figure 54. a. PCI transformation vectors represented via curves of the spectral channel or bands and b. via curves of the principal components.

c. Initial Input Channel Selection

In applying this procedure to fog depiction, a selection of specific spectral channels from the MODIS satellite observations were used rather than attempting to employ all 36 channels. Some of the 36 channels are not able to contribute to fog depiction such as the ocean color channels, and carbon dioxide channels for upper troposphere applications. This initial reduction in channels chosen is based on ability of the channel to show fog or contribute in some way to low-level moisture and low cloud determination. Table 9 lists the pre-selected channels chosen for testing fog depiction via PCA. A more complete description of the MODIS sensor can be found in Appendix A. The selected input channels are not only solely based on their physical capability to detect fog, but on their ability to do so differently. This offers the potential for the PCA process to come up with the best middle to low ordered PCI (such as the second or third PC) that will offer the best depiction of the fog.

Channels were selected from the portions of the spectrum observed by MODIS: in the visible, near-infrared, short wave infrared and infrared window. All of these selections have the capability of sensing to the lowest part of the atmosphere. Long-wave infrared channels were not selected due to their weighting functions peaking at higher levels of the atmosphere. (Baum and Platnick, 2006) The visible channel selected, 0.64 μm, will contribute via its reflectance of liquid water off of clouds, especially low clouds and fog. Three channels selected in the near infrared include, 1.24, 1.62, and 2.11 μm. This portion of the spectrum has absorption by liquid water found in the low clouds and fog. Reflectance of snow especially at 1.62 μm is low helping to depict low level water clouds and fog over snow. Two channels in the short-wave infrared,

3.78 and 3.97 μm, offer the combined solar reflection and infrared emission. In the Antarctic, during the austral summer, solar zenith angle even at the peak of the summer season will not have the solar reflection component maximized to the degree it is in middle and tropical latitudes. Finally, the infrared window channels, 11.0 and 12.0 μm, will offer pure emission of the low cloud and fog. Together, these channels tested via PCA offer the opportunity for the middle and low order PC (such as components 2 or 3) to provide some of the key differences between the channels that will be able to depict the low clouds and fog. The differences here are not simple spectral channel differences, but differences that fall out of the PCA process.

Table 9. A table of selected MODIS (on Terra) spectral bands tested in the PC method.

MODIS Channel or Band	Central Wavelength (microns)	Detection Properties	Atmospheric Radiative Properties
1	0.64	Visible Channel – clouds and land features	Reflectance of liquid water
5	1.24	Near infrared – land use	Absorption of liquid water
6	1.62	Near infrared – cirrus cloud features, land use, mineral discrimination	Absorption of liquid water, low reflectance of snow
7	2.11	Near infrared – land use	Absorption of liquid water
20	3.78	Shortwave infrared – fog and low clouds	Solar reflection and infrared emission
22	3.97	Shortwave infrared – fog and low clouds	Solar reflection and infrared emission
31	11.0	Infrared window – clouds, surface skin temperatures	Infrared emission
32	12.0	"Dirty" infrared window – sea surface temperatures and low level moisture.	Infrared emission

d. RGB PCI Fog Depiction and Final Input Channel Selection

Initial attempts tested a PCA on all eight of these channels. Extending the spectral color band combinations discussed above, tests of RGB combinations of the top three principal component images were created merging most of the explained variance into one depiction display. Figure 55 shows a combination of the first three components combined via an RGB combination (as described above). As an alternative, Figure 56 is the combination of just the first two principal components, with twice the weighting (via both red and green) on the second component image. The results reveal that this method could provide an alternative means for enhancing features including fog, as the fog and low cloud features in the image are subtly distinguished from other features in the field of view. However, investigation of the higher order PC images not shown here revealed that much less meteorological information and more noise was present. Hence, multiple combinations of the selected channels were tested for this example case (used throughout this chapter) to determine the best selection of channels from the collection to include in a PC depiction of the fog and low clouds. As a side note, both Figures 55 and 56 reveal that the white-blue enhancing of the low cloud and fog layers is also seen on the exposed, non-snow or ice covered land features along the Transantarctic Mountains. Since the near infrared channels used in this analysis are sensitive to minerals, this portion of the depiction indicates areas of the mountains that are snow free.
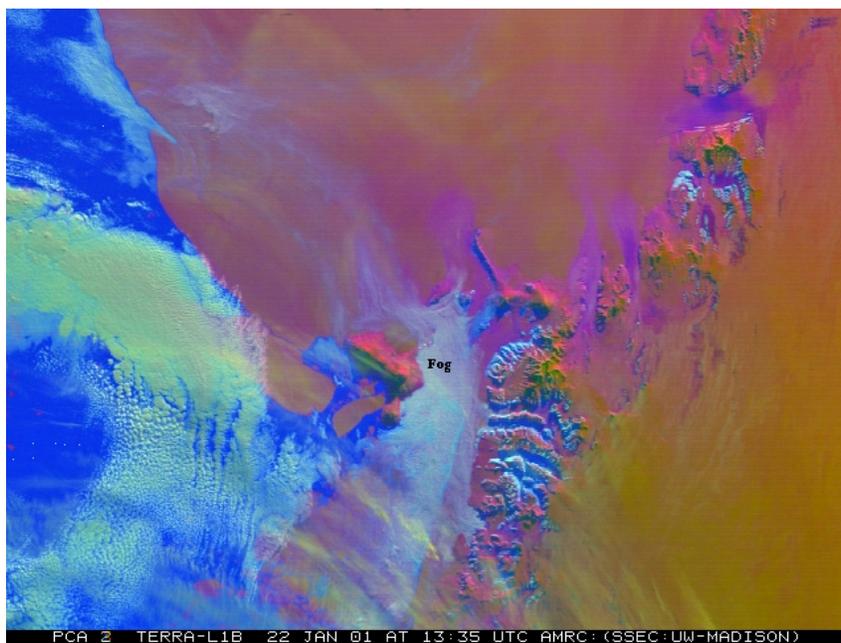
Figure 55. A RGB color combination of the first three principal component images shows fog and other features are enhanced.
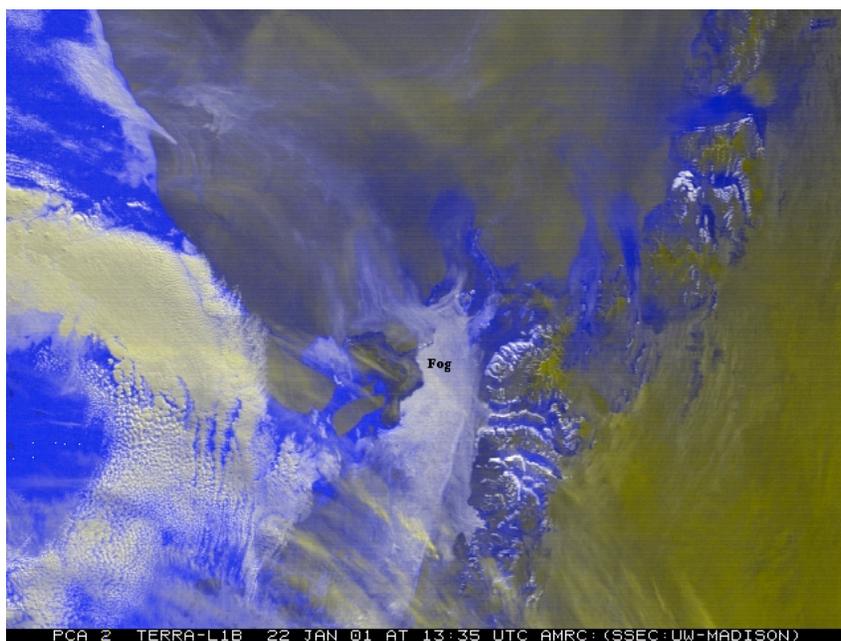
Figure 56. This is the same display as in Figure 55 with the RGB color combinations using only the first two principal component images. The weighting favors the second principal component, which is used in both green and blue.

As seen in Figure 51c, the application of only three MODIS spectral channels, chosen from the pre-selected list in Table 9, will generate one PCI display that may provide some enhanced depiction of the fog and low cloud region in the example test case. Hence, several combinations of three or more input spectral channels that resulted in at least one PCI visually depicting fog were examined. Example combinations include channels such as 1, 20, 31; 1,6,31; 1,6,20; 6,20,31; 1,6,7,31; and 1,6,7,20,31. A sample of the combinations with the best PCI depiction of fog and corresponding contributions are listed in Table 10. When considering the results of testing these combinations, some cases had the second PCI providing the best fog depiction and others offered the best depiction in the third PCI. Both the level of contribution and the visual ability to highlight fog were used in finding an optimum set of spectral channels.

Table 10. This summary table offers a sample of several combinations of spectral channel contribution values output from the PCA method. The contributions listed correspond to the best PCI visual depiction.

MODIS Band or Spectral Channel PC Input Combinations	Best PCI Visual Depiction	Band or Spectral Channel Contribution (scale -1 to +1)							
		1	5	6	7	20	22	31	32
1,5,6	2	-.562	.299	1.00					
1,5,20	2	-.001	.526			1.00			
1,6,7	2	-.079		1.00	.920				
1,6,20	2	.538		1.00		.791			
1,6,31	3	-.239		1.00				-.118	
1,6,32	3	-.233		1.00					-.110
1,7,20	2	.828			1	.954			
6,7,20	2			1.00	.753	-.371			
6,20,32	2			-.631		1			-.669
7, 20, 31	2				1.00	.505		-.425	
5,6,31	3		-.381	1.00				-.282	
1,6,20,31	2	.560		1.00		.477		-.531	
6,7,20,31	2			1.00	.886	.398		-.316	
1,6,7,22,32	2	.680		1.00	.858		.272		.358
1,6,7,20,31	2	.553		1.00	.861	.56		.061	
1,2,5,6,7,20,22,31,32	2	.496	.959	.84	.409	.328	.688	.663	.946

The final selection balances the visual depiction with a moderately low ordered PC and input channels offering critical contributions. Tests with some channels, such as band 32, provided results similar to using band 31. Other pairs of channels exhibiting this behavior included bands 20 and 22, and bands 1 and 2 (not all shown here). Hence, the redundant channels were removed from the selection (bands 22 and 32 in this case). Tests of the near infrared channels, bands 5, 6 and 7, resulted in band 6 offering the biggest impact, followed by band 7. The limited impact of band 5 led to its elimination from the final selection. Despite these eliminations, it is possible other combinations of spectral channels can and will provide similar results. One reason to eliminate extra channels that do not add information is to reduce computation time, although with the continued increase in speed of desktop computing, this is less of an issue in recent years. The final selection uses bands 1, 6, 7, 20, and 31 (Figure 57). This combination of spectral channels offers the best visual depiction of fog in the second PCI. Since band 6 is not available on the MODIS instrument on the Aqua satellite due to the degraded detectors for this channel, this combination is adjusted to either include band 5 observations in place of band 6 or even reduce the input channels to the remaining four.
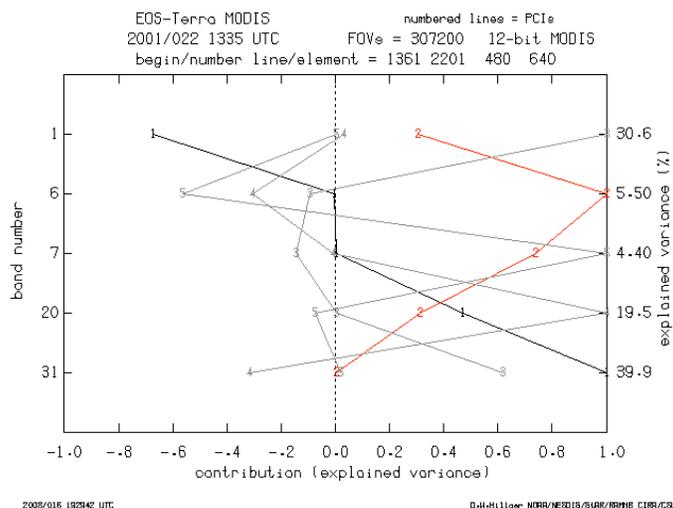
Figure 57. The PCI transformation vectors for input channels of 1, 6, 7, 20, and 31 for the test fog case. The first PCI is highlighted in black and the second PCI is highlighted in red, The different contributions these two PCI lead toward an RGB PCI Fog depiction.

As discussed above, a combination of the first, second, and third PCI through red, green and blue color combinations provides a means of being able to offer a depiction that includes characteristics of more than one PCI. Figure 58 shows the combination of first three PCI (PCI 1 - blue, PCI 2 – green, and PCI 3 – red) from our five-channel input. Here, the first PCI brightness representation is inverted before the RGB combination. However, with the third PCI having less variance explained, and little enhanced depiction of the fog and low clouds, an alternative combination, of only the first two PCI (PCI 1 – blue, PCI 2 – green, and PCI 2 – red) is shown in Figure 59 and one display with the first PCI brightness representation is inverted and one display without. The first PCI contains so much of the infrared window channel signal and some of the low clouds and fog signal, and when combined with the second PCI, which was one of the best depictions of low cloud and fog, provides a display that gives the fog and cloud features an appealing white color while having the ice features, so strongly seen in infrared imagery, blended

into the blue or sepia shaded background. This is the method of choice, RGB PCI, for the depiction of fog in the remainder of this project.
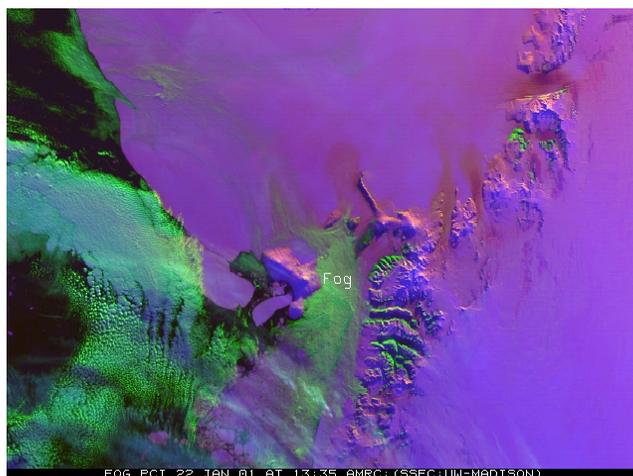
Figure 58. Fog depiction shown via a combination of the first three PC: Red: PCI 3, Green: PCI 2 and Blue: PCI 1.
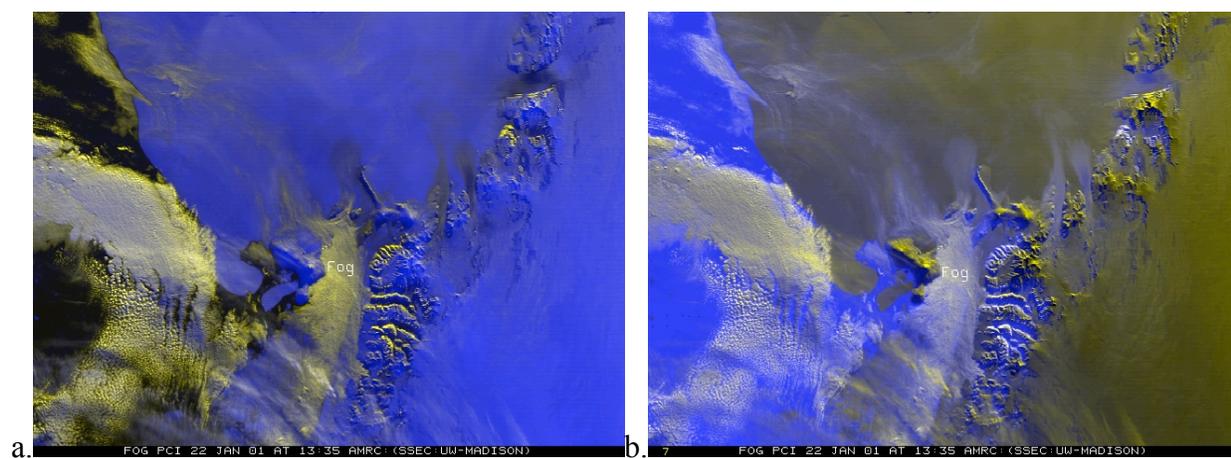
Figure 59. The RGB PCI depiction of fog and low cloud in this image is displayed via the combination of the first and second PCI: PCI 1 - blue, PCI 2 - green and red: Part (a) of the figure has the first PCI's brightness representation inverted, while in (b) the first PCI does not have this inversion.

e. Validation and Limitations

An abbreviated exercise was conducted to determine the validity of the RGB PCI fog product. Ten fog cases were used to test how well spatially the product compared to relative humidity observations from the AWS network. Although it is difficult, using the AWS network, to discern high relative humidity causes, as precipitation, blowing snow and fog (King and Turner 1997, Knuth 2007) are all plausible, it is the only spatially available independent observation network available for this informal validation. Figure 60 shows an example of how well the RGB PCI fog depiction compares to AWS relative humidity observations for approximately the same time.

The ten validation cases consisted of 105 satellite scenes centered on Ross Island and McMurdo. The region covered an area roughly 450 km (north/south) by 600 km (east/west). Scenes were selected in the 12 to 48 hour before the densest fog for each case. A breakpoint of 90% relative humidity from the AWS observations was used for the validation criteria. It is important to note that the relative humidity measurement has an accuracy of only +/- 5%, and can drift after installation. Hence, this selection of 90% may be too conservative in some situations.
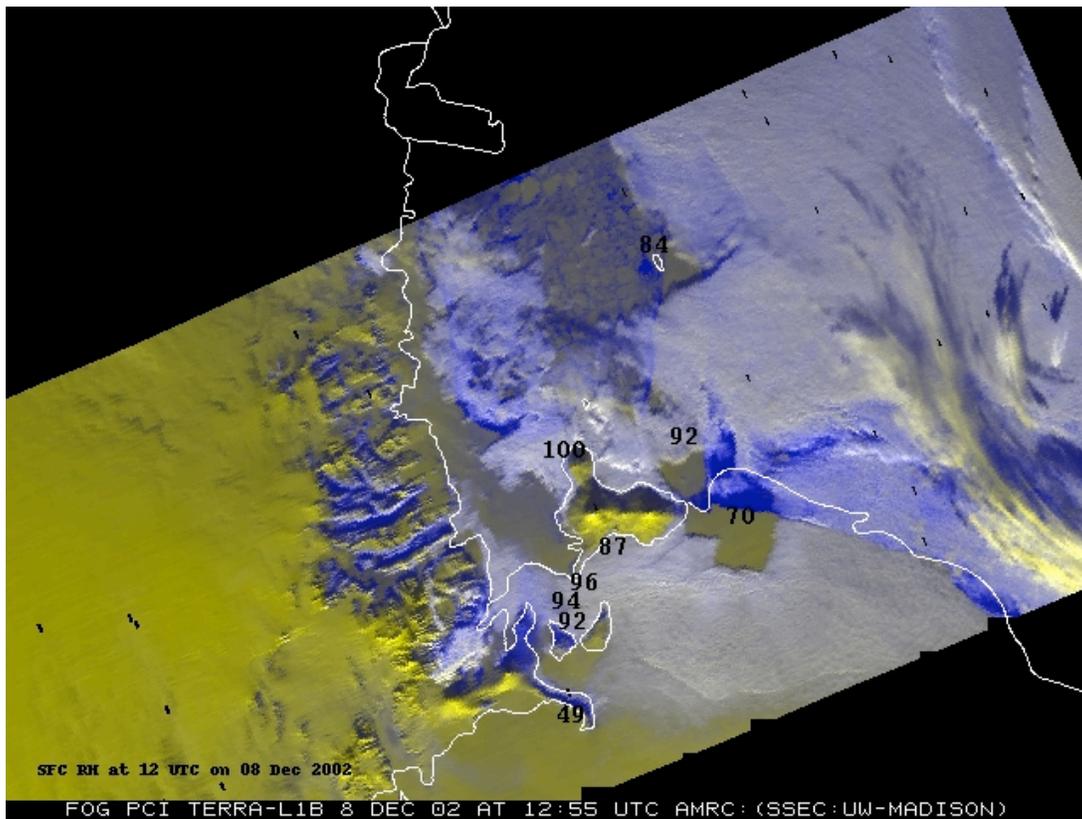
Figure 60. A sample RGB PCI fog depiction image with relative humidity observations from the AWS network plotted. Notice the high relative humidity reports occurring at AWS stations within the enhanced/highlighted white fog/low cloud regions, while there is lower relative humidity at Laurie II AWS, reporting 70%, in a clear region without fog. This example also shows the sepia tone ice background.

The procedure involved dividing the satellite data into regions that indicate fog and those that do not indicate fog. Next, the AWS observations were used for each of those types to determine if the observation matched or "hit" the satellite observation or did not match or "missed" the satellite observation. Hence, for regions that the satellite indicated fog/low cloud, a "hit" would be a match of the collocated AWS observations greater than or equal to 90% relative humidity. Conversely, a "miss" would be a relative humidity observation below 90% collocated

with the satellite indicating fog.   For regions the satellite does not indicate fog/low cloud, a "hit" denotes an AWS observation that matched with a value less than 90% while a "miss" indicates an AWS observation that did not match with an unexpected relative humidity greater than or equal to 90%. Approximately 903 AWS observations were used in the 105 scenes over the ten cases.

The results of the analysis are summarized in Table 11. From the perspective of the satellite indicated clear or "dry" regions, the method validated fairly well, with 287 AWS observations agreeing with the satellite observations with only 53 misses. Of those misses, some may be due to slight lags between the AWS observation time and the satellite observation time. Hence there are "near" misses, with some observations being very close to being proper observations of fog/low clouds. From the point of view of the satellite indicated fog/low cloud, the results of the validation on the surface has the satellite no better than a 50-50 chance of a correct depiction. However, this validation requires the consideration of comparison. The satellite is a topside view and cannot distinguish between fog and low cloud, for example. If there is a case of low cloud, the 3 meter tall AWS can very likely be correctly recording drier conditions in the layer of air below a low cloud deck. Of the 226 fog misses, some could be an indication of low clouds. Although this method cannot distinguish between the two, a low cloud deck can still violate landing criteria for classes of aircraft that utilize the airfields in the McMurdo area (e.g. C-17) Additionally, the accuracy of the relative humidity data and the possible issues with drift add to the uncertainty in this validation.

Table 11. Validation results of AWS relative humidity observations as compared to RGB PCI satellite observations.

Fog/Low Cloud Hit	Fog/Low Cloud Miss	Clear/Dry Hit	Clear/Dry Miss	Uncertain
223	226	287	53	114

The satellite depiction, as noted, does have limitations. An additional limit is the dependency on solar zenith angle. The performance of RGB PCI fog depictions during October is clearly impacted by the very low solar zenith angle.   This impact affects visual interpretation (Figure 61). This skews the peak months of usage toward the core austral summer months of November, December, January and February. There is some value to the depiction in the low light months of October and March; however, its interpretation will be different than the other months of the operational field season.
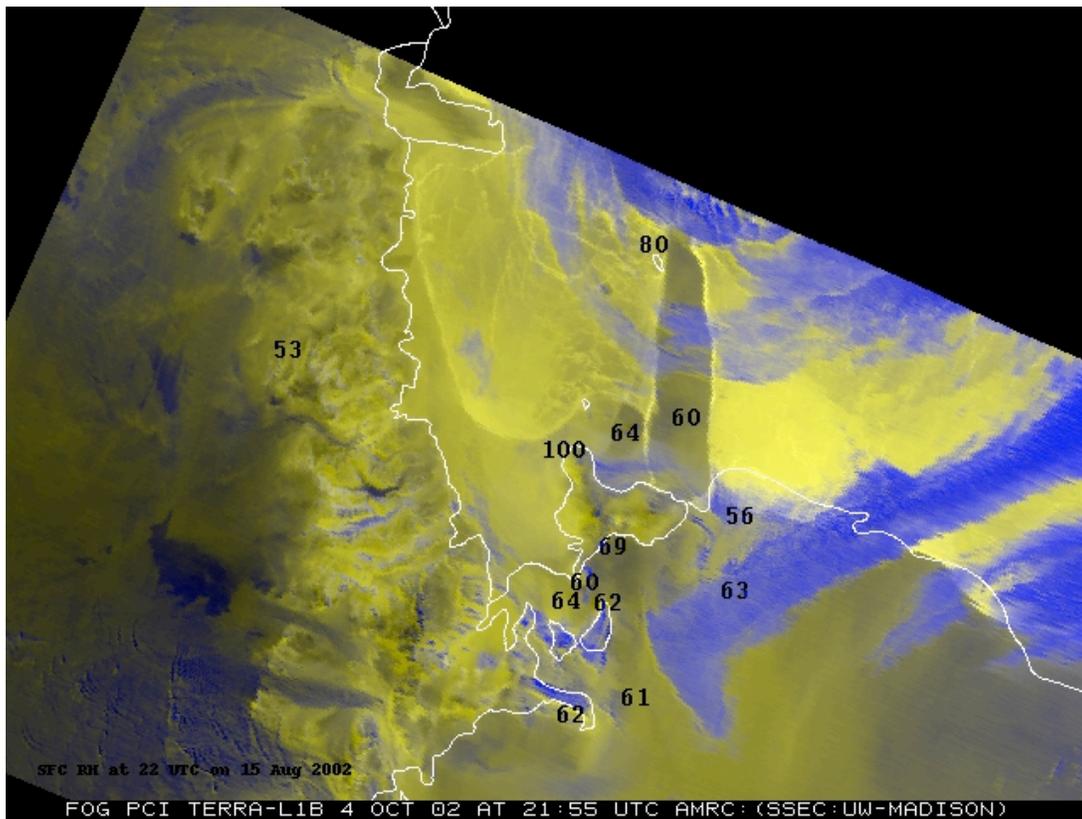
Figure 61. An example of an RGB PCI fog depiction that illustrates how the low zenith angle impacts the depiction and altering enhancement. In this case, suspected fog and low cloud areas are blue with the ice background in sepia tones.

3. Discussion

While single and two-channel methods will continue to have their place in monitoring fog, the multi-spectral tests introduced here present a step forward in the detection and depiction of fog and low clouds. The RGB PCI fog depiction provides a new and alterative approach to the SOFOS method. However, multi-spectral tests need more scrutiny to determine their value in an operational setting. The RGB PCI depiction method as outlined here does not perform the same

in low solar zenith angle periods of the year, and not all in the polar night. It will also have difficulty discerning between fog and other low clouds, but does have some skill to identify low cloud/fog features that can impede aviation operations. SOFOS method may work throughout the year, however, it requires ancillary data that the RGB PCI depiction method does not require. This is a clear advantage operationally in the USAP as there is limited bandwidth to off continent resources, such as not being able to acquire complete numerical model output that might be required by other determination methods. In any case, RGB PCI depiction does offer a means of accenting the features, and will be used in the next section as an areal depiction of fog in the Ross Island region as the behavior of fog is outlined.

Chapter 5: Fog Cases and Situation

With a climatological description of Antarctic fog and its relationship to the environment and armed with an improved satellite depiction method of Antarctic fog, this knowledge is applied in concert with analyses from a numerical weather prediction system and a back trajectory model to gain a more complete understanding of fog and its behavior. This chapter reviews representative example cases of fog, identifies possible fog source regions and introduces additional examples that provide greater understanding of fog behavior in this portion of the world.

1. Back Trajectories – Searching for Source Regions

The review of several fog cases during the satellite validation exercise along with additional cases for a total of 23, reveal none of the examined cases in this project had any clear local formation of fog close to Ross Island area. Aside from the suspected frontal fog cases (approximately 7 where fog is associated with precipitation), and a few undetermined cases (3), 13 fog events appear to be advective in nature. Advective fog differs from advection fog, meaning that the advective fog forms in another region by a formation process and then the already formed-fog moves or advects to the airfields and McMurdo Station. Where does the fog form before moving into the Ross Island area? Back trajectories analysis offers one means to establish fog source regions.

a. HYSPLIT

The HYbrid Single-Particle Lagrangian Integrated Trajectory (HYSPLIT) model, available from the NOAA Air Resources Laboratory (ARL) offers a means of generating back trajectories. HYSPLIT is designed for air pollution and dispersion applications. Used in its basic form, it offers single particle forward or backward trajectories treated, in essence, as a parcel of air (Rolph 2003, Draxler and Rolph 2003). HYSPLIT version 4.8 used in back trajectory computations was initialized with conditions from the Global Data Assimilation System (GDAS) one-degree by one-degree resolution data. In only a couple of cases where input data was not available from the GDAS, 2.5 by 2.5 degree resolution NCEP/National Center for Atmospheric Research (NCAR) reanalysis data was used as an alternate initialization. All back trajectories were computed to end at the Williams Field AWS location (-77.866° South, 166.983° East). Families of back trajectories are computed with final altitudes of 50, 100, 250, 500 and 1500 meters above ground level. A 48-hour back trajectory family set included six back trajectories - one inserted every 2 hours prior to the final end time. In all cases, the model's vertical velocity was used. The ending back trajectory date and time was selected from 20 fog cases, to match the occurrence of the fog. With fog often reported over several hours, the lowest visibility (or densest) portion of the fog, as reported from surface observations at McMurdo Station, was used as the final time of the back trajectory.

b. Results

The results of the back trajectories are summarized in Table 12. The largest source region for air is from the Southern Ross Ice Shelf, with approximately half of the events having this characteristic (Figure 62). For 23 percent of the events, air originating purely from the East Antarctic Plateau, may often come through the dry valleys over McMurdo Sound (Figure 63). As seen in the family of back trajectories in Figure 64, source air from both the East Antarctic Plateau and the Ross Ice Shelf were found in over a quarter of the cases. Here within the family of 6 back trajectories, a mix of the two source regions is seen in these cases. Finally a unique case of air that originally was from the south of McMurdo Sound on the Ross Ice Shelf, but then circled over the Sound (Figure 65). Overall, if the two Ross Ice Shelf categories are combined, 72% of the air that leads to fog comes from the south and east of Ross Island.

Table 12. The source regions of back trajectories computed with the HYSPLIT model, revealing the source regions that contribute to fog.

Source region	Percentage Occurrence
Southern Ross Ice Shelf	45%
Southern Ross Ice Shelf & East Antarctic Plateau mix	27%
East Antarctic Plateau	23%
South with circle over McMurdo Sound	5%
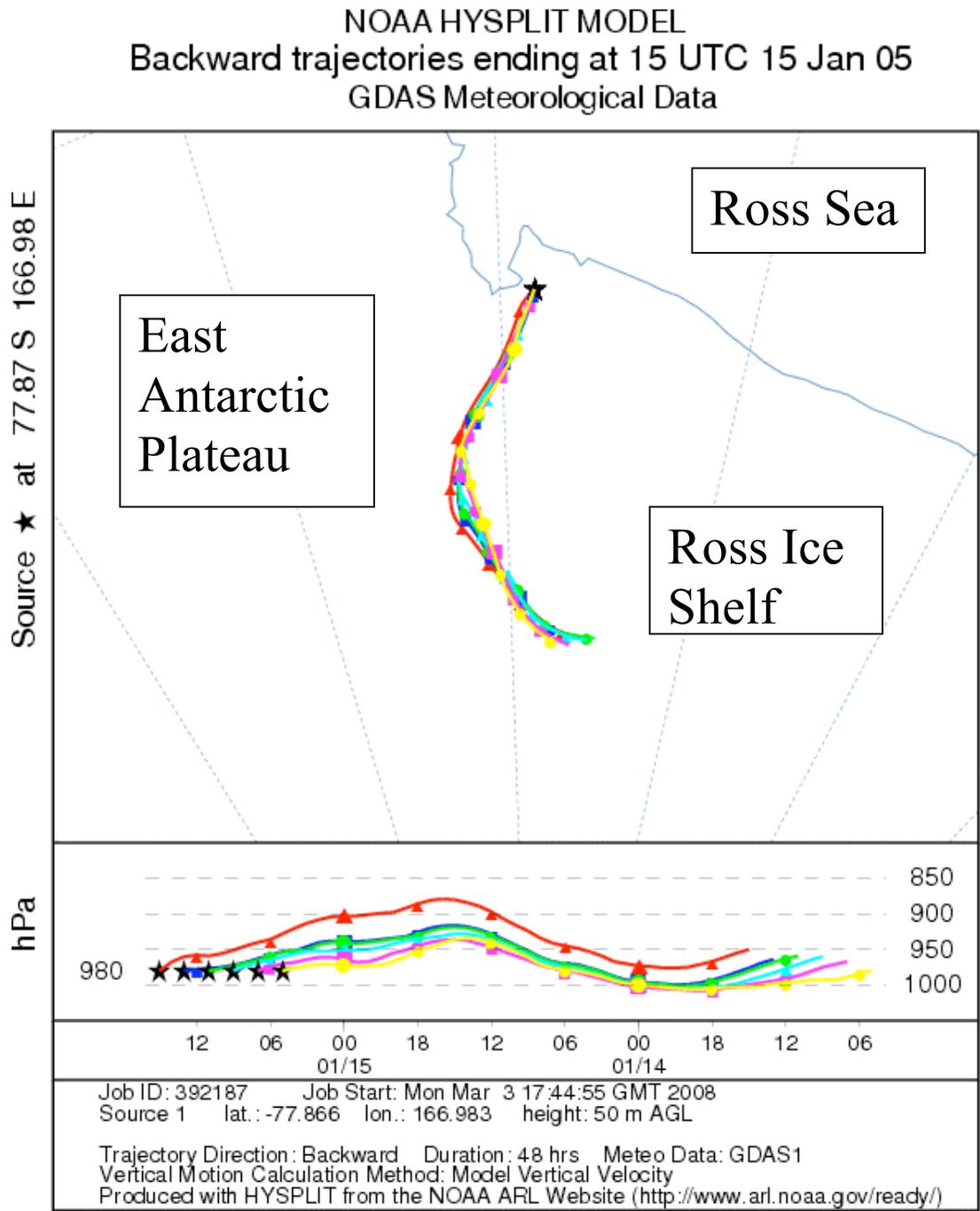
Figure 62. A family of six back trajectories, spaced two hours apart, with the last trajectory in red ending at the peak of the densest fog on 15 January 2005 at 15 UTC.
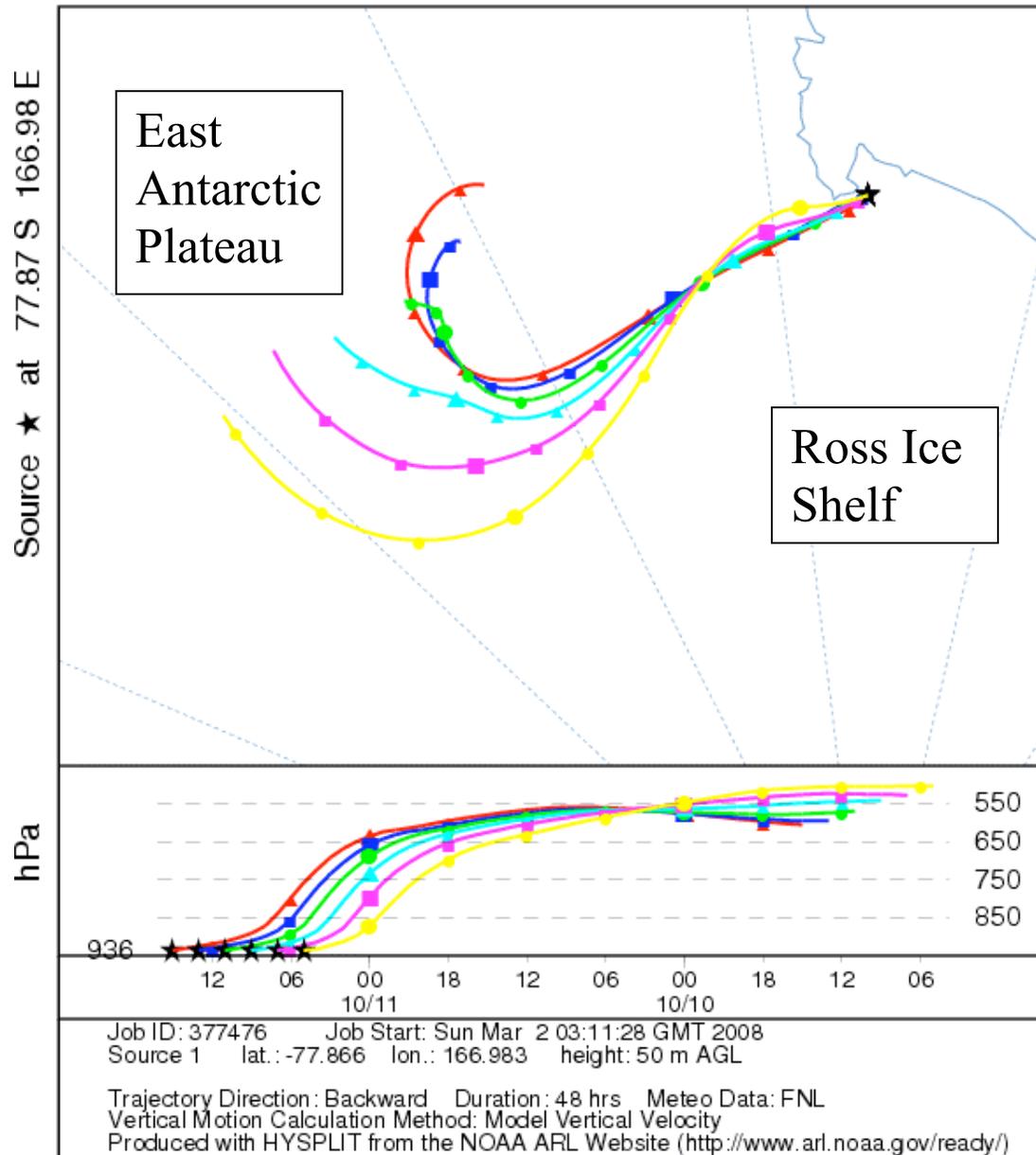
Figure 63. **A family of back trajectories with the source region over the East Antarctic Plateau.**
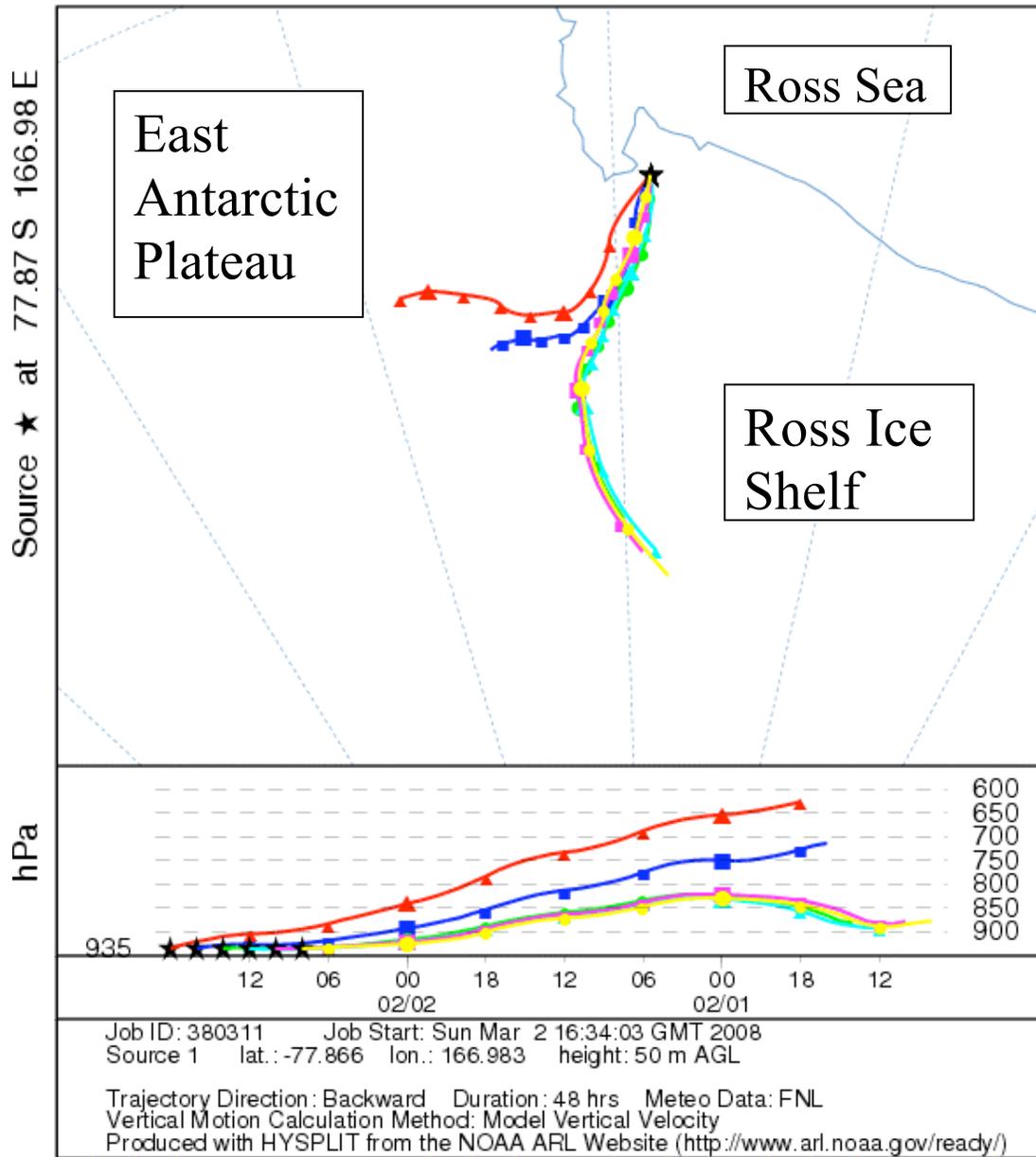
Figure 64. A family of back trajectories with two source regions: the East Antarctic Plateau and the Ross Ice Shelf.
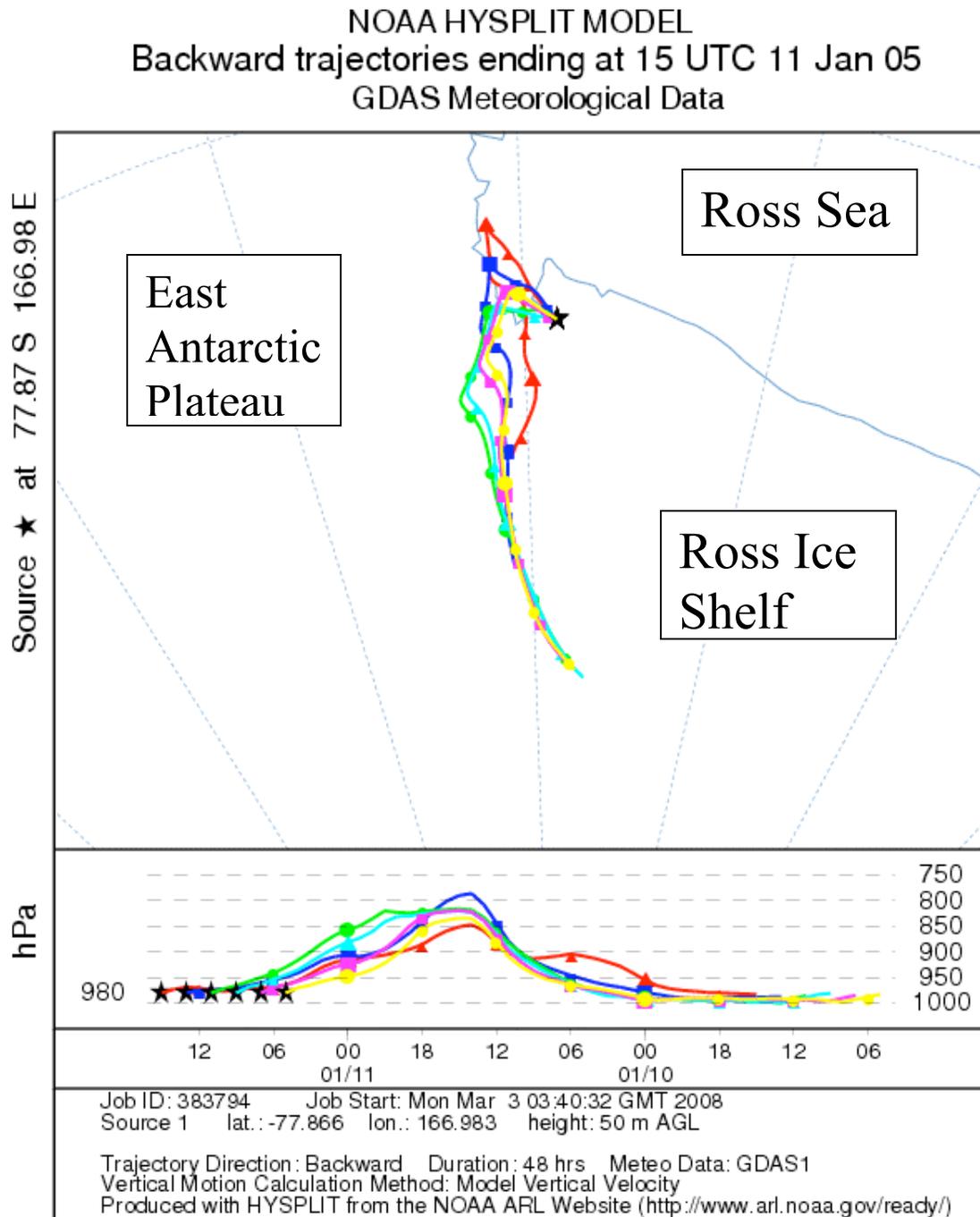
Figure 65. A family of back trajectories originating from the south and encircle the McMurdo Sound region from the north.

2. Antarctic Mesoscale Prediction System

The Antarctic Mesoscale Prediction System (AMPS) is based off of a version of the fifth generation Pennsylvania State University/NCAR Mesoscale Model (MM5) (Grell et al. 1995, Powers et al. 2003). Modifications have been made to the MM5 to improve its capabilities in the polar atmosphere (PolarMM5) and have been utilized over both the Arctic (especially over Greenland) and Antarctic (Bromwich et al. 2001, Cassano et al. 2001a, Cassano et al. 2001b). Key changes include revised cloud and radiation interactions, modified explicit ice phase microphysics, implementation of a sea ice surface type, improved treatment of heat transfer through snow/ice surfaces and optimized turbulence (boundary layer) parameterization based off of the NCEP Eta model (Bromwich et al., 2001, Manning personal communications, 2008). In the last two years, an Advanced Research Weather Research and Forecasting (WRF) model (Skamarock et al. 2005) was brought on-line in parallel with PolarMM5 (Manning 2006, Bromwich et al. 2006). The Polar WRF boundary layer is the Mellor-Yamada-Janjic turbulent kinetic energy scheme. Additional improvements made to both PolarMM5 and PolarWRF include better handling of heat transfer and snow surfaces and an added layer to the models with better upper boundary conditions. Additional changes to cloud physics schemes, land surface parameterizations, etc. have been under testing (Bromwich et al. 2006). Although skill between the models is similar on the synoptic scale, some differences still exist between the models with PolarMM5 able at times to outperform PolarWRF. For the remainder of this project, the PolarMM5 version of the AMPS will be primarily used in analyses here.

The AMPS model offers several domains including a 90-kilometer resolution hemispheric, 30-kilometer resolution Antarctic, 10-kilometer Ross Island, and 3.3-kilometer McMurdo domains. Additional domains have been added for other regions of the Antarctic including South Pole, and the Antarctic Peninsula. Starting in late 2005 the spatial resolution was increased for each of the domains to 60, 20, 6.7, and 2.2 kilometers respectively due to improved computing resources (Manning personal communications, 2008). The 30-kilometer (20-kilometer when available) domain is used here in this study due to its coverage area. In the vertical, the original 28 layers in AMPS were increased to 31 in 2003. The AMPS model is initialized with the real-time Global Forecast System (GFS) from the NCEP. Over the past decade additional datasets have been assimilated directly into AMPS including AWS observations and MODIS Polar Winds (Key et al., 2003). AMPS model output in gridded binary (GRIB) format was retrieved from the NCAR Mass Storage System (30/20 and 10/6.67 kilometer domains). Additional AMPS model output was utilized in this project and reprocessed into network common data format (netCDF) (30 and 20 kilometer domain).

This effort uses AMPS as an analysis tool. To gauge performance, the model output in the vertical was compared with the McMurdo Station radiosonde. Figure 66 is the same radiosonde shown in Figure 9 with the output from the AMPS model plotted in the pale colors and the radiosonde observations in matching bold colors. Here, the moisture profile from AMPS is in fair agreement with the observations. However, the low-level temperature profile is notably different between the observations and the AMPS model. The winds, especially the u-component, underestimate the actual observation in the boundary layer. Verification of model performance has been conducted (Monaghan 2003, Bromwich et al. 2005). Findings of these

studies suggest that AMPS has better verification statistics over larger domains, while able to maintain acceptable performance in the smaller, high spatial resolution domains. AMPS also does generally represent near surface winds well (Monaghan 2003), despite the example in Figure 66. While it is expected that AMPS will not be able to match the radiosonde in every detail, overall it captures the synoptic and broad mesoscale features.

McMurdo Radiosonde 17 January 2004 12 UTC
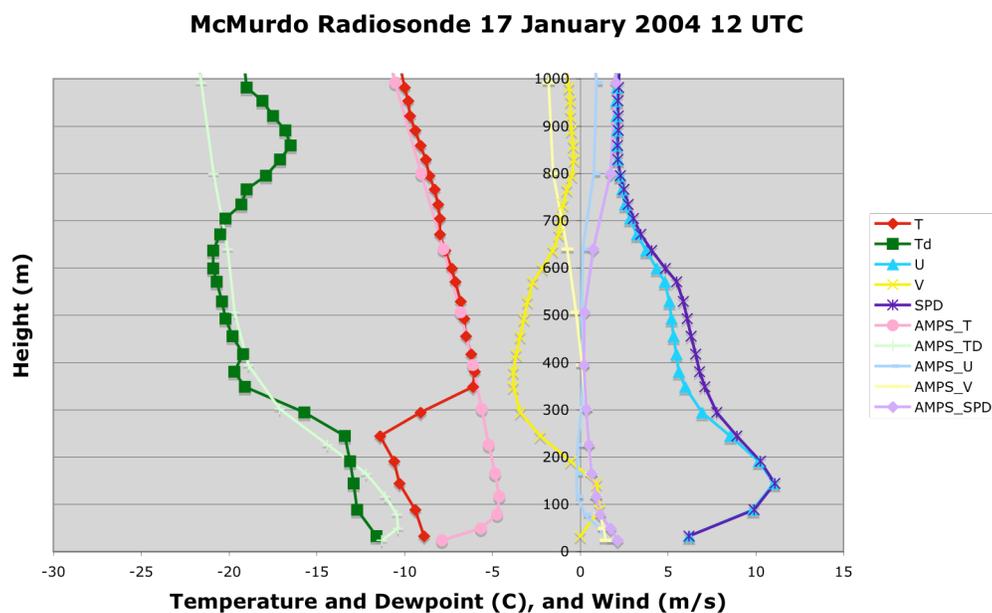
Figure 66. The same radiosonde sounding as in Figure 9, with the AMPS analysis valid for the same time.

3. Case Study: 22-24 January 2001

The 22-24 January 2001 fog case was directly observed by the McMurdo Weather forecasters (Cayette personal communications, 2001), and has been used in the prior sections as the example case to test the satellite techniques. This case represents a fog that has its origins from the

northeast of McMurdo Station. Although this case represents the minority of cases, this fog event significantly impacted aviation operations. The 3-day event caused the cancellation of 13 flights, the abort of 2 intercontinental flights after launch prior to point of safe return, and one flight was required to land in a designated "white-out" landing area due to the fog at the airfields (Cayette personal communications, 2001 and 2008).

a. Surface Observations

This fog event, observed at Williams and Pegasus airfields as well as McMurdo Station, began less than 24 hours after a snow event impacted the entire area. Mist and fog were first reported at Williams Field approximately 4 hours after the end of the snow event. However, this fog is short lived – lasting only two hours. The main fog event begins roughly 12 hours later just before 12 UTC on 22 January 2001, which is near local midnight (Figure 67, Table 13). Throughout the rest of the 22nd, fog continued to affect the airfields and McMurdo Station. Visibilities are reported as low as 100 meters at Williams Field (12-14, 18, 22 UTC 22 January 2001). At times, freezing fog is reported during this event. Freezing fog is defined as "a fog, the droplets of which freeze upon exposed objects and form a coating of rime and/or glaze" (AMS 2000); however, freezing fog may be reported regardless of deposition. There are some brief breaks in the fog near the 4 to 7 UTC time period as well as another at 12 UTC on the 23rd before a return to a mix of fog and mist. Freezing fog and fog returns in earnest from 13 UTC on the 23rd to the end of the event at 13 UTC on the 24th.

Due to the weather situation and operational status, weather observers were not assigned continuous duty at Pegasus field during this period. This resulted in a very limited set of observations from that airfield. Pegasus observations are a reflection of the observations made at Williams Field – visibility of 100 meters in fog and freezing fog (13-16 UTC 22 January 2001). McMurdo Stations synoptic observations also mirror Williams Field's observations; however the observing period of 3 hours offers fewer details than the airfields. All of the manned observing is consistent with those from the AWS in the region; however, since the majority of the fog came from the north primarily over McMurdo Sound, few AWS sites were able to observe it directly or were not equipped to observe it (e.g. Marble Point AWS site does not have a relative humidity sensor). As expected, winds at most surface sites are from the northern sector during the event. At the end of the event, winds switch back to the east at speeds up to 10 kts to as much as 20 kts and, the direction observed was the same as before the event began. Altimeter setting and station pressure during the event is seen to be decreasing. This is an indication that air is moving away from Ross Island during the event, which decreases the pressure locally. However, a review of additional fog cases finds that this is not always the rule for northwest advective fog situations.
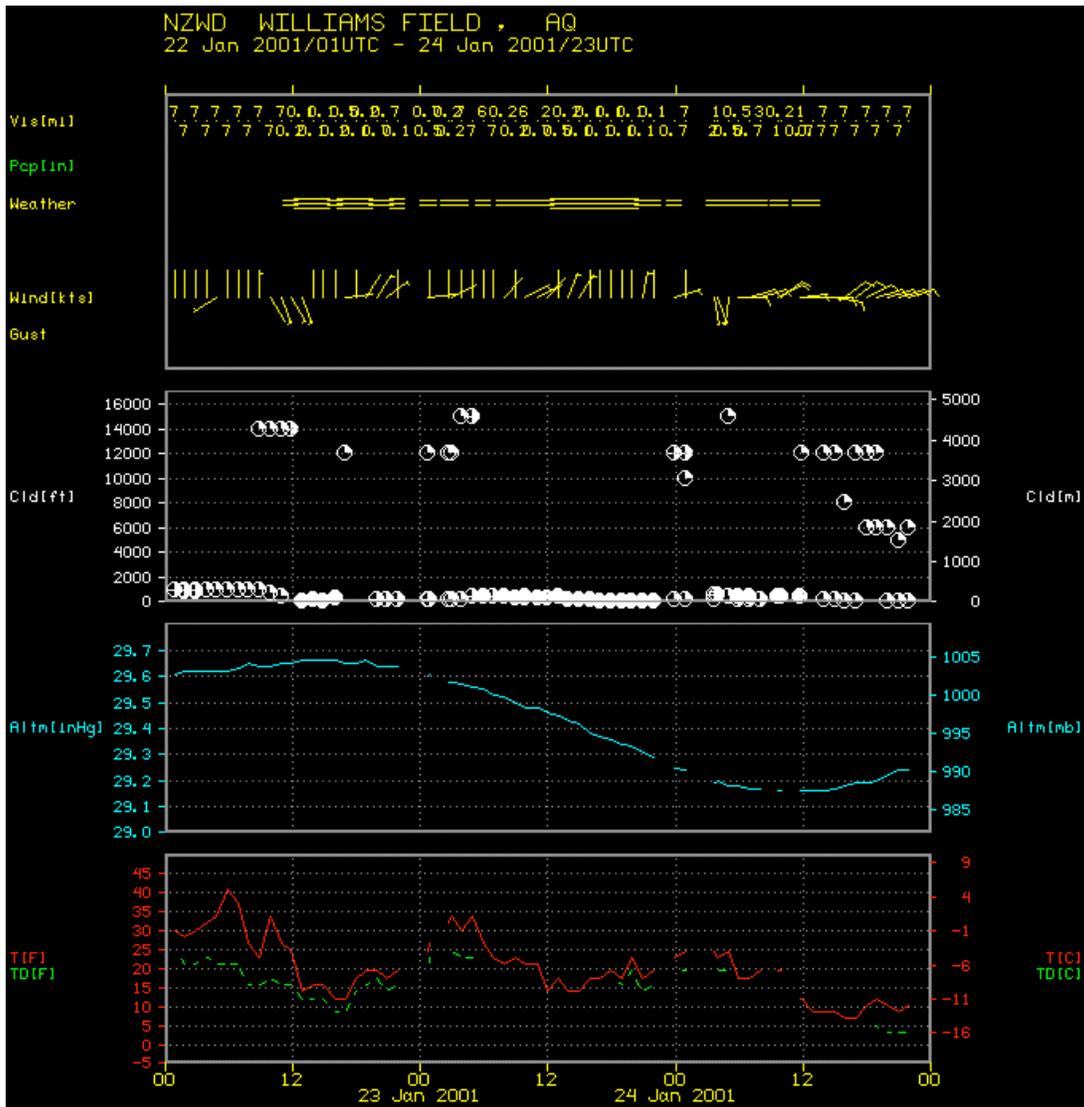
Figure 67. A meteorogram of the Williams Field surface weather observations during the fog event, 1 UTC 22 January through 23 UTC 24 January 2001.

Table 13. Synoptic observations from McMurdo Station, 22-24 January 2001.

DAY [CYD]	TIME [HMS]	T [C]	PST [hPa]	SPD [KTS]	DIR [DEG]	VIS [KM]	WX1	WXP	CA	ZCB [m]
2001022	0	-3.2	998.1	0.0	0				5	150
2001022	30000	-3.2	998.3	2.9	230	11.0			7	450
2001022	60000	-2.6	998.7	4.9	320	11.0			1	450
2001022	120000	-2.9	999.5	4.9	260	11.0			4	250
2001022	150000	-4.8	999.8	3.9	320	0.4	F	F	6	150
2001022	180000	-4.1	999.4	0.0	0	0.4	F	F	8	75
2001022	210000	-2.9	999.0	0.0	0	11.0			6	150
2001023	0	-3.1	998.7	2.9	300	11.0			2	75
2001023	30000	-3.3	997.3	2.9	300	4.8			6	150
2001023	60000	-4.2	996.2	4.9	320	3.2	F	F	8	150
2001023	90000	-2.0	994.4	8.0	360	11.0			8	150
2001023	120000	-4.0	993.4	3.9	340	11.0			8	150
2001023	150000	-3.1	991.7	2.9	340	0.5	F			25
2001023	180000	-6.3	989.8	3.9	310	0.6	F	F	8	75
2001024	0	-5.2	986.5	0.0	0	0.8	F	F	8	2500
2001024	30000	-5.6	984.6	0.0	0	0.6	F	F	8	150
2001024	60000	-4.7	983.3	9.9	110	11.0		F	1	2500
2001024	90000	-4.7	982.3	19.8	80	11.0			1	2500
2001024	120000	-2.8	982.5	15.9	60	11.0			1	2500
2001024	150000	-6.0	982.4	19.8	80	11.0			1	2500
2001024	180000	-8.2	983.6	7.0	80	11.0			1	800
2001024	210000	-10.8	984.4	9.9	80	11.0			1	800

b. Radiosonde Observations

The radiosonde observation at 12 UTC on 23 January 2001 at the height of the fog, seen in Figure 68, captures a well-defined boundary layer. The profile reveals the three typical portions of the boundary layer. The lowest and very shallow layer is a surface or friction layer as seen in the lowest two observation points, denoted by the slower wind at the surface. The fog layer above the friction layer is marked with equal or nearly equal temperature and dewpoint measurements, only slightly cooling with height. This layer is approximately 200 meters thick.

This fog layer is also marked by nearly constant wind speeds with height; however, there is directional shear found toward the top of the layer as the wind backs toward the west. Above this layer is the inversion layer at the top of the boundary layer. The inversion layer is roughly 200 meters thick and is marked with the increase in temperature with height, while the dewpoint decreases dramatically with height. Winds peak at this point, likely reaching geostrophic values at the top of the layer (Stull, 1988). Above the inversion layer is the free atmosphere, where a dissimilar air mass with markedly different characteristics, is found.

McMurdo Radiosonde
23 January 2001 McMurdo Station 12 UTC
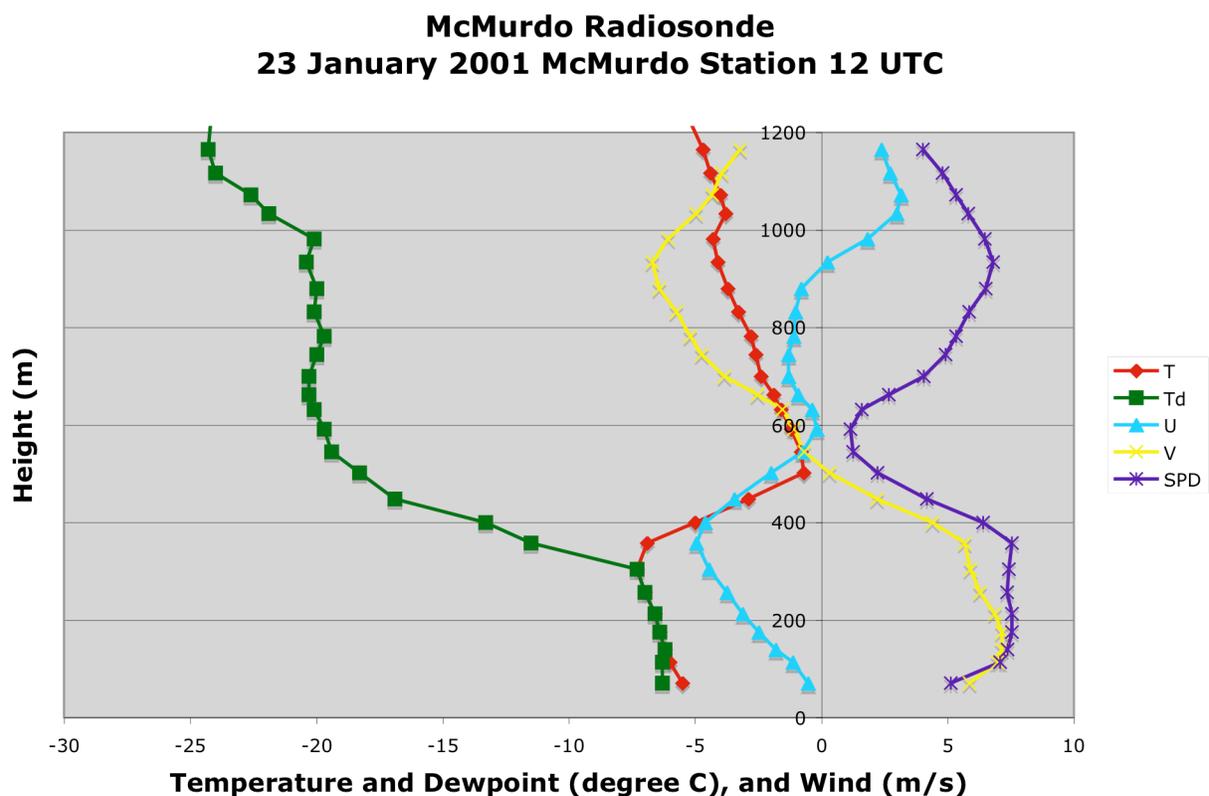
Figure 68. Radiosonde observation from 12 UTC 23 January 2001 exhibits the boundary layer structure during the peak of fog.

c. Satellite Observations

A review of Antarctic infrared composite satellite imagery with corresponding overlaid GFS model surface sea level pressure analysis provides the synoptic background in which the fog event takes place. Figure 69 displays the 22 January 2001 12 UTC satellite composite with the corresponding analysis. A weak pressure gradient is found in the vicinity of Ross Island. This conforms to the climate analysis and forecaster anecdotes of fog occurring primarily on the edges of high-pressure systems in weak pressure gradient situations. No strong synoptic-scale systems are influencing the western Ross Sea/Ice Shelf region.

Animations of the RGB PCI fog depiction show the fog source from the north and west of McMurdo Station, originating over McMurdo Sound just to the south of the Drygalski Ice tongue. With only Terra observations available for this analysis, a gap of several hours in orbital coverage leaves the source period of the fog formation unobserved. Figure 70 shows a sequence of RGB PCI images with the fog highlighted along with surface weather from the airfield(s) and matching relative humidity reports from the AWS network plotted as well. This sequence displays the complexity of fog in the region with other cloud systems in the field of view. Also noticeable is a second fog/low clouds bank in the last image to the east of Ross Island that forms also from the north of the island and is not associated with the stratocumulus clouds to the east over the southern Ross Sea.
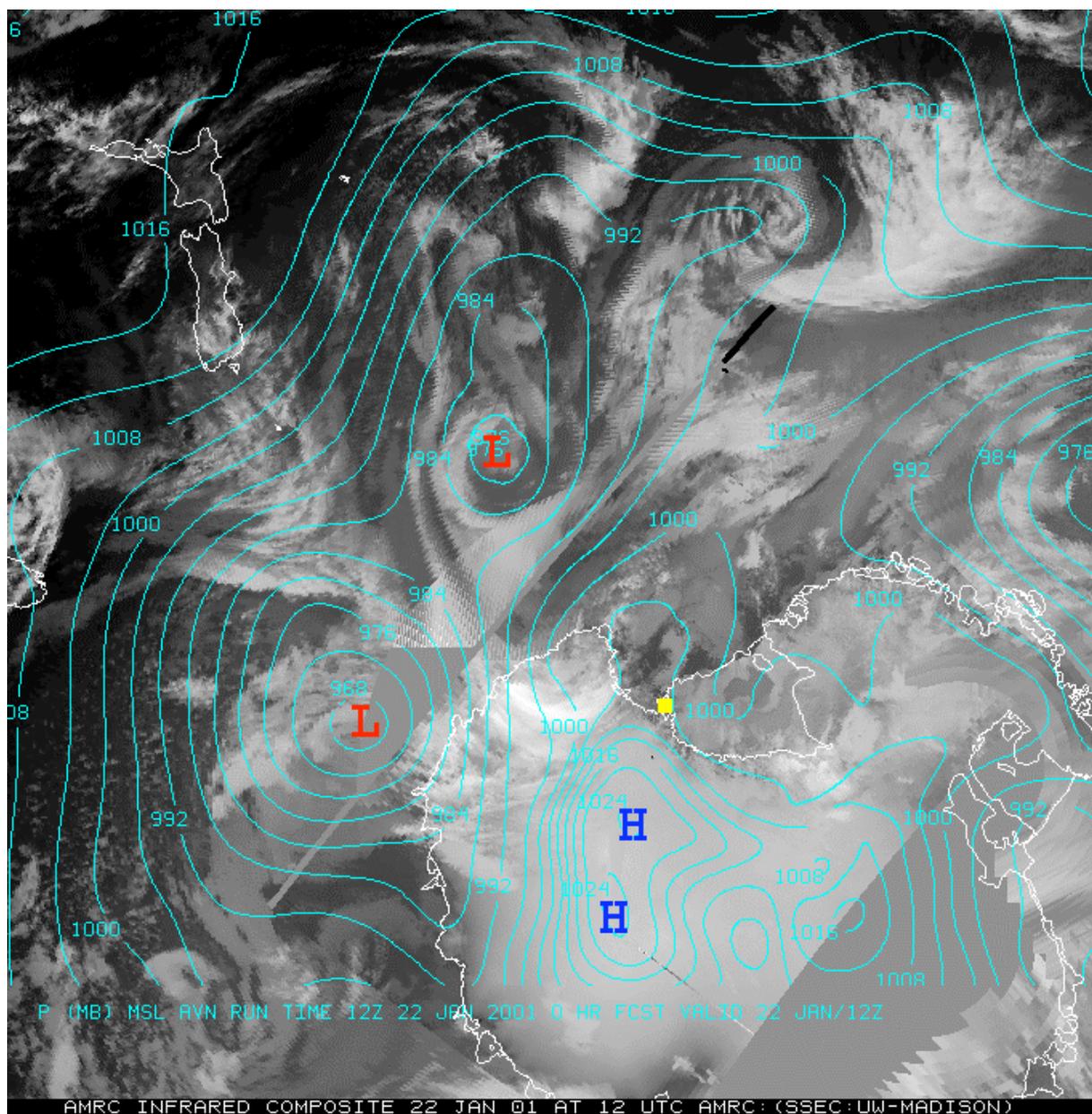
Figure 69. Antarctic infrared composite image from 12 UTC on 22 January 2001, just before the onset of the fog at McMurdo Station (marked in yellow), is plotted with the GFS surface isobaric analysis.
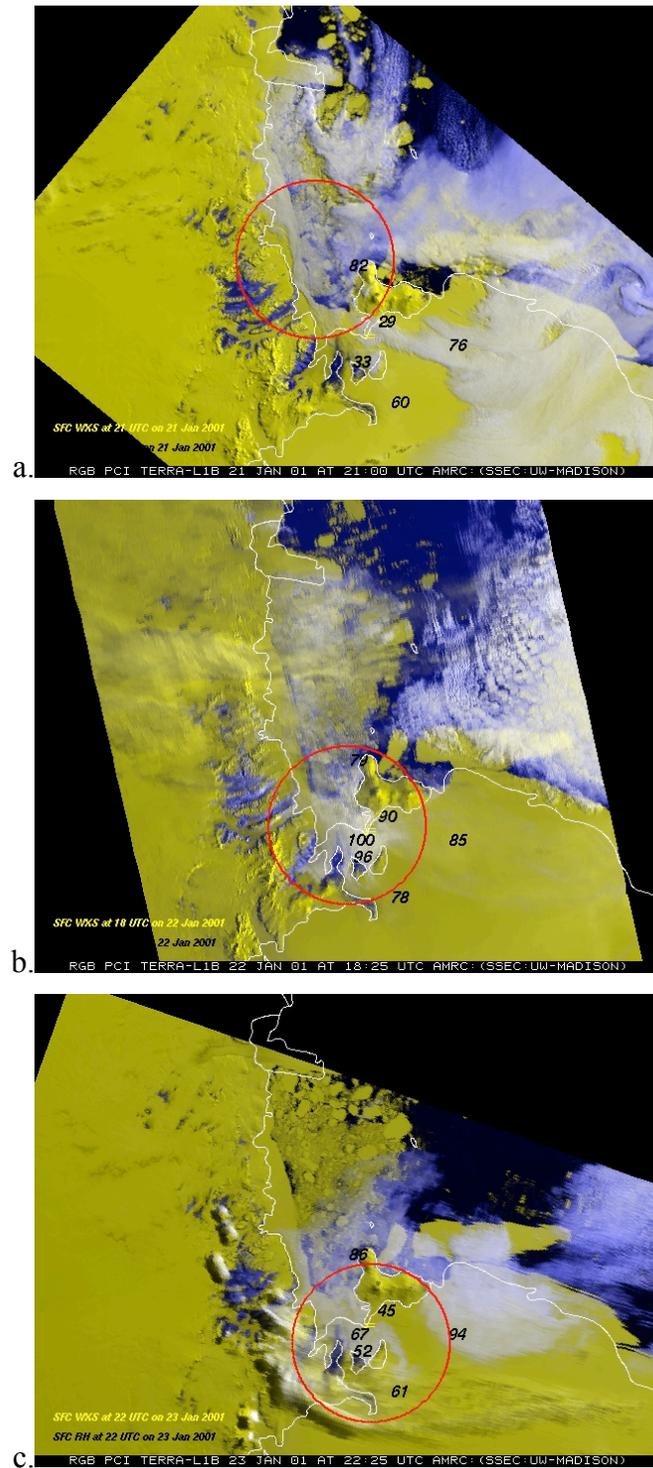
Figure 70. **RGB PCI satellite observation sequence of the fog over the McMurdo Sound region, 21 through 23 January 2001 along with surface weather from the airfields and matching relative humidity reports from the airfields. The red oval encircles the fog.**

d. Model Analysis

The back trajectory analysis of this case points to the source region for this fog coming from the East Antarctic plateau (Figure 71). This same signature is found at nearly all of the trajectories, regardless of the final altitudes above ground. The only variation was with the source of the air on the polar plateau. The more southern portion of Victoria Land was the source for the low altitude back trajectories (ending at 50, 100, 250 meters over Williams Field), while the northern portion of Victoria Land was the source for the higher altitude back trajectories (ending at 500, 1000, and 1500 meters over Williams Field). It is important to note that the back trajectory analysis is overly smooth, owing to the relatively low resolution of the initiating model fields used (GDAS) and very likely less detailed resolution of the topography in the region.

The AMPS model output used as an analysis verifies the airflow is off of the East Antarctic plateau, primarily down the David Glacier, and it then turns south as shown in Figure 72. This resulting situation has colder, drier plateau air flowing down from Victoria Land, over the open water of the northern McMurdo Sound, leading to fog formation along the fast ice edge of the Scott Coast. The fog then is advected towards the south, filling the southern part of McMurdo Sound, the McMurdo Ice Shelf, and affecting McMurdo Station and the nearby airfields, with fog. The weak pressure gradient in the region allows what forecasters term "glacial outflow" also known as a downslope flow or weak katabatic outflow from the higher altitude polar plateau. The proper environment at the base of the outflow along the Scott Coast leads to fog formation that then is advected south.
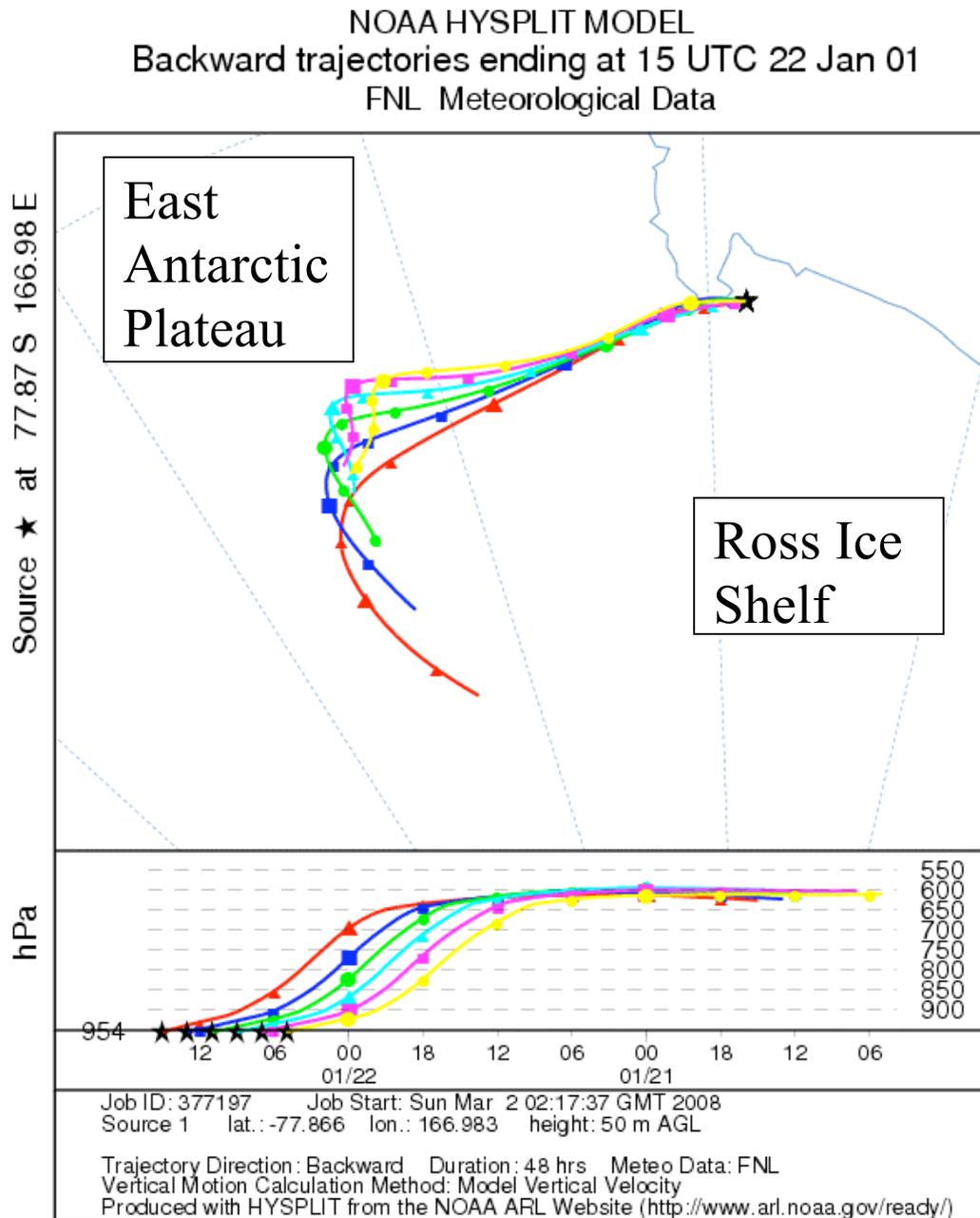
Figure 71. A family of back trajectories from the HYSPLIT model showing the source region for the air parcel from the East Antarctic Plateau.
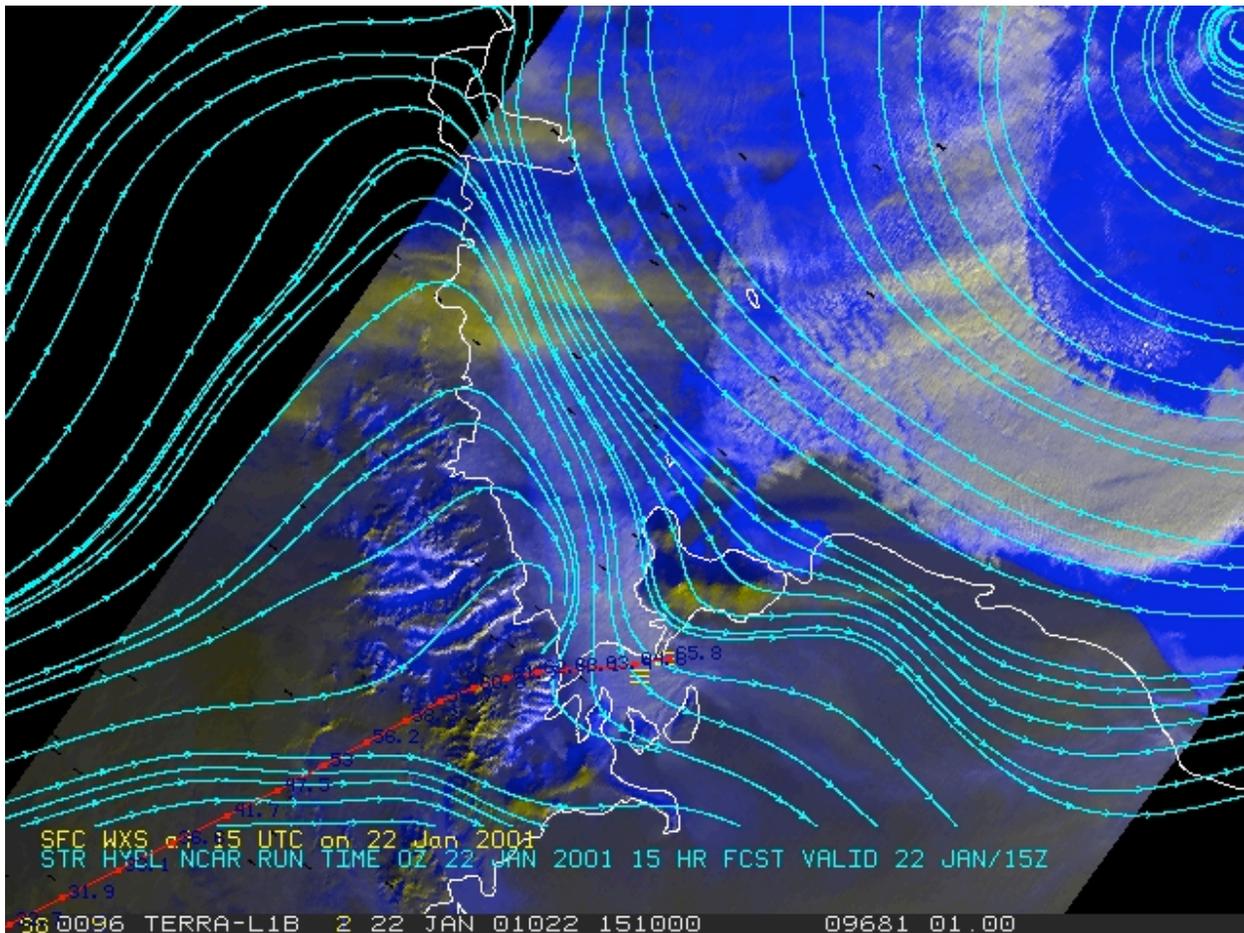
Figure 72. RGB PCI fog depiction from MODIS Terra at 15:10 UTC on 22 Jan 2001 shows the first onset of the fog event. AMPS streamlines from the second sigma level above the surface and the HYSPLIT model back trajectory with relative humidity are overlays on the satellite imagery.

4. Case Study: 24-25 January 2007

This fog case, occurring on Wednesday 24 January 2007 through Thursday 25 January 2007, represents an example of a fog event that is the more common type to affect the McMurdo region from the southeast. This event impacted aviation operations, canceling both regional and

intercontinental flights. As seen in Figure 73 and 74, this fog is shallow yet dense, and envelops Observatory Hill near McMurdo Station. Shortly after these photos were taken, McMurdo Station proper was encased in the fog, which affected the airfields the most with reduced visibilities.

Figure 73. Fog slowly consumes Observatory Hill on 24 January 2007 as a fog advects in from the south and east.
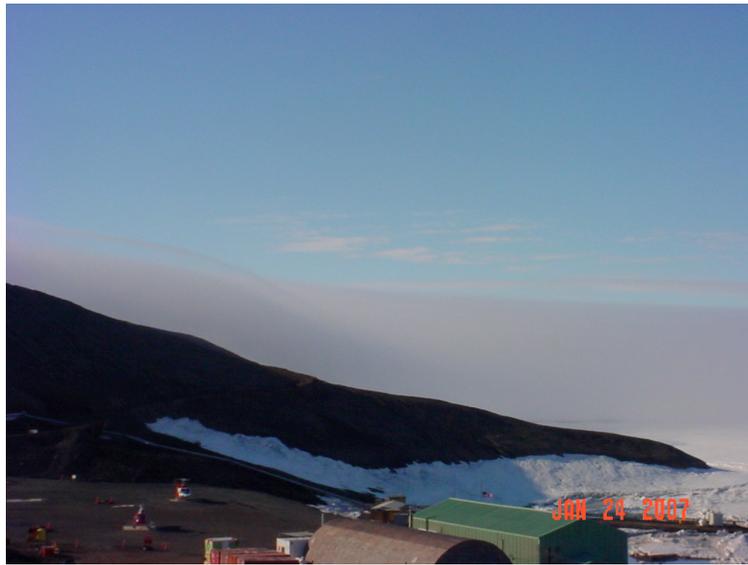
Figure 74. The 24 January 2007 fog event shows the depth of the fog as it flows around Cape Armitage at the foot of Observatory Hill with McMurdo helo pad in foreground.

a. Surface Observations

Surface observations from both operating airfields denote that this fog occurred on two days, with a break in between as shown in Figure 75. McMurdo observations do not reflect that, and instead indicate an on and off fog over the period (Table 14). Through the fog event, winds are from the eastern sector at 8 to 10 kts at Williams Field and 6 to 15 kts at McMurdo, and return to the northern sector at 3 to 8 kts after the event. Visibilities in fog and freezing fog are found to be as low as 200 meters in the first day of fog (20 UTC), and 100 meters on the second day (12 UTC). Unlike the prior case, this fog case has the station pressure and altimeter settings on the rise. This makes physical sense, as air is coming is from the south and east into Ross Island, and in effect "piles up" increasing the pressure locally. A review of additional fog cases did not find

a consistent pressure trend associated with southeast advective fog events, contrary to anecdotal

evidence (SPAWAR 2007a).

Figure 75. Surface observations from Williams Field from 11 UTC on 24 January 2007 through 5 UTC 26 January 2007.

Table 14. Table of surface weather observations from McMurdo Station on 24-26 January 2007.

DAY [CYD]	TIME [HMS]	T [C]	PST [hPa]	SPD [KTS]	DIR [DEG]	VIS [KM]	WX1	WXP	CA	ZCB [m]
2007024	0	2.9	983.4	8.9	350	11.0			3	800
2007024	30000	4.1	981.9	8.0	330	11.0			2	800
2007024	60000	3.8	980.9	9.9	350	11.0			2	1250
2007024	120000	1.8	979.3	0.0	0	11.0			1	2500
2007024	150000	2.6	979.0	0.0	0	11.0			2	25
2007024	180000	-4.4	979.3	7.0	100	11.0	F		1	450
2007024	210000	-6.2	980.0	15.0	100	11.0	F		1	2500
2007025	0	-3.9	981.4	11.8	100	11.0	F	F	3	2500
2007025	60000	-2.7	984.4	11.8	90	11.0			3	250
2007025	120000	-2.6	987.6	14.0	80	11.0	F	F	2	2500
2007025	150000	2.6	992.0	0.0	0	11.0	F		1	2500
2007025	180000	0.7	990.3	5.8	80	11.0		F	2	150
2007026	0	4.8	992.7	0.0	0	11.0		F	2	2500
2007026	30000	6.1	992.9	0.0	0	11.0			6	800
2007026	60000	1.8	993.6	8.0	310	11.0			6	2500
2007026	90000	0.1	994.1	4.9	310	11.0			6	2500
2007026	120000	-1.0	994.2	2.9	320	11.0			6	2500
2007026	150000	-0.2	993.7	2.9	0	3.2			0	1250
2007026	180000	2.8	993.7	3.9	280	11.0			7	2500
2007026	210000	3.3	993.6	3.9	180	11.0			1	2500

b. Radiosonde Observations

Weather balloon launches during the 2006-2007 field season suffered from reception problems leaving gaps in observations. Hence, the radiosonde in Figure 76 is from the closest successful radisonde launch during this fog case. As seen in Figure 75 and indicated in table 14, this case did have a break in the fog between the 24th and 25th of January The radiosonde shows the 00 UTC launch on the 25th, just as the first period of fog was coming to an end. Like many profiles

during fog, this profile is no exception with a shallow surface layer, a residual fog layer (where fog is dissipating), the inversion layer, and free atmosphere. Some critical differences in this profile include the peak wind occurring inside the boundary layer – just above the surface layer. This wind is likely topographically influenced, as the direction is from the northwest in the lowest part of the fog layer. The moisture profile shows a larger dewpoint depression in the lowest part of the fog layer and surface layer, with dewpoint depression decreasing toward the top of the residual fog layer and into the lowest portion of the inversion layer. The inversion layer actually has two portions denoted where the inversion changes slope in the temperature profile. This slope change corresponds to the dramatic shift in the dewpoint profile, where the upper portion of the inversion layer becomes much drier.

**McMurdo Station Radiosonde
25 January 2007 McMurdo Station 00 UTC**
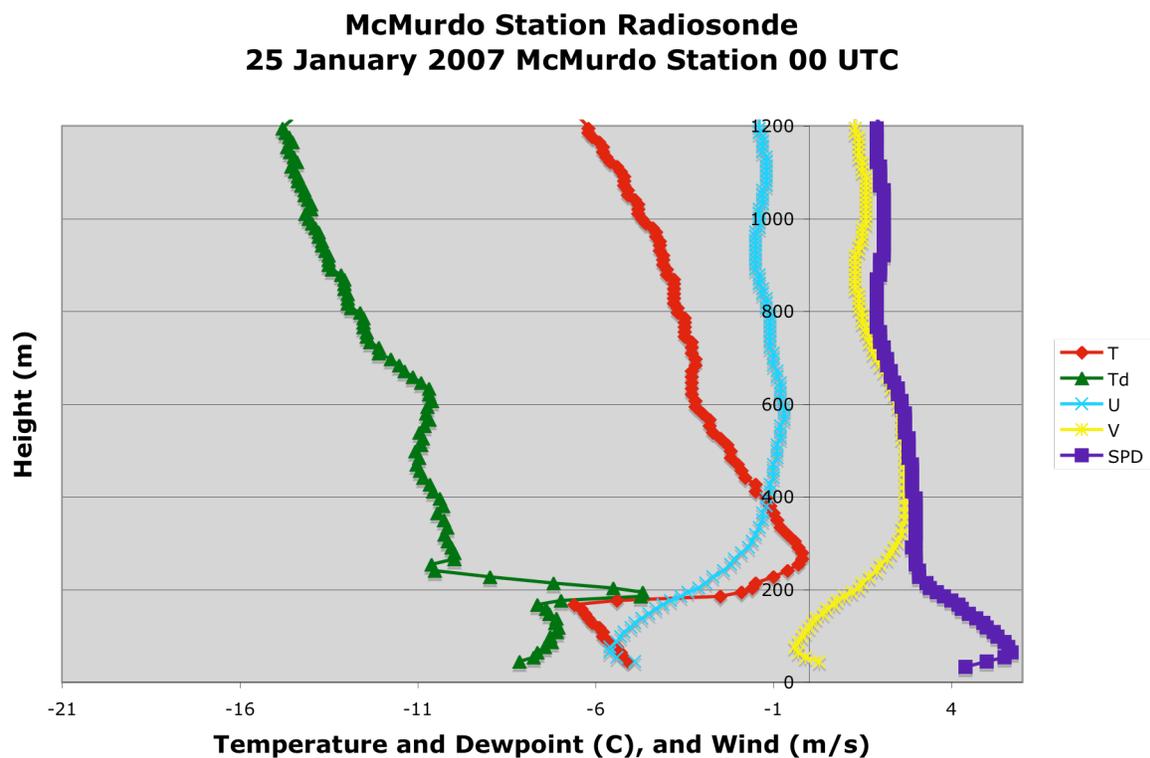
Figure 76. **Radisonde from the 00 UTC 25 January 2007 depicting the boundary layer structure for this fog case.**

c. Satellite Observations

As with the prior case, the Antarctic infrared composite imagery and isobaric analysis from the GFS places the Ross Island region into an area of weak pressure gradient and not under the direct influenced of low-pressure systems on the synoptic scale (Figure 77).
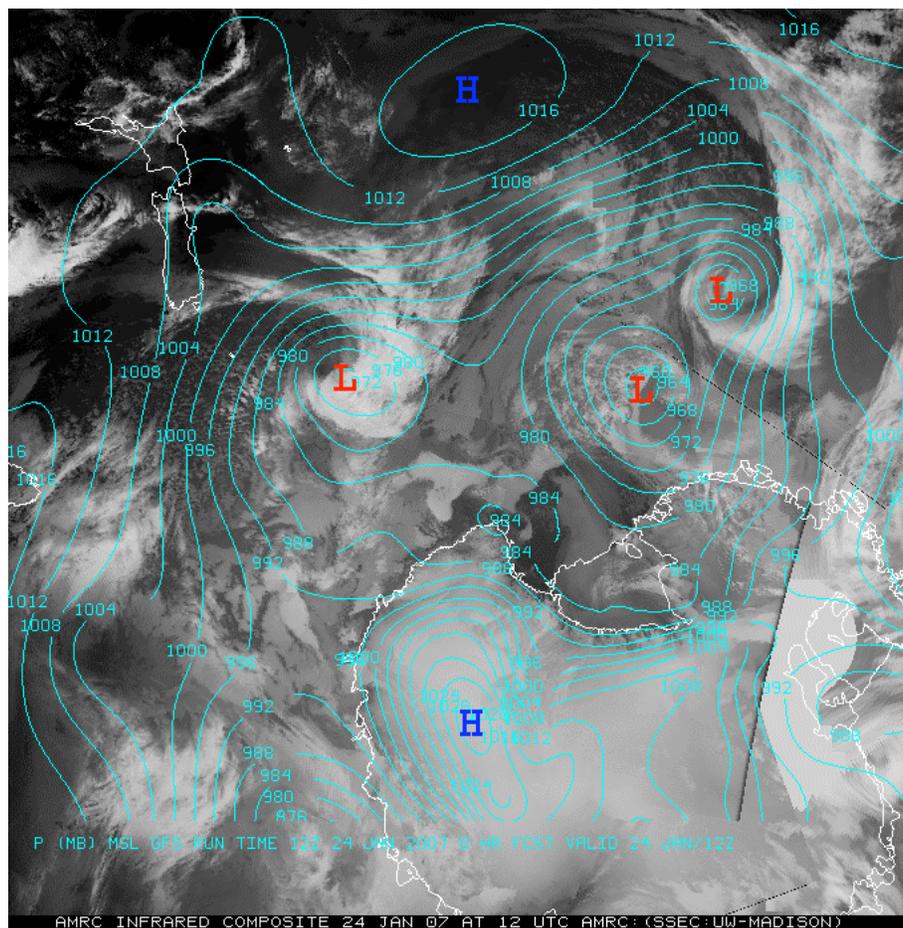
Figure 77. Antarctic composite satellite image with the GFS isobaric analysis valid 12 UTC on 24 January 2007 showing the synoptic situation before the fog event occurs later in the day.

The RGB PCI depiction sequence shown in Figures 78, 79 and 80 give a step-by-step view of the low clouds and fog over the Ross Ice Shelf to the south and east of Ross Island. Each frame shows the low clouds and fog advecting into the region and crossing the AWS line as denoted by the high relative humidity observations. The last frame in Figure 80 shows dissipation in progress with the low cloud and fog bank showing signs of breaking up and relative humidity on the decrease.
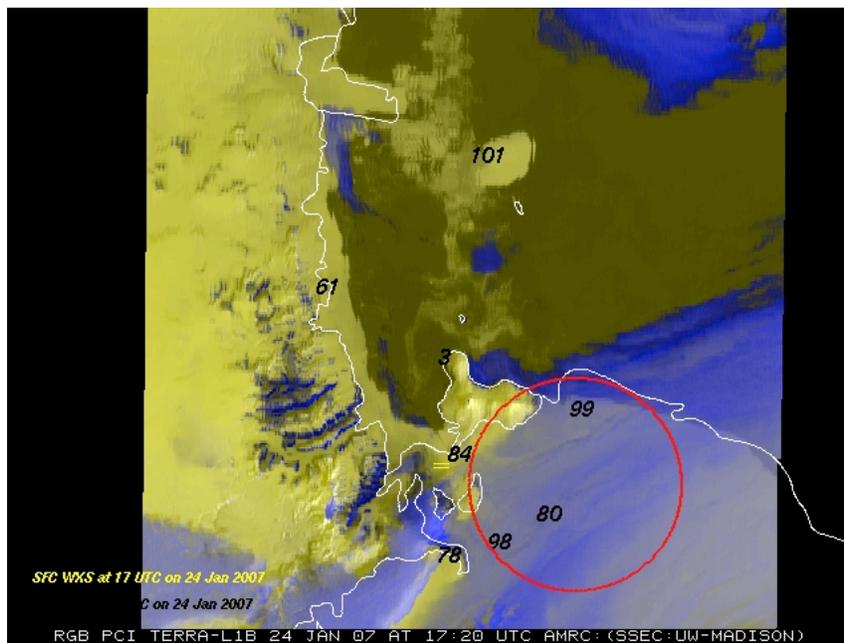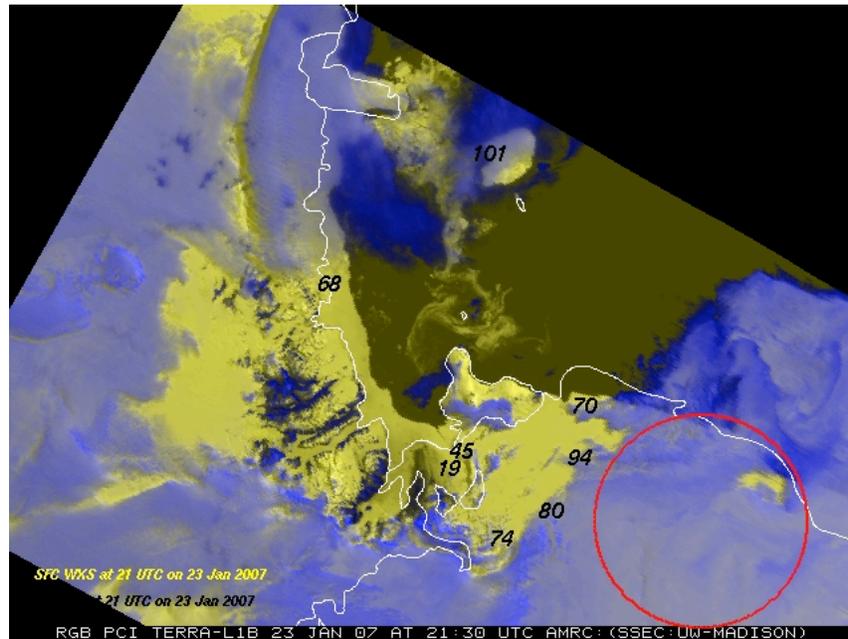
Figure 78. Part I: The first two frames of a sequence of RGB PCI fog depiction for the fog event on 24-25 January 2007. The AWS relative humidity observations and weather at the airfields are plotted. The fog is highlighted (red oval).
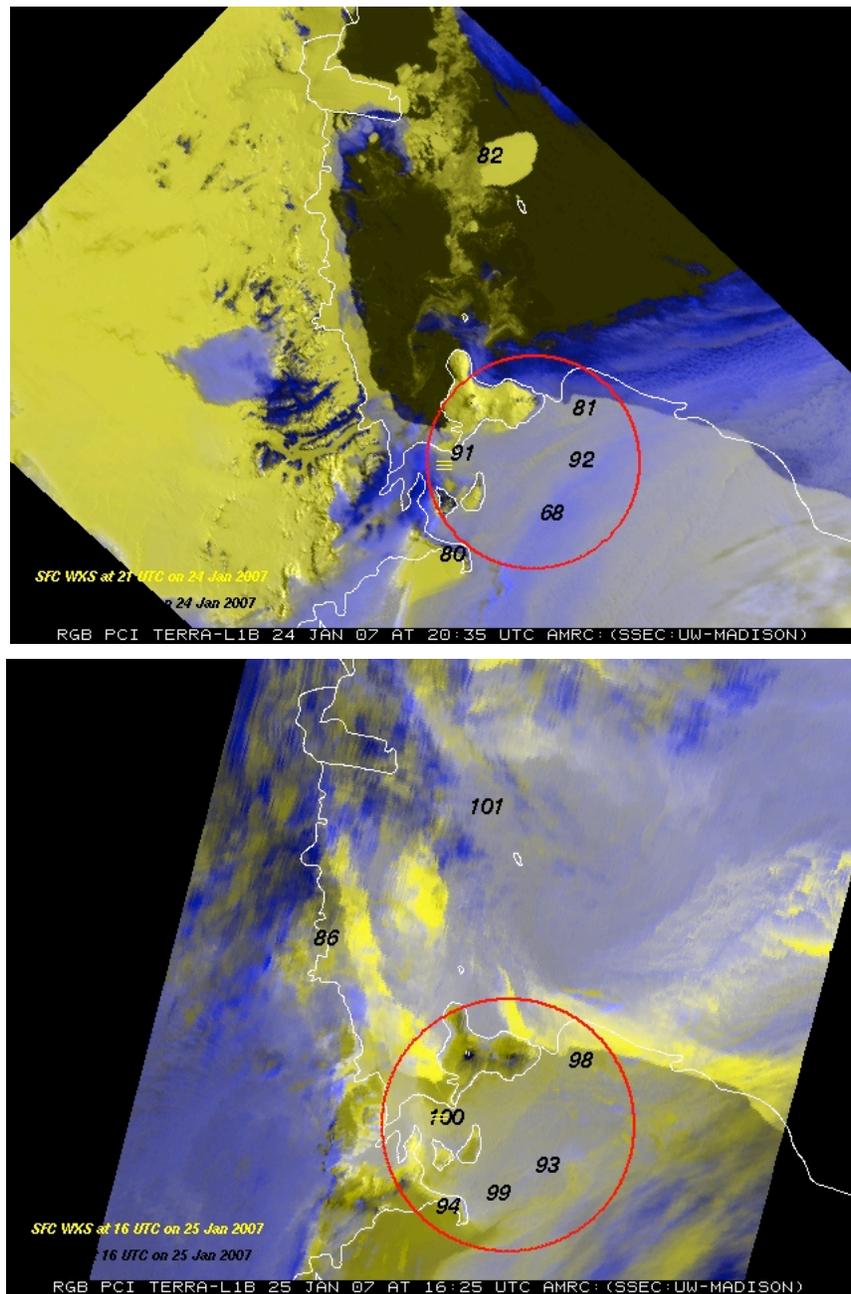
Figure 79. Part II: The next two frames of a sequence of RGB PCI fog depiction for the fog event on 24-25 January 2007. The AWS relative humidity observations and weather at the airfields are plotted. The fog is highlighted (red oval).
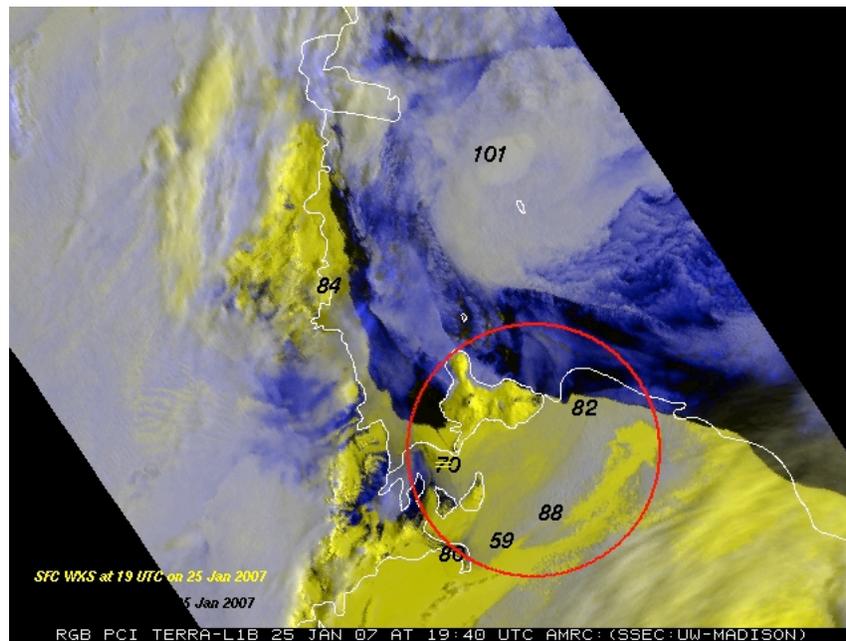
Figure 80.   Part III: The last frame of a sequence of RGB PCI fog depiction for the fog event on 24-25 January 2007. The AWS relative humidity observations and weather at the airfields are plotted. The dissipating fog is highlighted (red oval).

d. Model Analysis

The back trajectory analysis for this case depicts the common source region of air parcels that go into this fog from the southern or central Ross Ice Shelf. As seen in Figure 81, the air parcels go through a decrease in pressure, and hence an increase in altitude. Some of the air parcels as denoted here go into and over parts of the Transantarctic Mountains before reaching the Ross Island region. As noted above, the low resolution of the initialization to the HYSPILT model, coupled with likely poor representation of the dramatic terrain leads to this unlikely result. Additional runs of the back trajectory model further to the east reveal that these locations do not have the air parcel elevated over the mountains, but are found at the surface in the 12 to 18 hours

before arrival. As shown in more detail in Figure 82, the AMPS analysis of streamlines better captures the flow around the complex terrain, which in a mean sense matches the back trajectory analysis. Based on the satellite animation fog and low clouds go around these obstacles and not over them. In any case, the general analysis matches the airflow as depicted on animations of the satellite observations (both the Antarctic composite imagery as well as the RGB PCI depiction).
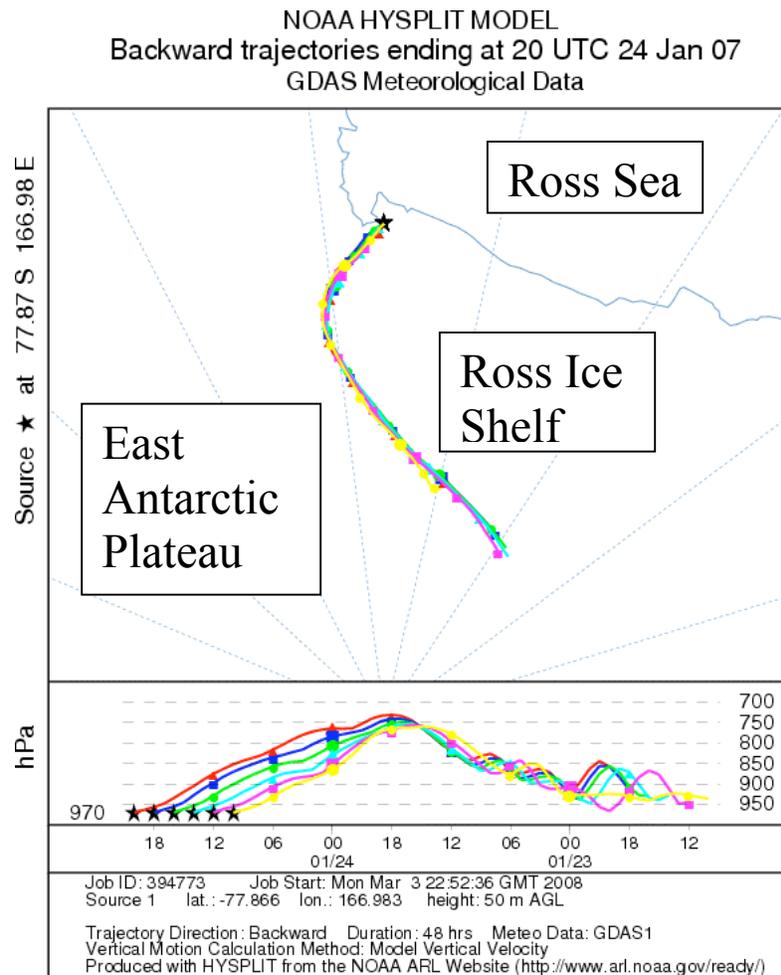
Figure 81. Back Trajectory analysis ending at 20 UTC 24 January 2007 during the densest fog on the first day of the event. Air parcels from the southern part of the Ross Ice Shelf are the common source regions for this time of event.
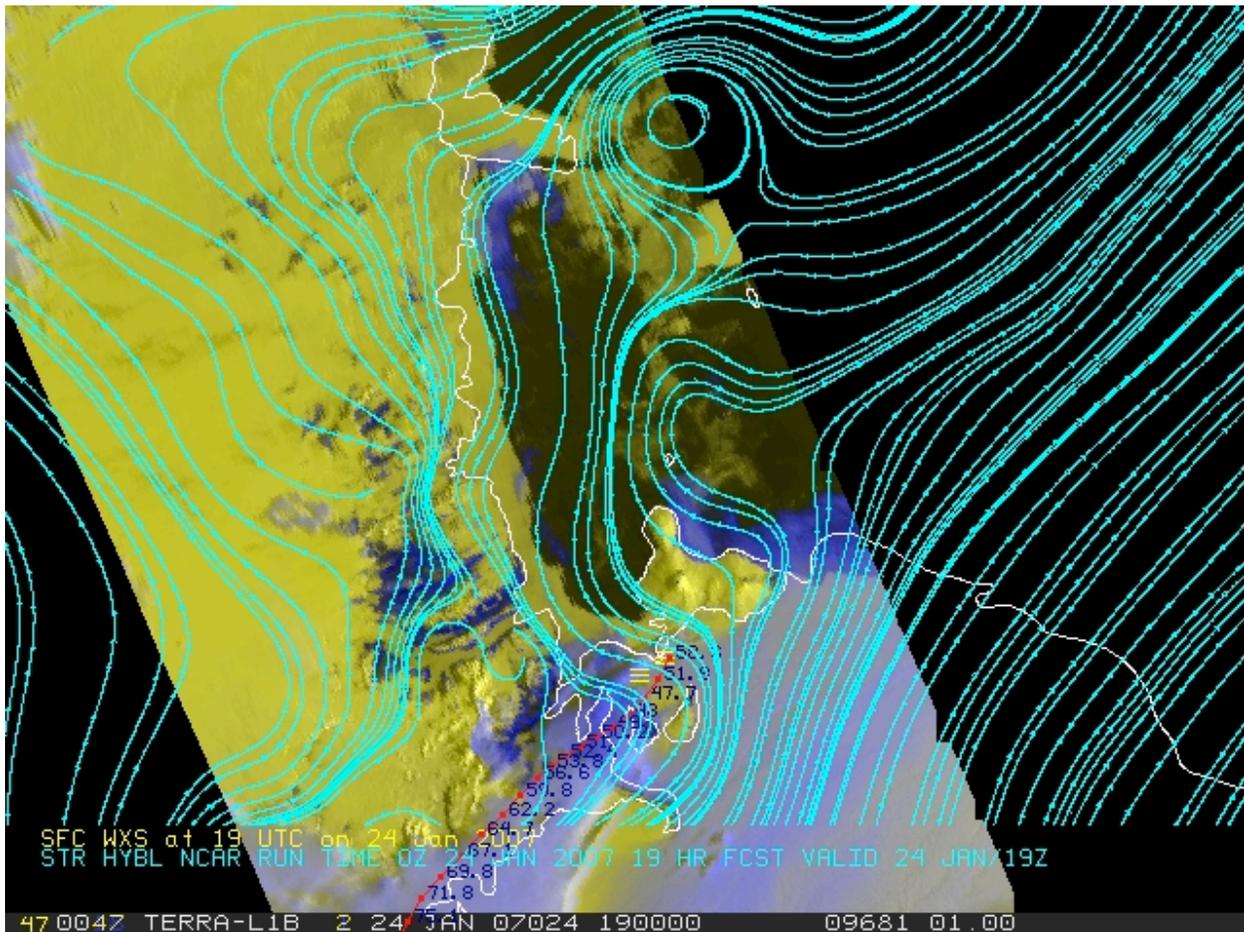
Figure 82. RGB PCI Fog depiction with AMPS streamlines at the second sigma layer above the surface and HYSPLIT back trajectory with valid at 19 UTC 24 January 2007.

5. Additional Examples

Of the analyzed fog cases, none appeared to match anecdotes of fog forming via radiative-advective means around Cape Crozier on the east end of Ross Island and forming in the Windless Bight and advecting over the airfields. In fact, none of the back trajectory analyses

supported any cases with the Ross Sea as a source region for fog (at least 48 hours prior to the densest part of the fog event). Additionally, none of the events reviewed here provided any examples of fog that was compatible with "pop-up" fog unexpectedly impacting the airfields as a locally formed fog (Mullen 1987). This section provides possible alternative explanations for these two situations. The single examples offered here do not disprove the existence of these fog types, but illustrate potential connection of these categories to the southeast advective fog common in the region.

a. "Cape Crozier" fog

This section provides an alternative possible explanation for the anecdotal thinking that fog has a source from the Ross Sea, hooking around Cape Crozier, pooling over Windless Bight and/or the airfields. As shown in Figures 83 and 84, fog at this time may actually be special cases of the fog that has formed to the south and east of Ross Island. Due to its route into the area, it appears to be a fog that formed in Windless Bight, which is not the case. The example shown here is from late on 11 January 2002 through 12 January 2002.
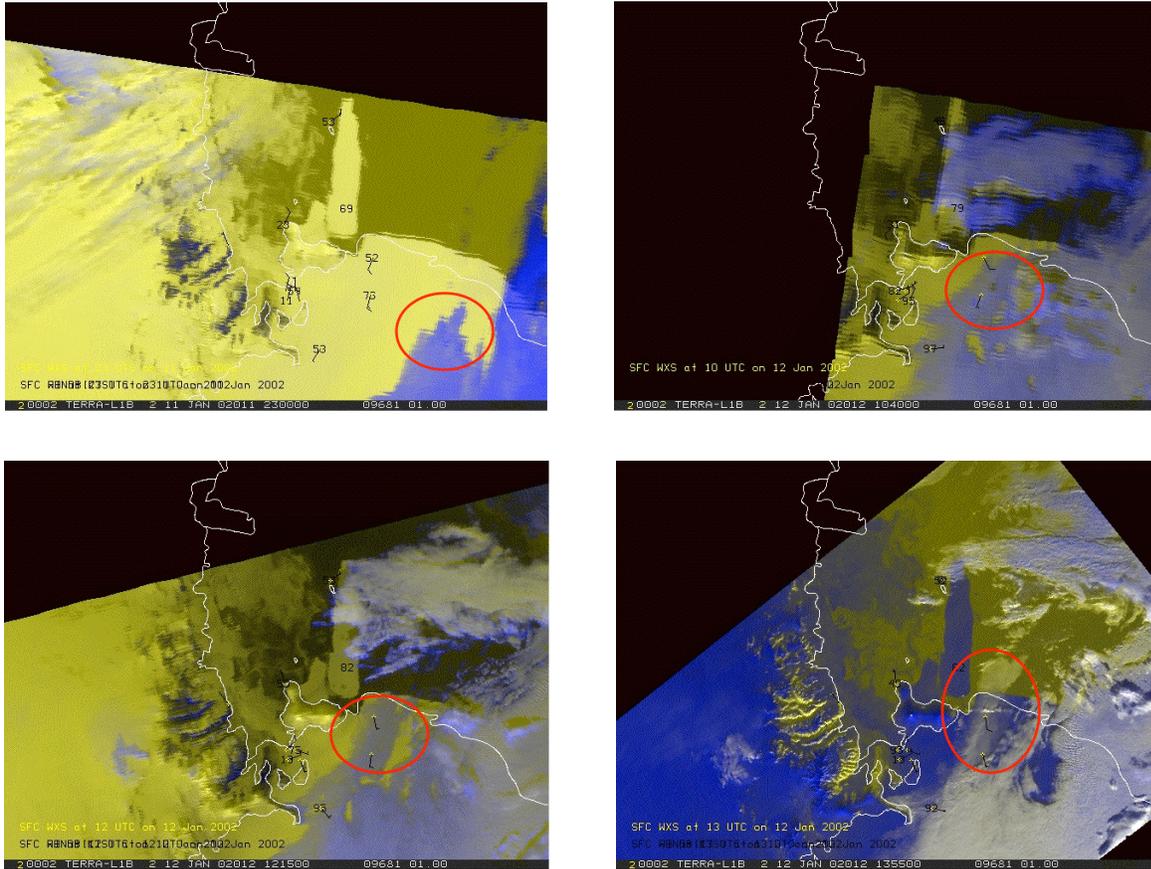
Figure 83.   Part I of II of a case that does show fog from the "due-east" as highlighted by the red oval from 23 UTC 11 January 2002 through 13:35 UTC 12 January 2002. Relative humidity and wind barbs are also plotted.
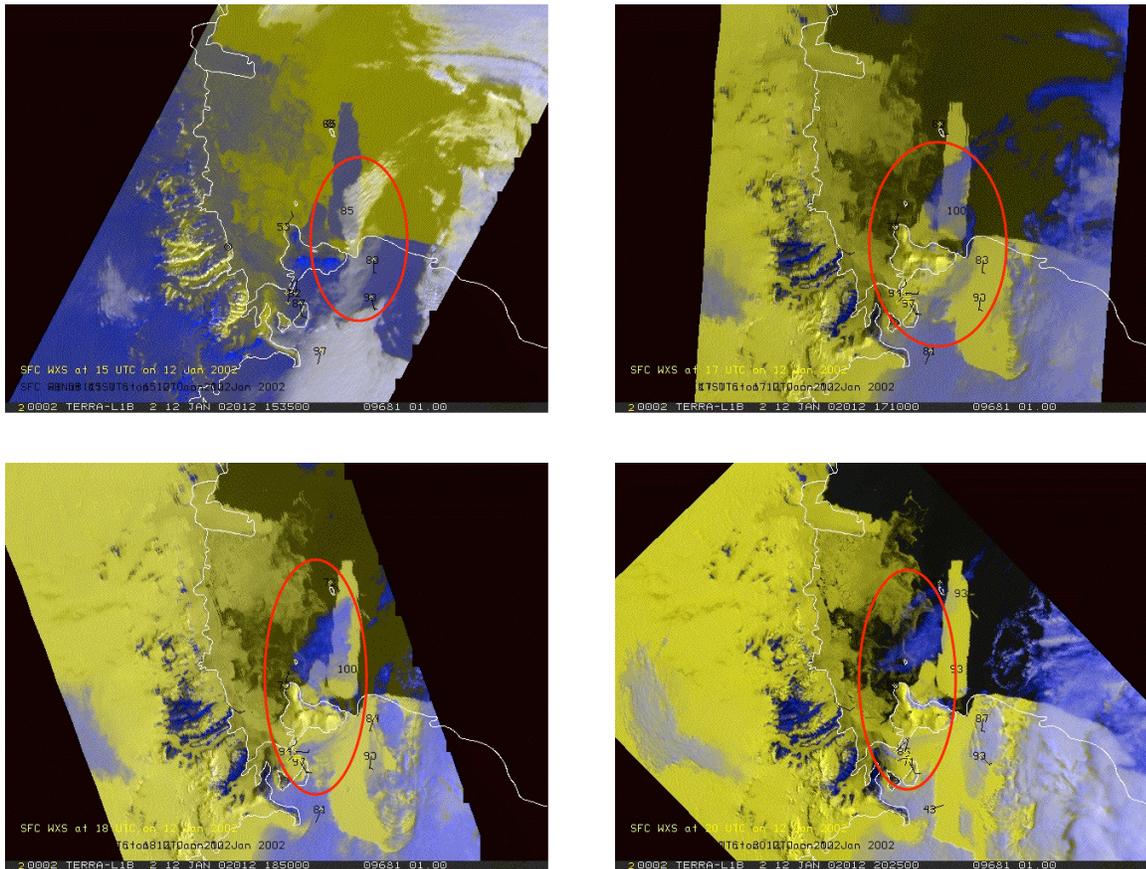
Figure 84. Part II of II of fog from the "due-east" as highlighted by the red oval from 15:35 UTC 12 January 2002 through 20:25 UTC 12 January 2002. Relative humidity and wind barbs are plotted. Note the spilt in the low cloud/fog bank as it moves around Ross Island.

In this case, the RGB PCI satellite depiction indicates a bank of low stratus/fog to the south and east of Ross Island. Relative humidities inside the AWS network are fairly dry (most below 70%). Winds at the outer AWS sites are from the south-south-west while closer to McMurdo Station and the airfields reveal light winds from the north. As time progresses, and winds at the outer AWS sites decrease, yet remain generally out of the south, the fog/low stratus bank has a portion that advects due west toward Ross Island. Through this time period, relative

humidities at the AWS increase and eventually fog is reported at Pegasus Field at 17 UTC on 12 January 2002.

In this case, the fog/stratus signature on the satellite image has a northern and southern branch. The northern portion goes to the north of Ross Island, passing over Iceberg B-15A. The AWS installed on the iceberg observes the fog, as the relative humidity report from the stations increase into the 90% to 100% range as the fog mass advects past the stations. The southern branch, which is seen in the satellite imagery, hugs close to the gap between White Island and Ross Island (especially seen in the 18:50 UTC satellite image) and arrives at the airfields from due east. Winds from Williams Field AWS switch to the east at initially 11 kts as the fog goes by. Finally, a dry slot comes behind this wave. Reports at 20:25 UTC from Linda AWS confirms that the drier air is moving into the region as its relative humidity decreases to below 50%. While this case is only one example, it gives credence to the possibility that other cases exist. Further investigation into these specific fog situations is required.

b. Local "pop-up" fog

A very recent case of fog that was captured in photographs illustrates what might be classified as a "pop-up" fog event, as anecdotally discussed by previous forecasters (e.g. Mullen 1987). However this event appears to not have local origins. On 12 January 2008 a brief fog event was recorded as seen in Figure 85. This fog, lasted no more than 2.5 hours, and never impacted McMurdo Station or even Pegasus Field. It was recorded only at Williams Field, and seen advecting over Hut Point and moving into the McMurdo Sound (Figure 85).

Figure 85. a. A patch of fog as captured coming over Hut Point peninsula at 20:49 UTC (10:49 am local time) 12 January 2008 seen from Observatory Hill. b. The bank of fog is seen 20 minutes later toward the west at 21:09 UTC (11:09 am local time) 12 January 2008 in (*Photos courtesy of Kirk Beckendorf*).

Approximately 30 minutes before the photographs of the fog first hitting Hut Point peninsula were taken, the Terra satellite was able to catch this fog as it was approaching Ross Island (Figure 86). The origin of this fog bank is seen 100 minutes before as a part of the low stratus and fog found over the Ross Ice Shelf to the southeast. It is as if this bank of fog "peeled" off the main cloudiness and fog region and moved toward the north and west. This particular bank of fog is very small, approximately 40 km long by 5 km wide. Only the southern and western end of the fog bank affected Williams Field as reported in its observations (not shown).

This fog was not forecast, as only a hint of it is seen in the Terminal Aerodrome Forecasts for Williams Field, calling for 6 km visibility and mist, when fog in the vicinity and mist with visibilities as low as 3.2 km was observed. This situation would indeed be a difficult one to forecast: Such a small area of fog to break away from the main flow that is on the order of only a few grid points large, even with a high resolution mesoscale model such as AMPS, is very difficult to capture. However, this may indeed be the kind of fog that has been anecdotally discussed for many years at McMurdo Station – small breakaway banks that come as quickly as they go, and in the meantime, impact operations in the process. As with the Cape Crozier fog, one example is not proof enough, but does offer an alternative explanation that this may be an advective fog. Further study is required to come to a more complete understanding of this specific scenario and the value of satellite observations to forecasting fog.
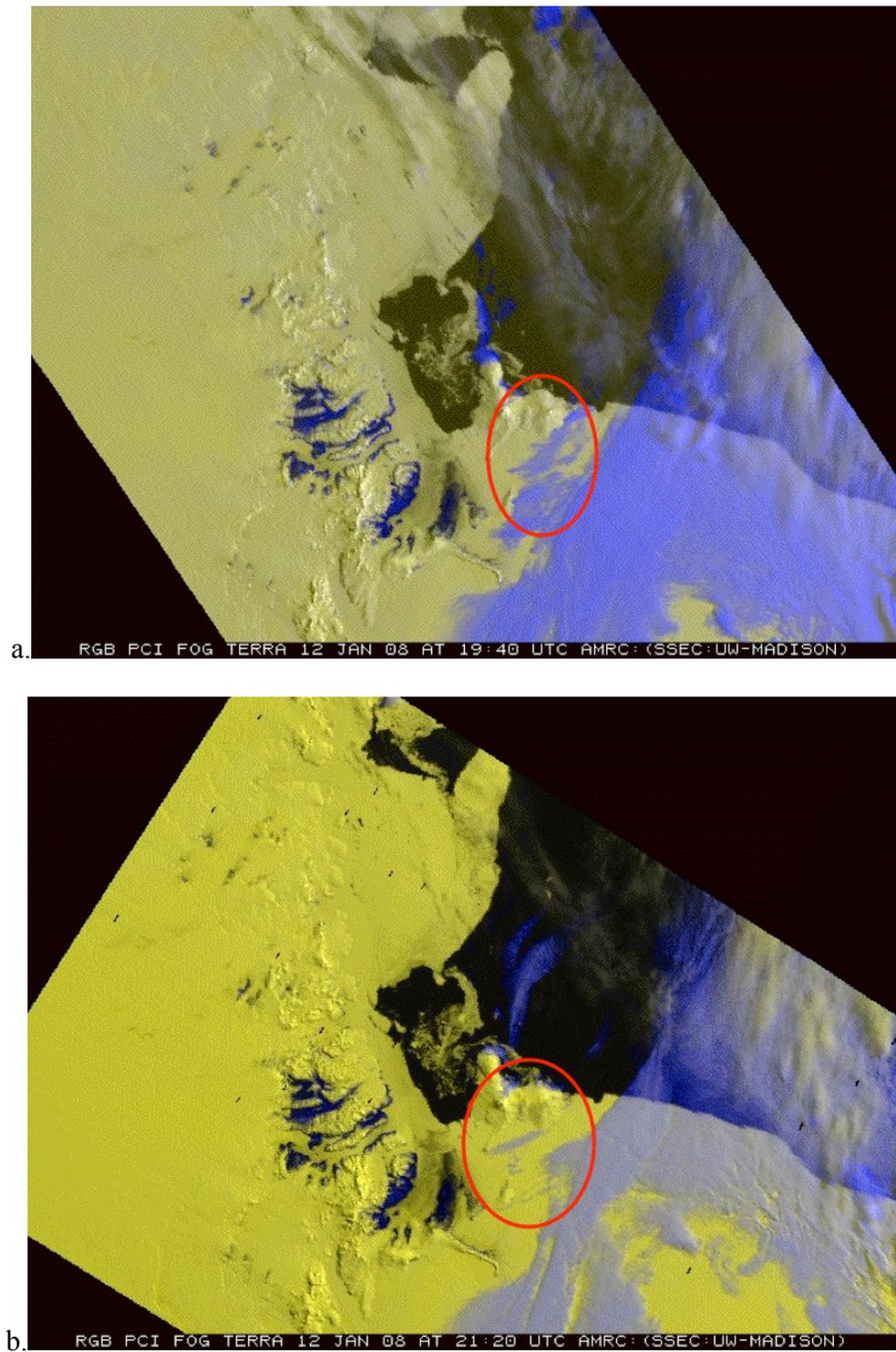
Figure 86. RGB PCI depiction sequence of "pop up" fog on 12 Jan 2008 shown as a fog band (red oval) peeling from a larger low cloud/fog area to the southeast of Ross Island.

6. Discussion

Fog does not often, if at all, initially form in the McMurdo Sound/Ross Island region during the austral summer season. As demonstrated here, fog is primarily advective, having formed elsewhere via other means. As shown in the back trajectory analysis, there are two key areas that should be monitored for fog formation: The Ross Ice Shelf (especially to the south and east of McMurdo Station), and the East Antarctic Plateau and the interaction of that airflow over the fast ice (annual or multi-year ice attached to the continent) region to the north and west of McMurdo Sound. Two case studies reviewed here demonstrate each of these two regimes. Two additional cases briefly illustrate the connection between the dominant fog regime from the southeast, to local "pop-up" fog and Cape Crozier fog.

In the boundary layer, fog formation can be aided by several factors in the region. The mixing of air parcels of different characterstics that form a new saturated parcel is one possible option. The existence of a trapping inversion may take advantage of the large gradient of moisture between the snow and air or the ocean and air. In the case of radiation fog and advective-radiation fog, radiative flux divergence that cools the air can lead to fog (Fleagle and Businger 1963). However, during the core austral summer, in the eight years of this study, no examples of this could be found. As seen in the northeast fog case, drier, cooler air from the East Antarctic plateau descends over the warmer Ross Sea ocean water where the molecular diffusion coefficient for water vapor is larger than the thermal diffusivity of heat leading to the formation of fog. Hence, water from the ocean surface evaporates into the layer of air above it. Over time

this situation saturates or even supersaturates the lowest layer of air in contact with it, increasing the likelihood fog will form. On the other hand, several situations can lead to fog dissipation or prevent formation from occurring in the first place. A lack of an inversion, or the ability to maintain an inversion, can allow for low-level moisture to be turbulently mixed away or advected away, preventing the boundary layer from reaching saturation. Near the surface, there are many hygroscopic surfaces – including the snow/ice surface itself as well as the ocean (Fleagle and Businger 1963). However, these sinks can be limited and do not reach through the whole boundary layer.

This study did not determine if fog requires a "preconditioned" environment to allow it to form. However, the analysis of the radiosonde observations over 27 cases reveals that the low level inversion capping the boundary layer is a key ingredient in over two-thirds of the cases reviewed. This has been known to forecasters as an important ingredient for fog formation (Hay personal communications, 2007) The cases of fog from the northwest all had components of East Antarctic airflow coming into the Ross Island region which under a northern quadrant wind has air mass influences from McMurdo Sound and the western Ross Sea, providing an opportunity to increase moisture in the boundary layer. The cases of fog from the southeast are possibly the result of decaying synoptic and mesoscale weather systems that advect onto the Ross Ice Shelf on the eastern side. These systems bring moisture with them that can become fog. Other "preconditioned" factors may exist beyond these that lead to fog formation.

Chapter 6: Conclusions and Future Efforts

1. Conclusions

The examination of fog occurrence in the Ross Island region of the Antarctic has found most austral summer fog events to be "advective" in nature. Satellite observations along with corroborating model and back trajectory analysis reveal austral summer fog events often form outside the current Mac Weather AWS fog network. The analysis identifies two key source areas. The primary region is from the south and east of Ross Island over the Ross Ice Shelf. A secondary region, of very few events, is from the north and east along the northern Scott Coast of McMurdo Sound.

A climatological review of fog reports compared to surface observations at McMurdo Station over a greater than 30-year period revealed that fog occurrences are decreasing from 1973 to mid-2007. Fog has two peak seasons at McMurdo, with a primary peak in January in the middle of austral summer, and a secondary peak in September, late austral winter. Meteorological conditions during fog occurrence are not significantly different than McMurdo's general climatology. Most fog events last for 1 to 3 hours. However, it is possible for fogs to persist for as long as 30 hours. Fog is more likely to occur at the nearby airfields than at McMurdo Station itself. This is consistent with the type of fog reported at the station, where fog is in the distance but not at the station.

Time series of the number of monthly fog events inspired assessing possible causes for the observed temporal variability. Large-scale climate circulation forcing, including El Niño/Southern Oscillation, and Antarctic Oscillation were found to be uncorrelated with fog occurrence. Also, the limited correlations of fog occurrence with sea ice concentration challenges the current anecdotal thinking that fog is related to open water, near Ross Island and especially further a field.

A multi-channel fog depiction method via principal component analysis has been developed using MODIS satellite observations. The method requires no ancillary data, which is of benefit to direct broadcast reception sites in the remote Antarctic, where communication links are limited and may not have bandwidth for required ancillary data. A basic validation using the AWS network reveals the depiction method to have some ability in distinguishing fog and low cloud from non-fog and non-low cloud. However, uncertainties remain with interpretation given limited validation observations.

Of the sample fog events examined, the occurrence of "pop-up" fog appears to be a special case of advective fog. Additionally, back trajectory analysis does not find the eastern Ross Sea as a source region, nor trajectories of airflow that hook around Cape Crozier giving fog to the region, the "common wisdom" shared by forecasters. Two examples are briefly discussed that offer possible alterative explanations: Both of these situations could simply be special cases of the primary fog that affects the region. The review of these and other cases find that fog occurrence is not always tied to a particular trend in station pressure. Additionally, a review of radiosonde observations during and near fog events show that approximately two-thirds have elevated inversion characteristics associated with them. The in-situ and satellite observations

combined with the numerical model and a back trajectory model offer additional tools for forecasters that may lead toward improved monitoring and predictions.

2. Future Efforts

With an improved understanding of fog in this portion of the Antarctic, questions remain. What is the microphysical structure of Antarctic fogs throughout their life cycle, and can that information be used to better monitor, model, and forecast fog? The fog collection effort, conducted as a part of this project, only scratches the surface. A complete microphysics observational field campaign has never been conducted on Antarctic fog and should be undertaken to specifically measure the microphysical and thermodynamic structure of the fog, both source regions and as it advects away. In particular, an intensive observational study is needed in the source regions to understand how fog is being created there, which in turn impacts the Ross Island area.

What are the characteristics and behaviors of austral winter fog (or "camp" fog)? The formation mechanisms and the microphysics are unknown. Additionally, the assumed anthropogenic cause to this fog has not been verified. This type of fog impacts the airfields during the critical "winter fly in" or WINFLY airlift operation, and was not considered in this study.

Can the back trajectory information be maximized in future fog studies? The initialization of the HYSPLIT model with a mesoscale analysis, such as AMPS, rather than the courser resolution from a global analysis would lead to improved depiction of advective fog.

With the topography playing an important role in the region, high-resolution analysis is important to gaining a better depiction of the dynamics and thermodynamics of the boundary layer. Such a system may also better define source regions, lead to a refined conceptual model of fog behavior in the region and be an useful diagnostic tool for forecasters.

References

Ackerman, S.A., K.I. Strabala, W.P. Menzel, R.A. Frey, C.C. Moeller, and L.E. Gumley, 1998 Discriminating clear sky from clouds with MODIS. *J. Geophys. Res.*, **103**, 32,141-32,157.

AMS, 2000: *Glossary of Meteorology* 2nd ed. American Meteorological Society, 850 pp.

AFCCC, 2002: Pressure Reduction Ratios (R- Factors), US Air Force Combat Climatology Center [Available online at: https://www2.afccc.af.mil/html/rapid_rfactor.html.]

Aguado, E., J. E. Burt, 2001: *Understanding Weather and Climate*. Prentice-Hall, 505 pp.

Anton, H.,1987: *Elementary Linear Algebra*. Fifth ed. John Wiley and Sons, 475 pp.

ATS, 1999: McMurdo Weather. Aviation Technical Services (ATS), Space Naval Warfare System Center (SPAWAR), Charleston, SC. 56 pp. (Unpublished)

Bader, M. J., G. S. Forbes, J. R. Grant, R. B. E. Lilley and A. J. Waters, 1995: *Images in Weather Forecasting: A Practical Guide for Interpreting Satellite and Radar Imagery*. Cambridge University Press, 499 pp.

Baliles, 1959: History of observational instructions on fog. United States Weather Bureau. Washington, DC. 8 pp.

Bendix, J, B. Thies, and J. Cermak, 2003: Fog detection with Terra-MODIS and MSG_SEVIRI. *Proceedings, 2003 Met. Sat. Users' Conf. Weimar (Germany), 29.9.-3.10.2003, EUMETSAT,* 429-435.

Bendix, J., B. Thies, and J. Cermak, 2004: Fog detection with Terra-MODIS and MSG-SEVIRI. *Proceedings, 2003 Met. Sat. Conf., Darmstadt*, 427-435.

Bendix, J., B. Thies, J. Cermak, and T. Nauss, 2005: Ground fog detection from space based on MODIS daytime data - a feasibility study. *Wea. Forecasting*, **20**, 989-1005.

Baum, B., and S. Platnick, 2006: *Introduction to MODIS Cloud Products. Earth Science Satellite Remote Sensing*, Vol. 1: Science and instruments. *J. J. Qu*, W. Gao, M. Kafatos, R. E. Murphy, and V. V. Salomonson, Eds., Tsinghua University Press (Beijing) and Springer-Verlag (Berlin), 74-91.

Bromwich, D. H., J. J. Cassano, T. Klein, G. Heinemann, K. M. Hines, K. Steffen, and J. E. Box, 2001: Mesoscale modeling of katabatic winds over Greenland with the Polar MM5. *Mon. Wea. Rev.*, 129, 2290-2309.

Bromwich, D. H., A. J. Monaghan, K. W. Manning, and J. G. Powers, 2005: Real-time forecasting for the Antarctic: An evaluation of the Antarctic Mesoscale Prediction System (AMPS). *Mon. Wea. Rev.*, **133**, 579-603.

Bromwich, D. H., K. M. Hines, and L. Bia, 2006: Development and validation of polar WRF. *Antarctic Meteorological Observation, Modeling and Forecasting Workshop, Boulder, CO*, pages?

Brown, H. A., and B. A. Kunkel, 1985: Water vapor, precipitation, clouds and fog. *Handbook of Geophysics and the Space Environment*, A. S. Jursa, Ed. US Air Force Geophysics Lab, Air Force Systems Command, pp. 16-1 - 16-59.

Byrd, R.E., 1935: *Little America: Aerial Exploration in the Antarctic The Flight to the South Pole*. G.P. Putnam's Sons, 422 pp.

Carrasco, J. F., D. H. Bromwich, and A. J. Monaghan, 2003: Distribution and characteristics of mesoscale cyclones in the Antarctic: Ross Sea east to the Weddell Sea. *Mon. Wea. Rev.*, **131**, 289-301.

Carrasco, J. F., and D. H. Bromwich, 1996: Mesoscale cyclone activity near Terra Nova Bay and Byrd Glacier, Antarctica during 1991. *The Global Atmosphere and Ocean System*, **5**, 43-72.

Cassano, J. J., J. E. Box, D. H. Bromwich, L. Li, and K. Steffen, 2001: Evaluation of Polar MM5 simulations of Greenland's atmospheric circulation. *J. Geophys. Res., Special Issue on the PARCA (Program for Arctic Regional Climate Assessment)*, **106**, 33,867-33,890.

Cassano, J. J., J. E. Box, D. H. Bromwich, L. Li, and K. Steffan, 2001: Verification of Polar MM5 simulations of Greenland's atmospheric circulation. *J. Geophys. Res.*, **106**, 13867-13890.

Cayette, A. M., 1998: 1997/1998 Season weather phenomena case studies: Case studies of weather phenomena in and around Ross Island. ATS, SPAWAR, Charleston, SC. (Unpublished)

Cayette, A. M., 1999: 1999/1999 Season weather phenomena case studies: case studies of weather phenomena in and around Ross Island. ATS, SPAWAR, Charleston, SC. (Unpublished)

Cermak, J., 2006: SOFOS – A New Satellite-based Operational Fog Observation Scheme. PhD Thesis, Philipps-Uiversitat Marburg, 147 pp. [Philipps-Universitat, Karl-von-Frisch-Straβe 4, 35032 Marburg, Germany].

Cermak, J. and J. Bendix, 2007: Dynamical Nighttime Fog/Low Stratus Detection Based on Meteosat SEVIRI Data – A Feasibility Study. *Pure App. Geophys.*, **164**, 1179-1192.

Collett, Jr., J. L., Moore, K. and Straub, D. (1998) Two new multistage impactors for drop size dependent fog and cloud sampling. *Proceedings, 1st International Conference on Fog and Fog Collection, Vancouver, Canada*, pp. 133-136.

Croft, P.J., R.L. Pfost, J.M. Medlin, and G.A. Johnson, 1997: Fog Forecasting for the Southern Region: A Conceptual Model Approach. *Wea. Forecasting*, **12**, 545-556.

Draxle, R .R. and G. D. Rolph, 2003: HYSPLIT (Hybrid Single-Particle Lagrangian Integrated Trajectory). NOAA Air Resources Laboratory, Silver Spring, MD. [Model access via NOAA ARL Ready Website http://www.arl.noaa.gov/ready/hysplit4.html]

Ellrod, G. P., 1991: Nighttime fog detection with bi-spectral GOES-VAS imagery. *Proceedings, 4th International Conference on Aviation Weather Systems,* Paris, France. Amer. Meteor. Soc., 71-75.

Ellrod, G .P., 1994: Detection and analysis of fog at night using GOES multispectral infrared imagery. NOAA Technical Report NESDIS 75, US Department of Commerce, Washington, DC. 22 pp.

Ellrod, G. P., 1995: Advances in the detection and analysis of fog at night using GOES multispectral infrared imagery. *Wea. Forecasting*. **10**, 606-619.

Evans, E. R. G. R., 1921: *South with Scott*. W. Collins and Sons Co., 283 pp.

Eyre, J. R., J. L. Brownscombe, and R. J. Allam, 1984: Detection of fog at night using Advanced Very High Resolution Radiometer (AVHRR) imagery. *Meteor. Mag.*, **113**, 266-271.

Falconer, T. R. and A .R. Pyne, 2004: Ice breakout history in southern McMurdo Sounds, Antarctica (1988-2002). Antarctic Data Series No 27. Antarctic Research Centre: Victoria University of Wellington, Wellington, New Zealand. [Available online at "ftp://ftp.geo.vuw.ac.naz/ARC/ADS27 IceBreakouthistory.pdf"]

Fleagle, R .G. and J. A. Businger, 1963: *An Introduction to Atmospheric Physics*. Academic Press, 346 pp.

Grumbine, R. W., 1996: Automated Passive Microwave Sea Ice Concentrations Analysis at NCEP. Technical Note Ocean Modeling Branch Contribution 120, NOAA-NWS-NCEP. Washington, DC.

Grell, G. A., J. Dudhia, and D. R. Stauffer, 1995: A description of the fifth-Generation Penn State/NCAR Mesoscale Model (MM5). NCAR Tech. Note TN-398+STR, 122 pp. [Available from UCAR Communications, P.O. Box 3000, Boulder, CO 80307.]

Hillger, D. W., 1992: Image and graphical analysis of principal components of satellite sounding channels. *Proceedings*, *6th Conf. on Satellite Meteorology and Oceanography*, *Atlanta, GA*, Amer. Meteor. Soc 28-31.

Hillger, D. W., 1994: Use of truncated principal component analysis to improve images from satellite sounding channels. *Proceedings,.7th Conference on Satellite Meteorology and Oceanography*, Monterey, CA, Amer. Meteor. Soc., 540-541.

Hillger, D. W., 1996: Meteorological features from principal component image transformations of GOES imagery. *Proceedings of the International Symposium on Optical Science, Engineering, and Instrumentation*, Denver, CO, 4-9 August, SPIE, vol. 2812, 111-121.

Hutchison, K. D., and A. P. Cracknell, 2006: *Visible Infrared Imager Radiometer Suite: A New Operational Cloud Imager*. CRC Taylor & Francis Group, Boca Raton, FL. 230 pp.

Key J.R., D.A. Santek, C.S. Velden, N. Bormann, J.-N. Thepaut, L.P. Riishojgaard, Y. Zhu, and W.P. Menzel, 2003: Cloud-drift and Water Vapor Winds in the Polar Regions from MODIS, *IEEE Trans. Geosci. Remote Sensing*, **41**, pp. 482-492.

King and Turner, 1997: *Antarctic Meteorology and Climatology*. Cambridge University Press. 409 pp.

Knuth, S. L., 2007: Estimation of snow accumulations in Antarctica using automated acoustic depth gauge measurements. MS thesis, University of Wisconsin-Madison, Department of Atmospheric and Oceanic Sciences. UW Met Publication Number 07.00.K1. 82 pp.

Kyle P. R., Aster R., Crain J., Dunbar N., Esser R., McIntosh W. C., Richmond M., Ruiz M., and Wardell L. J., 2003: Monitoring Volcanic Activity at Mount Erebus, Antarctica. *IX International Symposium on Antarctic Earth Science*.

LaDochy, S. and M.R. Witiw, 2007: Dense fog trends in West Coast U.S. locations since 1991. *Program and Abstracts, 4th International Conference on Fog, Fog Collection and Dew, La Serena, Chile,* 415-418.

Lazzara, M.A. K.C. Jezek, T.A. Scambos, D.R. MacAyeal, and C.J. van der Veen, 1999: On the Recent Calving of Icebergs from the Ross Ice Shelf. *Polar Geog.* **23**, 201-212.

Lazzara, M. A., L. M. Keller, C. R. Stearns, J. E. Thom, and G. A. Wiedner, 2003: Antarctic Satellite Meteorology: Applications for Weather Forecasting. *Mon. Wea, Rev.,.***131**, 371-383.

Lee, T. F, F. J. Turk, and K. Richardson, 1997: Stratus and fog products using GOES-8-9 3.9 micron data. *Wea. Forecasting*, **12**, 664-677.

Liu Z., and D.H. Bromwich, 1993: Acoustic remote sensing of planetary boundary layer dynamics near Ross Island, Antarctic. *J. Appl. Meteor.,* **32**, 1867-1882.

Manning, K. W., 2006: AMPS Status and Update. *Antarctic Meteorological Observation, Modeling and Forecasting Workshop, Boulder, CO.*

Monaghan, A.J., 2003: Real-time forecasting for the Antarctic: An evaluation of the Antarctic mesoscale prediction system (AMPS). MS Thesis, The Ohio State University, Department of Geography, Atmospheric Sciences Program. 171 pp.

Mullen, D. P., 1987: Forecasting for the Frigid Desert of Antarctica. *Weatherwise*, **40**, 304-311.

Nilsson, E. D. and E. K. Bigg, 1996: Influences on formation and dissipation of high arctic fogs and their interaction with aerosol during summer and autumn. *Tellus,* **48B**, 234-253.

NOAA, 1988: Federal Meteorology Handbook No. 2: Surface Synoptic Codes, NOAA, US Department of Commerce, pp. 131.

NSFA, 1990: Forecaster's Handbook. Naval Support Force, Antarctica (NSFA). (Unpublished)

Ohtake, T., 1977: X-Ray analyses of nuclei in individual fog droplets and ice nuclei. *Proceedings, 9th International conference on Atmsopheric aerosols, Condensation, and Ice Nuclei, University College, Galway, Ireland.*

Operation Deep Freeze '60, Task Force 43. Edited by James S. Hahn. Norfolk, VA, Liskey Lithograph Corp., n.d. 210 pp.

Powers, J. G., A. J. Monaghan, A. M. Cayette, D. H. Bromwich, Y-H. Kuo, and K. W. Manning, 2003: Real-time mesoscale modeling over Antarctica: The Antarctic Mesoscale Prediction System (AMPS). *Bull. Amer. Met. Soc.*, **84**, 1533-1545.

Pruppacher, H. R. and J. D. Klett, 1997: *Microphysics of Clouds and Precipitation*. Kluwer, 954 pp.

Rolph, G. D., 2003: Real-time Environmental Applications and Display sYstem (READY) NOAA Air Resources Laboratory, Silver Spring, MD. [Available online at http://arl.noaa.gov/ready/hysplit4.html.]

Sallee, R. W., and A. Snell, 1970: Antarctic forecasters handbook, [Antarctic Support Activities, Detachment Charlie, Fleet Post Office, New York, NY 09501.]

Saxena V.K and Ruggiero, 1985: Real-time measurements of droplet size distribution in Antarctic coastal clouds. *Antarctic Journal of U.S.*, **19**. 198-200.

Saxena, V.K., and Curtin, 1983: Air-sea interactions over the Ross Ea in the surface boundary layer, *Antarctic Journal of the U.S.*, **18**, 241-243.

SCAR PACA READER Project, 2000: *XXVI SCAR Working Group on Physics and Chemistry of the Atmosphere (PACA)*, July 2000, Tokyo, Japan. [available on-line at http://www.antarctica.ac.uk/met/READER/]

Schwerdtfeger, W. 1984: *Weather and Climate of the Antarctic.* Elsevier, 261 pp.

Scott, R. F., 1905: *The Voyage of the 'Discovery'*. Volume II, London, Smith, Elder and Co./New York, Charles Scribner's Sons. 440 pp.

Seefeldt, M. W., G. J. Tripoli, and C. R. Stearns, 2003: A high-resolution numerical simulation of the wind flow in the Ross Island region, Antarctica. *Mon. Wea. Rev.*, **131**, 435-458.

Skamarock, W. C., J. B.Klemp, J. Dudhia, D. O. Gill, D. M. Baker, W. Wang, and J. G. Powers, 2005: A description of the advanced research WRF version 2. NCAR/Technical Note-468+STR, 88 pp. [Available from UCAR Communications, P.O. Box 3000, Boulder, CO 80307.]

Smith, L. I.; 2002: A tutorial on principal components analysis. Department of Computer Sciences, University of Otago, Dunedin, New Zealand. [Available online at: http://csnet.otago.ac.nz/cosc453/student_tutorials/principal_components.pdf]

Souders, C. G. and R. J. Renard, 1984: The visibility climatology of McMurdo/Williams Field, Antarctica. *Proceedings, 10th Conference on Weather Forecasting and Analysis, Clearwater Beach, FL*. Amer. Meteor. Soc., 98-101.

SPAWAR, 2007a: McMurdo Forecasting Handbook OPSEA 06-07, SPAWAR System Center, Charleston, SC, 38 pp.

SPAWAR, 2007b: McMurdo Weather Observer Handbook OPSEA 07-08, SPAWAR System Center, Charleston, SC, 117 pp.

Stearns, C. R. and G.A. Weidner, 1999: Meteorological Observations related to fog events at Williams Field, Antarctica. Internal document/letter to NSF/USAP. (Unpublished)

Stearns, C.R. and G.A. Weidner, 1990: The Polar automatic weather station project of the University of Wisconsin. *Proceedings, International Conference on the Role of the Polar Regions in Global Change*, Fairbanks, AK, Vol. I, 58-62.

Stearns, C. R, L. M. Keller, G. A. Weidner, and M. Sievers, 1993: Monthly Mean Climatic Data for Antarctic Automatic Weather Stations. *Antarctic Meteorology and Climatology: Studies Based on Automatic Weather Stations*. D.H. Bromwich and C.R. Stearns, Eds., Antarctic Research Series, Vol. 61, AGU, Washington, DC., 1-21.

Stringer, G. L. and S. J. Newell, 2001: Design and installation of the fog prediction system in the Antarctic. *17th Conference on IIPS*, Albuquerque, NM, Amer. Meteor. Soc., 6-9.

Stull, R.B., 1988: *An Introduction to Boundary Layer Meteorology*. Kluwer, 666 pp.

Turner, J., and S. Pendlebury, 2004: *The International Antarctic Weather Forecasting Handbook*. Cambridge University Press. 663 pp.

Turner, J., S.R. Colwell, G.J. Marshall, T.A. Lachlan-Cope, A.M. Carleton, P.D. Jones, V. Lagun, P.A. Reid and S. Iagovkina, 2003: The SCAR READER Project: Toward a high-quality database of mean Antarctic meteorological observations. *J. Clim.*, **17**, 2890-2898.

Turner, J., Allam, R. J., and Maine, D. R., 1986: A case study of the detection of fog at night using channels 3 and 4 on the Advanced Very High Resolution Radiometer (AVHRR). *Meteorol. Mag.*, **115**, 285-290.

Wendler, G, and Y. Kodama, 1993: The Kernlose Winter in Adelie Coast. *Antarctic Meteorology and Climatology: Studies Based on Automatic Weather Stations*. D.H. Bromwich and C.R. Stearns, Eds. Antarctic Research Series, Vol. 61, AGU, Washington, D.C., 139-147.

Witiw, M. R., J. Barrs, and K. Fischer: 2002: Fog in the Las Angeles Basin: Influence of El Nino Southern Oscillation and the Pacific Decadal Oscillation. *Proceedings, 16th Conference on Probability and Statistics in the Atmospheric Sciences, Orlando, Florida*. Amer. Meteor. Soc.

Witiw, M. R. and S. LaDochy, 2004: Variations of fog in the Los Angeles Basin. Programme. Abstracts, *Proceedings, 3rd International Conference on Fog, Fog Collection and Dew, Capetown, Republic of South Africa*.

WMO, 1983: Guide to Climatological Practices No. 100. Secretariat of the World Meteorological Organization, Geneva, Switzerland.

Appendix A: Satellite Sensor Technical Specifications

1. AVHRR/3 Technical Specifications

Adapted from: http://www2.ncdc.noaa.gov/docs/klm/html/c3/sec3-1.htm
http://www.ssec.wisc.edu/mcidas/doc/users_guide.html

Spacecraft:	NOAA and MetOp satellites
Orbit:	833 km or 870 km, nominal sun-synchronous, polar orbiting
Swath Dimensions:	+/- 55.4 degrees scan
Telescope:	20.32 cm diameter afocal Cassegrain
Size:	31.33 x 14.35 x 11.5 in.
Weight:	73 kg
Power:	27 W (average)
Data Rate:	665.4 kbps (HRPT/GAC/LAC); 2.66 Mbps (Playback)
Spatial Resolution:	1.1 km (at nadir)
Design Life:	2 years required

Band	Wavelength (µm)	Primary Uses
1	0.63	Visible cloud and surface features
2	0.86	Visible aerosols over water, vegetation
3*	3.74	Infrared low-level cloud/fog, fire detection
4	10.8	Infrared surface/cloud-top temperature
5@	12.0	Infrared surface/cloud temperature/low-level water vapor
6*	1.61	Near-infrared surface, cloud phase (NOAA-15 and later)

*For NOAA-15 and later, channels 3A and 3B are often labeled as bands 6 and 3, respectively.

@Band 5 on NOAA-10 is not available

2. MODIS Technical Specifications

From http://modis.gsfc.nasa.gov/about/specs.html

Spacecraft:	Terra and Aqua satellites
Orbit:	705 km, 10:30 a.m. descending node (Terra) or 1:30 p.m. ascending node (Aqua), sun-synchronous, near-polar, circular
Scan Rate:	20.3 rpm, cross track
Swath Dimensions:	2330 km (cross track) by 10 km (along track at nadir)
Telescope:	17.78 cm diam. off-axis, afocal (collimated), with intermediate field stop
Size:	1.0 x 1.6 x 1.0 m
Weight:	228.7 kg
Power:	162.5 W (single orbit average)
Data Rate:	10.6 Mbps (peak daytime); 6.1 Mbps (orbital average)
Quantization:	12 bits
Spatial Resolution:	250 m (bands 1-2) 500 m (bands 3-7) 1000 m (bands 8-36)
Design Life:	6 years

Primary Use	Band	Bandwidth[1]	Spectral Radiance[2]	Required SNR[3]
Land/Cloud/Aerosols Boundaries	1	620-670	21.8	128
	2	841-876	24.7	201
Land/Cloud/Aerosols Properties	3	459-479	35.3	243
	4	545-565	29.0	228
	5	1230-1250	5.4	74
	6	1628-1652	7.3	275
	7	2105-2155	1.0	110
Ocean Color Phytoplankton Biogeochemistry	8	405-420	44.9	880
	9	438-448	41.9	838
	10	483-493	32.1	802
	11	526-536	27.9	754
	12	546-556	21.0	750
	13	662-672	9.5	910
	14	673-683	8.7	1087
	15	743-753	10.2	586
	16	862-877	6.2	516
Atmospheric Water Vapor	17	890-920	10.0	167
	18	931-941	3.6	57
	19	915-965	15.0	250

[1] Bands 1 to 19 are in nm
[2] Spectral Radiance values are (W/m^2 -μm-sr)
[3] SNR = Signal-to-noise ratio

Primary Use	Band	Bandwidth[1]	Spectral Radiance[2]	Required NE[delta]T(K)[4]
Surface/Cloud Temperature	20	3.660-3.840	0.45(300K)	0.05
	21	3.929-3.989	2.38(335K)	2.00
	22	3.929-3.989	0.67(300K)	0.07
	23	4.020-4.080	0.79(300K)	0.07
Atmospheric Temperature	24	4.433-4.498	0.17(250K)	0.25
	25	4.482-4.549	0.59(275K)	0.25
Cirrus Clouds	26	1.360-1.390	6.00	150 (SNR)[3]
Water Vapor	27	6.535-6.895	1.16(240K)	0.25
	28	7.175-7.475	2.18(250K)	0.25
Cloud Properties	29	8.400-8.700	9.58(300K)	0.05
Ozone	30	9.580-9.880	3.69(250K)	0.25
Surface/Cloud Temperature	31	10.780-11.280	9.55(300K)	0.05
	32	11.770-12.270	8.94(300K)	0.05
Cloud Top Altitude	33	13.185-13.485	4.52(260K)	0.25
	34	13.485-13.785	3.76(250K)	0.25
	35	13.785-14.085	3.11(240K)	0.25
	36	14.085-14.385	2.08(220K)	0.35

[1] Bands 20 to 36 are in μm
[2] Spectral Radiance values are (W/m2 -μm-sr)
[3] SNR = Signal-to-noise ratio
[4] NE(delta)T = Noise-equivalent temperature difference

3. VIIRS Technical Specifications

From resources at http://npoesslib.ipo.noaa.gov/u_listcategory_v3.php?50

Spacecraft:	NPP and NPOESS satellites
Orbit:	833 km, nominal cross times of 7:30, 13:30, 21:30, sun-synchronous
Scan Rate (Period):	1.786 seconds
Swath Dimensions:	+/- 56.063 degrees, 3029 km scan
Telescope:	19.1 cm aperture114 cm focal length
Size:	65 x 129 x 138 cm
Weight:	160-199 kg
Power:	134 W (177 W Peak)
Data Rate:	10.8 Mbps (peak); 6.7 Mbps (orbital average)
	(Using 2:1 Rice compression)
Spatial Resolution:	0.371 km (I channels) 0.742 km (M channels)
Design Life:	7 years (plus 8 years storage)

VIIRS Channel Listing (adapted from Hutchison and Cracknell, 2006)

Band Number	VIIRS Channel Designator	Central Wavelength (µm)	Bandwidth (µm)
1	DNB	0.7	0.4
2	M1	0.412	0.02
3	M2	0.445	0.018
4	M3	0.488	0.020
5	M4	0.555	0.020
6	I1	0.640	0.080
7	M5	0.672	0.020
8	M6	0.746	0.015
9	I2	0.865	0.039
10	M7	0.865	0.039
11	M8	1.240	0.020
12	M9	1.378	0.015
13	I3	1.610	0.060
14	M10	1.610	0.060
15	M11	2.250	0.050
16	I4	3.740	0.380
17	M12	3.700	0.180
18	M13	4.050	0.155
19	M14	8.550	0.300
20	M15	10.763	1.000
21	I5	11.450	1.900
22	M16	12.013	0.950

DNB = 0.742 km resolution at nadir and at 55.8 degrees
I channels = 0.371 km resolution at nadir and 0.8 km at 55.8 degrees
M channels = 0.742 km resolution at nadir and 1.6 km at 55.8 degrees

Appendix B: Observing Systems Specifications

1. University of Wisconsin-Madison AWS Specifications

From Technical Manual for Automatic Weather Stations, by George A. Weidner, Department of Meteorology (now Atmospheric and Oceanic Sciences), University of Wisconsin-Madison, 1985.

Variable	Sensor	Specifications
Air Pressure	Paroscientific Model 215 A	Range: 0 to 1100 hPa Resolution: 0.050 hPa Accuracy: +/- 0.2 hPa (0.2 hPa/year long term drift)
Air Temperature	Weed PRT Two-wire bridge	Range: to -100 C minimum Resolution: 0.125 C Accuracy: +/- 0.5 C * Lowest Recorded is -85.2 C at Dome Fuji 17 July 1996
Humidity	Vaisala HMP-35A (and other models)	Range: 0 to 100% Resolution: 1.0 % Accuracy: +/- 5.0 % down to -55 C Corrections possible for lower temperatures
Wind Direction	10 K Ohm pot.	Range: 0 to 355 Degrees Resolution: 1.5 Degrees Accuracy: +/- 3.0 Degrees
Wind Speed	Bendix/Belfort RM Young Hydro-Tech	Resolution/Accuracy: 0.25 +/- 0.5 m/s Resolution/Accuracy: 0.20 +/- 0.5 m/s Resolution/Accuracy: 0.33 +/- 2% * Maximum speed along Adelie Coast ~50 m/s
Temperature String	Thermocouple Two junction Copper-Cons.	Resolution: 0.06 C Accuracy: +/- 0.125 C

2. McMurdo Station Radiosonde Specifications

The following specifications are from Vaisala Oyj, Helsinki, Finland.

Variable	Sensor	Specifications
Pressure	Vaisala BAROCAP	Range: 3 to 1080 hPa, Resolution: 0.1 hPa, Accuracy: 0.3-1.5 hPa
Temperature	Vaisala THERMOCAP	Range: -90 to 60 C, Resolution: 0.1 C, Accuracy: +/- 0.5 C
Humidity	Vaisala HUMICAP	Range: 0 to 100 %, Resolution: 1 % Accuracy: +/- 5%
Positioning/Wind	GPS	Accuracy: 10 m horizontal, 20 m vertical, +/- 0.2 m/s velocity

* Lowest level reported data is taken from the PASOS system atop the McMurdo Operations/McMurdo Weather, building 165, at McMurdo Station – near the McMurdo Balloon Facility, building 82, launch point for radiosondes.

3. McMurdo Station and Airfields PASOS Specifications

The following specifications were made available by SPAWAR/Mac Weather and/or are from the Portable Automatic Surface Observing System Installation and Maintenance manual, Systems Management Inc. Hunt Valley, Maryland.

Variable	Sensor	Specifications
Pressure	Setra 470T	Range: 572.3 to 1066.7 hPa Resolution: ~0.15 hPa Accuracy: +/- 0.003 hPa
Temperature	Rotronics MP 101A-C4	Range: -54 to 60 C Resolution: 1 C Accuracy: +/- 0.5 C (Aspirated)
Humidity/Dew point	Rotronics MP 101A-C4	Range: 0 to 100 % Resolution: 1 C (Converted from humidity) Accuracy: +/-0.5 C (Converted from humidity) (Aspirated)
Wind Direction	RM Young	Range: 0 to 355 degrees (5 degree dead zone) Resolution: 1.5 degrees Accuracy: +/- 3 degrees
Wind Speed	RM Young	Range: 0 to 60 m/s Resolution: 0.2 m/s Accuracy: +/-1 m/s

"…The sun, a pale and watery yellow, was gleaming through the mist just above the west wall of the hollow in which they lay; north, south and east, beyond the wall the fog was thick, cold and white. The air was silent, heavy and chill… The hobbits sprang to their feet in alarm, and ran to the western rim. They found that they were upon an island in the fog. Even as they looked out in dismay towards the setting sun, it sank before their eyes into a white sea, and a cold grey shadow sprang up in the East behind. The fog rolled up to the walls and rose above them, and as it mounted it bent over their heads until it became a roof: they were shut in a hall of mist..."

- J.R.R. Tolkien

from *The Lord of Rings* Part I: <u>The Fellowship of the Ring</u> "Fog on Barrow-Downs"